Post-processing of Photonic Crystal Fibres and Standard Fibres

Witkowska, Agata

Award date:
2009

Awarding institution:
University of Bath

Post-processing of photonic crystal fibres and standard fibres

Agata Witkowska

A thesis submitted for the degree of Doctor of Philosophy

University of Bath

Department of Physics

January 2009

Abstract

This thesis describes work on fibre transitions made in photonic crystal fibres (PCF) and conventional standard fibres. Three post-processing techniques were used to make the transitions: fibre tapering, ferrule drawing and a new technique – PCF hole inflation. All these methods change the fibre dimensions on a centimeter scale while maintaining very low loss.

In the hole inflation technique, cladding holes are pressurized and can be enlarged while heat-treating, unlike other techniques where the holes can only be reduced in size. Controlled hole expansion was used to produce devices for applications such as supercontinuum generation. Furthermore, differential pressurization of holes could create a diversity of core shapes in a PCF section. For example they were investigated to improve interfacing of laser diodes to fibres.

Differential pressurization was also used to introduce new cores into PCFs. Introducing a larger core asymmetrically by the original core resulted in a fundamental to second-order mode conversion with a high extinction ratio. Alternatively, similar mode conversion was demonstrated by fusing two unequal standard fibres. Also with standard fibres, low-loss multimode to single-mode fibre transitions were made using a modified fibre fabrication technique.

These fibre transitions and optical devices have a wide range of potential applications, for example in supercontinuum generation and low-loss interfacing of fibres to other optical systems.

Acknowledgements

There are a lot of people I should thank for their help and support during my PhD. Firstly I would like to thank my supervisor, Tim Birks, for his support and unlimited enthusiasm.

Many thanks to all the members of the optogroup (today CPPM) for their everyday willingness to help (do I look like a person who needs so much help?), but first of all their great company during all these 4 years. I would especially like to thank Sergio and Lai for sharing not only all the knowledge and experience but also all these precious moments in the labs and the office. Thanks Mat for introducing me to the secrets of the fibre tapering. It was great to have William and Chunle, our “nonlinear gurus”. Alan and Steve, thank you for all your helpful advices during long fibre drawing sessions. For great energetic badminton sessions I need to thank Kevin (the guy making the best Chewbacca impression) and Alexey. Fetah and Francois, a french team for their warmth and OSA sharing. Aline and Purna for trying to be nice to me while hole blocking. Thank you also to all of you who I have just omitted.

I would like to acknowledge and thank Philip Russell and Jonathan Knight for giving me the opportunity to work in such a prestigious environment.

Finally I would like to thank my parents for letting me go and all their support through all my life. And you Laurent for your critical view into my thesis and everyday little help. Thank you my son for the nicest smile in the world.

Publications

The following is a list of papers published or submitted to refereed journals as a result of work done in this Ph.D.

1. W.J.Wadsworth, A.Witkowska, S.G.Leon-Saval, T.A.Birks: "Hole inflation and tapering of stock photonic crystal fibres", Optics Express, 13, August 2005, pp.6541-6549.

2. C.Xiong, A.Witkowska, S.G.Leon-Saval, T.A.Birks, W.J.Wadsworth: "Enhanced visible continuum generation from a microchip 1064nm laser", Optics Express, 14, June 2006, pp.6188-6193.

3. A.Witkowska, K.Lai, S.G.Leon-Saval, W.J.Wadsworth, T.A.Birks: "All-fibre anamorphic core-shape transitions", Optics Letters, 31, September 2006, pp.2672-2674.

4. K.Lai, S.G.Leon-Saval, A.Witkowska, W.J.Wadsworth, T.A.Birks: "Wavelength-independent all-fibre mode convertors", Optics Letters, 32, February 2007, pp.328-330.

5. A.Witkowska, S.G.Leon-Saval, A.Pham, T.A.Birks: "All-fiber LP_{11} mode convertors", Optics Letters, 33, February 2008, pp.306-308.

6. P.Nandi, Z.Chen, A.Witkowska, W.J.Wadsworth, T.A.Birks, J.C.Knight: "Characterization of photonic crystal fiber mode converter using low coherence interferometry", Optics Letters, 34, March 2009, pp. 1123-1125.

The following is a list of publications in national and international conferences as a result of work done during the course of this Ph.D.

7. W.J.Wadsworth, T.A.Birks, S.G.Leon-Saval, A.Witkowska: "Photonic crystal fibre devices, processing and interfacing", presented at the IEEE Seminar on Photonic Crystal Fibres (London, UK), September 2005 (invited).

8. A.Witkowska, W.J.Wadsworth, S.G.Leon-Saval, T.A.Birks: "Novel optical devices made by inflating the holes of a photonic crystal fibre", presented at the IOP meeting on In-Fibre Bragg Gratings and Special Fibres (Coventry, UK), Photonex Europe 05, October 2005.

9. K.Lai, A.Witkowska, S.G.Leon-Saval, W.J.Wadsworth, T.A.Birks: "Fibre core shape transitions for optical interfacing", Proceedings of the Optical Fiber

Communication Conference (OFC, Anaheim, California), March 2006, paper PDP4 (postdeadline).

10. K.Lai, A.Witkowska, S.G.Leon-Saval, W.J.Wadsworth, T.A.Birks: "Low-loss anamorphic transitions to high-aspect-ratio fibre cores", Proceedings of the Conference on Lasers and Electro-Optics (CLEO, Baltimore, Maryland), May 2006, paper CMM7.

11. C.Xiong, A.Witkowska, T.A.Birks, W.J.Wadsworth: "Visible continuum generation from a microchip 1062 nm laser source", Proceedings of the Conference on Lasers and Electro-Optics (CLEO, Baltimore, Maryland), May 2006, paper CTuA6.

12. N.Y.Joly, S.G.Leon-Saval, A.Witkowska, T.A.Birks, P.St.J.Russell: "Evolution of soliton behavior in adiabatically tapered photonic crystal fiber", Proceedings of the Conference on Lasers and Electro-Optics (CLEO, Baltimore, Maryland), May 2006, paper CThV1.

13. T.A.Birks, S.G.Leon-Saval, K.Lai, A.Witkowska, W.J.Wadsworth: "Interfacing to photonic crystal fibres", Proceedings of the Optoelectronics and Communications Conference (OECC, Kaohsiung, Taiwan), July 2006, paper 5D2-1 (invited).

14. K.Lai, S.G.Leon-Saval, A.Witkowska, W.J.Wadsworth, T.A.Birks: "Wavelength-insensitive LP_{01} to LP_{02} fibre mode convertor using photonic crystal fibre inflation", Proceedings of the European Conference on Optical Communication (ECOC, Cannes, France), September 2006, paper Th4.2.3 (postdeadline).

15. A.Witkowska, S.G.Leon-Saval, K.Lai, T.A.Birks: "LP_{01} to TE_{01} fibre mode convertor", Proceedings of the European Conference on Lasers and Electro-Optics (CLEO/Europe, Munich, Germany), June 2007, paper CE5-3-WED.

16. T.A.Birks, A.Witkowska, S.G.Leon-Saval, K.Lai: "Broadband mode convertors in photonic crystal fibres", Proceedings of the International Conference on Transparent Optical Networks (ICTON, Rome, Italy), July 2007, paper We.B2.1 (invited).

17. S.G.Leon-Saval, T.A.Birks, A.Witkowska, K.Lai, W.J.Wadsworth: "Post-processing and tapering of PCFs", Proceedings of the IEEE/LEOS Winter Topical Meeting, January 2008, paper WD2.1 (invited).

18. T.A.Birks, A.Witkowska, S.G.Leon-Saval, K.Lai, W.J.Wadsworth: "Post-processing of photonic crystal fibres", presented at the 1st Mediterranean Conference on Nano-Photonics (Istanbul, Turkey), October 2008 (invited).

19. P.Nandi, Z.Chen, A.Witkowska, W.J.Wadsworth, T.A.Birks, J.C.Knight: "Characterization of photonic crystal fiber mode converter using low coherence interferometry", submitted to the Optical Fiber Communication Conference (OFC, San Diego, California), March 2009.

Patents filed from work done during this PhD:

20. T.A.Birks, K.Lai, S.G.Leon-Saval, W.J.Wadsworth, A.Witkowska: "Microstructured optical fibres and methods relating thereto (differential fibre inflation)", British patent application number 0519503.7, September 2005; international patent publication number WO2007/034186, March 2007.

Articles appeared in technical press from work carried out during this PhD:

21. T.A.Birks, S.G.Leon-Saval, A.Witkowska, K.Lai, W.J.Wadsworth: "Novel methods pair holey fibers with conventional fibers", Laser Focus World, 42, April 2006, pp.70-73.

22. K.Lai, S.G.Leon-Saval, A.Witkowska, W.J.Wadsworth, T.A.Birks: "Wavelength-independent all-fibre mode convertors", Virtual Journal on Nanoscale Science and Technology, 15, February 2007.

Table of contents

Chapter 1 Introduction

Optical fibres are very fine fibres of glass. Typically they consist of a glass core of a few or a few tens of micrometres diameter, surrounded by a glass optical cladding giving an outside diameter of about 125 μm (Fig. 1.1). Light entering one end of the fibre is guided to the other end.

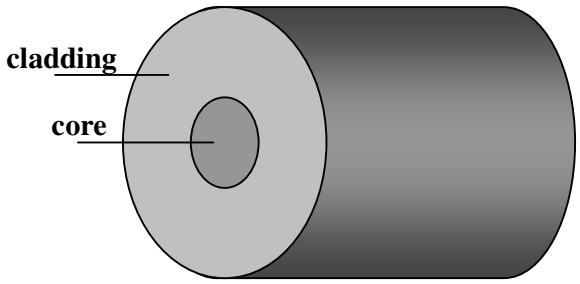

Fig.1.1 The cross-section of a conventional optical fibre.

The light-guiding principle behind optical fibers (total internal reflection) was first demonstrated by Irish inventor John Tyndall in the 1840s and first practical applications for medical purposes based on uncoated plastic fibres appeared early in the twentieth century [Crisp 01]. Modern fibres suitable for telecommunication with a silica core surrounded by a silica cladding were demonstrated in the late 1970s. Optical fibers are widely used in telecommunication to transmit a modulated laser beam. The rate at which information can be transmitted by a wave (light, radio) is proportional to the frequency. Infrared and visible-light waves guided by optical fibres have much higher frequency than radio waves, so a modulated laser beam can transmit an enormous amount of information through a single fibre-optic cable. Another advantage of fibre-optic cables is that they are electrical insulators. They are immune to electrical interference from lightning and other sources and they don't allow unwanted currents between source and receiver. Optical fibers are also used to form sensors, and in a variety of other applications.

More recently, a new type of fibre called the photonic crystal fibre (PCF) has been developed [Knight 96, Birks 97, Cregan 99, Russell 03] and my research mainly

concerns their properties. PCFs have generated much attention offering many degrees of freedom in their design that are not available in standard optical fibres. Amongst their main advantages towards the latter are single-mode guidance over very wide wavelength ranges [Birks 97], extremely small or large mode areas [Knight 98 b], unusual dispersion properties [Knight 00] and many others.

In this Chapter I outline some principal optical properties of conventional single-mode fibres (SMFs) and photonic crystal fibres (PCFs), both used in my research. I will use the abbreviation SMF to denote conventional single-mode fibres, even though at short-enough wavelengths they do become multi-mode. Only fibres made from fused silica glass are considered.

1.1 Conventional optical fibres

1.1.1 Structure and fabrication

To maintain total internal reflection, the core of the fibre in Fig. 1.1 must be given a higher refractive index than the cladding [Born 64].

There are two main stages to the manufacture of optical fibres: the making of the preform which is a glass rod of about 25 mm in diameter and a meter in length (eg using the Modified Chemical Vapour Dispersion (MCVD) technique) and the drawing of the fibre from the preform. The MCVD technique [Nagel 92] relies on chemical reactions where a precursor gas placed in a hollow substrate tube reacts with oxygen at high temperatures (~1800 K). The tube serves afterwards as a part of the cladding. The inside wall is covered with a number of glass layers forming the outer of the cladding and then the inner most layers with small amounts of index-raising dopants forming the core. Further heating collapses the tube making the preform ready to draw to the fibre.

In order to draw the fibres, the preform is passed vertically through a furnace to soften one end which is then stretched to form a glass fibre. The interior of the fibre retains a very similar refractive index structure as the preform with the same relative dimensions. The fibre passes through a coater which coats it with a plastic buffer protecting the fibre from the contamination and damage. Finally the fibre is wound on to a drum.

1.1.2 Guiding mechanism

The core is doped with impurities such as germanium or other dopants (unlike the cladding) to increase the refractive index of this region. The light can be guided through such a fibre due to the difference between the core (n_1) and the cladding (n_2) refractive indices, making use of total internal reflection (TIR) to confine light within the core of the fibre [Born 64, Marcuse 72].

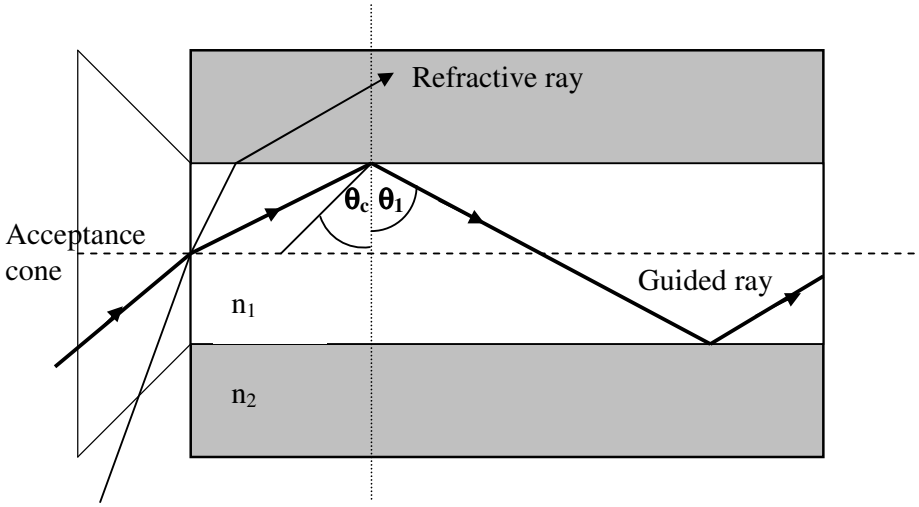

Fig. 1.2 Guiding and refractive rays in a step index fibre. The acceptance cone determines the maximum angle within which light will be accepted by the fibre.

As shown in Fig. 1.2 TIR occurs at the intersection of two media where $n_1 > n_2$ providing that the incident angle θ_1 is larger than a critical angle θ_c. The condition for TIR is:

$$\theta_1 \geq \theta_c = \sin^{-1}\left(\frac{n_2}{n_1}\right) \tag{1.1}$$

1.1.3 Optical modes

Fig. 1.2 shows a single ray propagating in a zigzag path reflecting at θ_1. Each ray propagates along the downward/upward path with wavevector $k_1 = k_0 n_1$. Each reflection changes transverse k_T but not longitudinal k_L. The longitudinal component is therefore invariant and is referred to as the propagation constant β:

$$\beta = k_1 \cdot \sin\theta_1 = n_1 k_0 \sin\theta_1 \tag{1.2}$$

where $k_0 \equiv \frac{\omega}{c} = \frac{2\pi}{\lambda}$ is the free space phase constant, λ is the wavelength of light measured in vacuum, and ω is the optical angular frequency.

The propagating wave changes with the direction of propagation z as $e^{-i\beta z}$. A light wave that propagates without change except for its phase is called a mode of the fibre. The electric field distribution of a mode can be expressed as [Marcuse 72]:

$$\vec{E}(x, y, z, t) = \vec{E}(x, y) e^{i(\omega t - \beta z)} \tag{1.3}$$

In order to avoid destructive interference between the various reflected component waves, the round trip phase change in the transverse plane needs to be a multiple of 2π. For a given wavelength, core size and choice of indices only certain values of θ_l satisfy this requirement. Each allowed incident angle θ_l corresponds to a mode of the guide.

β as a θ_l dependant constant is responsible for a diversity of mode orders. The higher β is, the lower is the order of the mode. The first mode (with the highest β) is called the fundamental mode.

The number of guided modes N depends on the wavelength, core size and refractive index differences and is determined by a parameter called the normalised frequency or V-value as follows:

$$V = \frac{2\pi}{\lambda} a \left(n_1^{\,2} - n_2^{\,2}\right)^{\frac{1}{2}} = \frac{2\pi}{\lambda} aNA \tag{1.4}$$

where a is the core radius and NA is the numerical aperture. If $V>>1$ and both polarizations are present the number of modes is [Diament 90]:

$$\mathrm{N} \sim \frac{V^2}{2} \tag{1.5}$$

In general, a fibre will support many modes of propagation. However by reducing the V-value the mode of lowest β stops being guided and is cut off. When $V < 2.405$ the fibre becomes single-mode and only the fundamental mode is guided. However, the fundamental mode exists in two perpendicular states of polarisation. Thus a single-mode fibre really guides two perpendicularly polarised modes. If these modes have different β, such a fibre becomes birefringent.

1.1.4 Kinds of modes and mode patterns

The exact modes of a step index fibre are known [Marcuse 72, Snyder 83] but complicated. Depending on the field distribution they divide between transverse electric (TE) transverse magnetic (TM) and hybrid (HE and EH) sets. In a TM mode the magnetic field lies entirely in the transverse plane and in a TE mode the electric field does. In the hybrid modes neither field is completely transverse.

In general the direction of electric vector $\vec{E}$ varies across the fibre cross-section. However, in the weak guidance approximation, where the refractive index difference between core and cladding is small, the direction of $\vec{E}$ can be assumed constant. This means that modes are linearly polarized (LP_{lm}) and TE, TM, HE and EH modes can be represented by LP modes instead [Marcuse 72]. Generally, the parameters l and m of a $LP_{l,m}$ mode can help to visualize the mode's intensity pattern. $2l$ gives the number of intensity maxima in the azimuthal direction, while the second index m gives the number of intensity maxima in the radial direction. The intensity patterns of some lower-order modes are shown in Fig. 1.3.

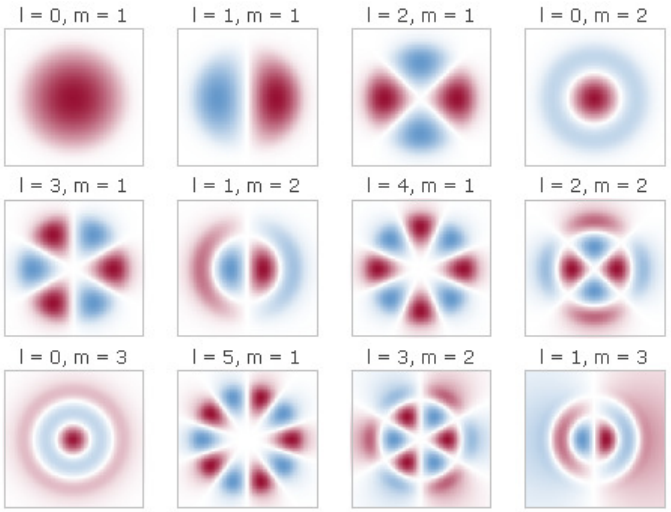

Fig. 1.3 Electric field amplitude profiles for guided modes of a multimode fibre. The two colors indicate different signs of electric field values.

Certain groups of LP modes become degenerate, meaning they have the same value of β. Their fields maintain the same relative phasing at all values of z, and so

their fields can be superimposed to form a new mode. The second order mode LP_{11} is composed of TE_{01}, TM_{01} and two degenerate HE_{21} modes whose field distributions and orders are presented in Fig. 1.4. This particular mode is of special interest in Chapters 5 and 6.

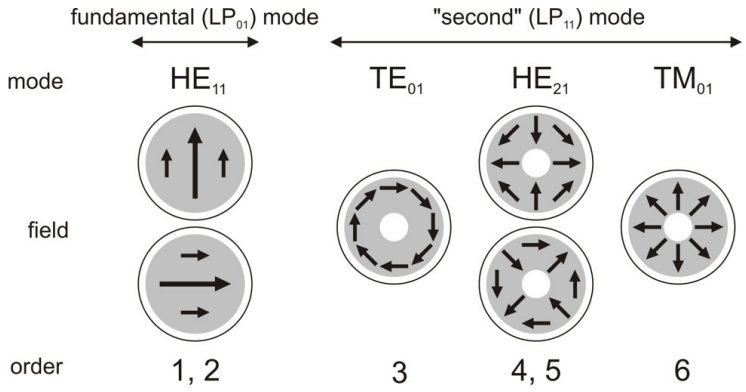

Fig. 1.4 The electric field directions of the six lowest-order polarisation modes of a circular multimode fibre core. The propagation constant decreases and the mode order increases from left to right. The HE modes are degenerate pairs.

When looking at mode patterns two descriptive images can be obtained: either in the nearfield or in the farfield. In the nearfield a lens is used to image the endface of the fibre on the camera, while the farfield is a Fraunhofer diffraction pattern which can be obtained with a lens or without. It is the Fourier transform of the nearfield pattern.

The intensity *I(r)* of the mode pattern is proportional to the square of the amplitude *A(r)*:

$$I(r) \propto A^2(r) \tag{1.6}$$

1.1.5 Directional coupling

Light may couple between parallel cores, forming a fibre optic directional coupler [Kawasaki 81]. If their modal fields are close enough they can overlap and thus interact leading to power transfer. Such a set of two separate cores can be considered as a single two-core composite waveguide (Fig. 1.5).

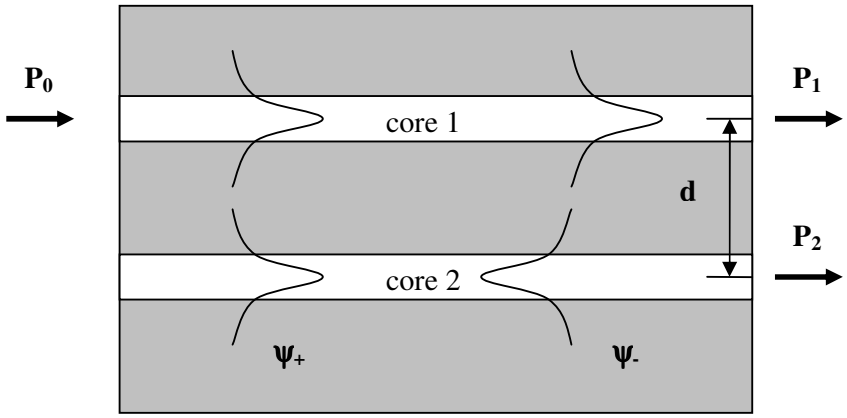

Fig. 1.5 Fiber optic directional coupler with two identical cores. When power is launched into one arm of the symmetrical coupler the lowest-order modes of the composite waveguide (even mode ψ_+ and odd mode ψ_-) are excited with equal amplitudes.

The behaviour of a directional coupler depends on the dissimilarity of the cores, which is represented by the F^2 factor. A good review to this field is given in [Jeunhomme 83, Buck 04].

$$F^2 = \frac{1}{\left(1 + \frac{(\beta_1 - \beta_2)^2}{4C^2}\right)} \tag{1.7}$$

where β_1 and β_2 are the propagation constants of the fundamental modes present in the isolated first and second cores respectively and C is the coupling coefficient. C is a function of wavelength and of the core separation, size and refractive index.

In a symmetric coupler the two cores are identical and when considered in isolation their fundamental modes have the same propagation constants $\beta_1=\beta_2$ so as seen in Eq. 1.7 $F^2=1$. This happens for any value of C. In this case complete power transfer between the two cores can be reached.

Otherwise the coupler is asymmetric $\beta_1\neq\beta_2$ and $F^2<1$. However in this case if C is large compared to the difference of propagation constants $C >> |\beta_1 - \beta_2|$ then $F^2\approx 1$ and significant (if not complete) power transfer between the two cores can be achieved. Otherwise, small values of C (large core separation, short wavelength, small core diameter) makes $F^2 \rightarrow 0$. This extreme case is called the null coupler described in

[Birks 94, Birks 95]. In the null coupler there is negligible power transfer between the two cores provided they are weakly interacting or very dissimilar [Leon-Saval 05 b, Wadsworth 02].

The null coupler has been studied and implemented in fibre mode convertor experiments where the fibre transitions play the crucial role. This issue will be explained in the Section 2.2.2 of Chapter 2.

The power in both cores can be determined using:

$$P_2 = F^2 P_{in} \sin^2\left(\frac{CL}{F}\right) \tag{1.8}$$

$$P_1 = P_{in} - P_2 \tag{1.9}$$

where P_1 and P_2 are the optical powers in the 1st and 2nd core respectively, P_{in} is the input power and L is the length of the coupler.

The normal modes of the composite waveguide are combinations of the fundamental modes of the isolated cores. If the coupler is symmetric these are the even and odd combinations. By launching light into one of the cores, both normal modes are equally excited. As they have different propagation constants β_+ and β_- they develop a phase difference while propagating through the system. It can be shown that:

$$\beta_+ - \beta_- = \frac{2C}{F} \tag{1.10}$$

1.1.6 Loss

The reduction of power as light travels along a fibre or through a fibre device is known as loss. Loss in a straight piece of fibre is due to absorption and scattering by the material it is made from or leakage through the cladding. Additional loss can also be caused by bending of the fibre: bend loss [Jeunhomme 83, Snyder 83].

A loss in transmission also arises in the interface between two fibres. In order to keep low interface loss the modes ψ_1 and ψ_2 (Eq. 1.11) of the fibres must be well-matched, as is the case when the core diameter and numerical aperture are the same. Furthermore the ends of the fibre must be brought together in close proximity and they must be accuretely aligned.

Fusion splicing is the most permanent and lowest loss method of connecting optical fibres. The fibres must first be stripped of their coatings, cleaned and cleaved. In

a typical case, the fibres are inserted into the vee-grooves and moved until the ends of the fibres meet guide lines visible through a lens or camera. After clamping them in position and choosing the splicing program, they are aligned and prefused (by an electric arc between two electrodes) in order to clean and dry the end surfaces. Afterwards the fibres are brought together and some additional end pressure is applied while a second fusing arc is generated to connect the fibres.

The transmission coefficient across a perfect intereface is [Snyder 83]:

$$T = \left| \int \psi_1 \psi_2 dA \right|^2 \tag{1.11}$$

where ψ_1 and ψ_2 are normalized field distributions of the modes of the two fibres and the integral is evaluated over the transverse cross-section (dA). This shows that $T<1$ unless $\psi_1=\psi_2$, so for low loss the mode fields need to be well matched. In particular it is necessary for the mode sizes to be matched. The parameter describing the spatial extent of the mode is the mode field diameter (MFD) [Gambling 77]:

$$MFD = 2\left(\frac{\int_0^\infty r^2 I dA}{\int_0^\infty I dA} \right)^{\frac{1}{2}} \tag{1.12}$$

where I is the mode field intensity distribution.

The more dissimilar two fibres are, the higher is the loss due to significant light coupling to the cladding modes. Therefore mode field diameter for low loss transmission in fibre systems should be similar when interfacing fibres.

It is also necessary for the mode shape to be matched. However, in most normal fibres, mode shape is the same (ie circular).

Fibre transmission loss is expressed in decibel units dB:

$$loss(dB) = 10 \log_{10} \frac{P_o}{P_i} \tag{1.13}$$

where P_i is the input power of the fibre and P_o is the output power.

The loss per unit length of a fibre is called attenuation and can be expressed in dB/km.

Loss can be measured using the cutback technique [Derickson 97]. This method is based on the measurement of the power P_o at the output of a fibre. Then a short piece of

the fibre is cut at the input without changing the input conditions and the power P_i leaving this piece is also measured. Their ratio, Eq. 1.13, gives the loss of just the piece that was cut out.

1.2 Photonic crystal fibres

1.2.1 Structure

Photonic crystal fibres (PCFs) [Russell 03] are typically formed from just one material – pure silica. The cladding has a periodic structure of parallel air holes constituting an array along the fibre length as shown in Fig. 1.6.

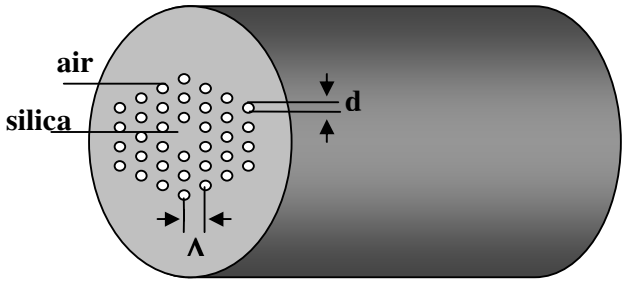

Fig. 1.6 PCF cross-section. d is the hole diameter, Λ is the pitch.

Light is guided along a core created by a defect in the above-mentioned periodicity [Knight 96, Birks 97]. The defect can be a missing air hole in the centre or perhaps a larger hole [Knight 98 a, Cregan 99].

1.2.2 Fabrication

Drawing the PCFs is a multi-step process [Knight 96]. First a silica tube and silica rod with diameters of several centimetres are drawn down to a diameter of approximately 1-2 mm using the drawing tower. A stack is then constructed by stacking the capillaries and rods by hand in a hexagonal array, where usually one rod is placed in the centre surrounded by capillaries, forming the core and the cladding respectively of the eventual fibre. More sophisticated designs can be implemented at this stage by

for example omitting one or more capillaries (forming a hollow core), placing doped or birefringent elements and so on. Such a prepared stack is placed in a silica tube (of around 20 mm diameter) to hold the stack together ready to be drawn down in the tower. A vacuum is applied between the capillaries while drawing to collapse the air-space between them. The product is a preform or cane composed of air-holes arranged in a regular hexagonal array. The preform can be then placed in a jacketing tube and then drawn down into PCF. The final diameter of the fibre is about 30-200 μm. Fig. 1.7 is a summary of the stack and draw process.

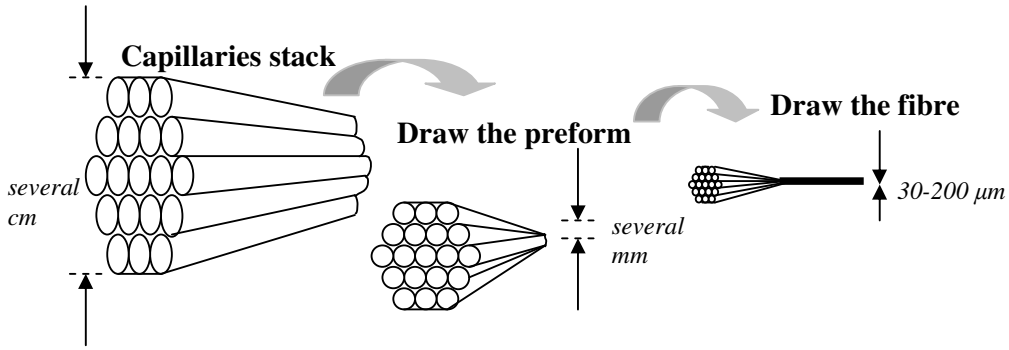

Fig. 1.7 Summary of the stack and draw process.

A photo of the drawing tower is given in Fig. 1.8. The perform feeding mechanism consists of a chuck mounted on a precision lead screw and this slowly feeds the preform into the furnace at a speed ranging from several to tens of mm/min. The furnace consists of an argon-purged graphite element which heats up (up to 2200 ^{0}C) when a current is applied to it. The cane puller is a set of two touching wheels with a precision speed control that pulls thick silica rods, capillaries or canes (1-5 mm diameter) out of the furnace at speeds from several mm/min to several m/min. In the case of fibre drawing (~ 100 μm diameter) its role is replaced by a capstan consisting of a set of wheels and springs and a drum winder controlling the tension on the drum. A coating monomer is applied to the fibre and cured using a UV lamp to increase the strength of the fibre.

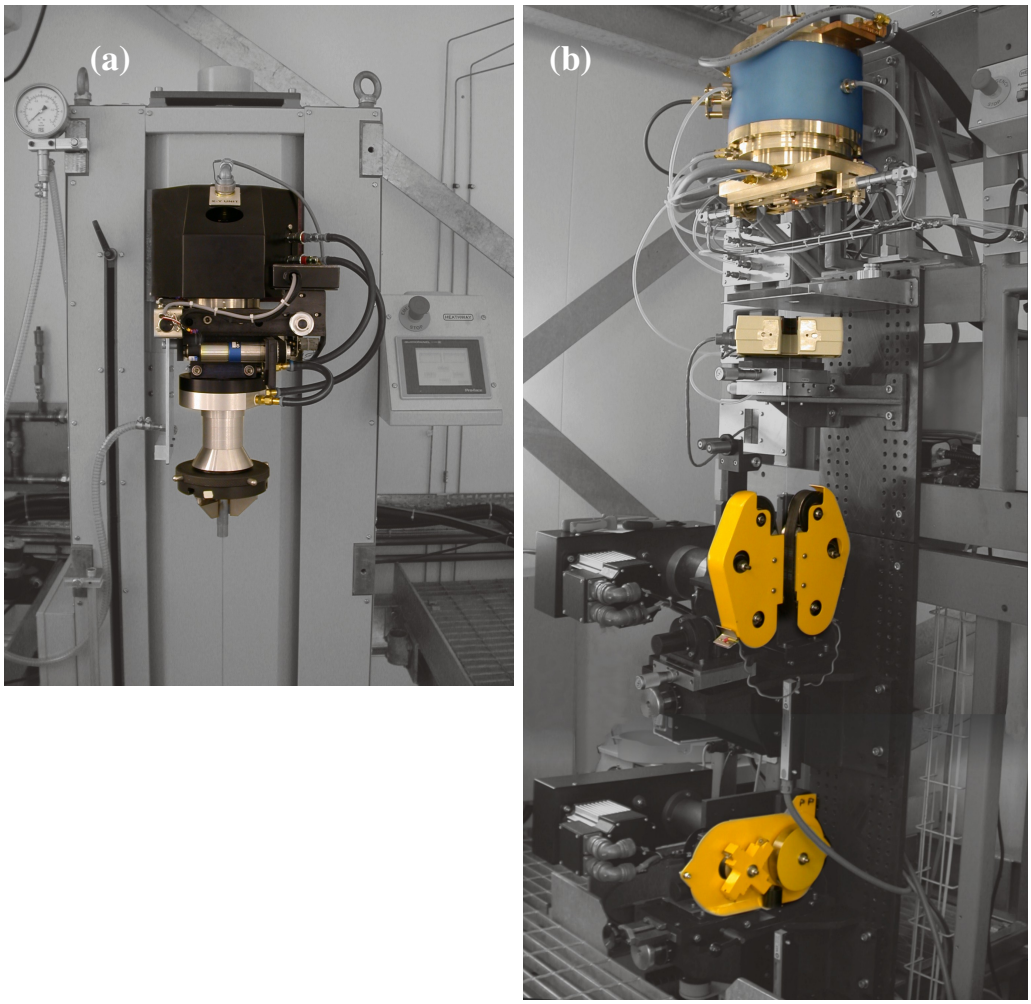

Fig. 1.8 The drawing tower (a) feeding mechanism, (b) furnace, diameter monitor and cane puller.

1.2.3 Guiding mechanism

A PCF guides light by one of two complementary guidance mechanisms. In the first case for an index-guiding PCF the guidance principle is analogous to that for conventional fibres. Total internal reflection occurs as the inner cladding made from air and silica has a lower effective refractive index than the solid core. The main difference is that the effective index of the cladding is a function of the wavelength of the transmitted light which affects the optical properties of the fibre. Additionally unlike in conventional fibres there is no need for the use of dopants.

For bandgap-guiding PCFs the structure in the cladding creates a photonic bandgap where the light is trapped in the core and cannot leak out even if the core refractive index is lower than that of the cladding. This can be used to make hollow-core fibres but is not restricted to air and silica [Alkeskjold 04, Steinvurzel 04, Luan 04]. It can be satisfied for example in an all-solid structure consisting of germanium-doped silica and pure silica materials [Argyros 05 a, Argyros 05 b].

1.2.4 Endlessly single-mode fibres.

The normalised frequency parameter V for standard fibres was introduced in Section 1.1.3. PCF has a similar expression for the effective V parameter:

$$V = \frac{2\pi}{\lambda}\Lambda\left(n_1{}^2 - n_2(\lambda)^2\right)^{\frac{1}{2}} \tag{1.14}$$

where λ is the wavelength, Λ is the pitch or centre-to-centre separation of holes in the cladding (which approximates the core radius), n_1 is the refractive index of the core and n_2 is the effective refractive index of the cladding.

It can be shown that, unlike in conventional fibres, V for a PCF tends to a finite value as $\lambda \rightarrow 0$, and a PCF can be single mode for any wavelength (or "endlessly single mode", ESM) if this finite value is less than the second-mode cutoff V value for the fibre [Birks 97, Kuhlmey 02 b]. The strong wavelength dependence of the cladding refractive index counteracts the explicit λ dependence of the V parameter. At longer wavelengths the field reaches further across the fibre and therefore experiences a cladding index closer to the average of the cladding. Conversely, light of shorter wavelengths becomes more confined to the silica regions and avoids the holes. This results in an increase of the effective cladding index with decreasing wavelength which reduces the dependence of V on wavelength - V becomes almost constant for short wavelengths [Birks 97]. Unlike in conventional SMFs, the endlessly single-mode regime in PCFs does not depend on the core size (if the core is made from a single solid unit cell) and is only determined by the relative hole size d/Λ. For $d/\Lambda < 0.4$ the PCF stays endlessly single-mode. For larger d/Λ ratios, the isolation of the core from the cladding increases and therefore such a fibre can become multimode.

1.2.5 Supercontinuum in PCFs

Supercontinuum (SC) generation in PCFs is a nonlinear process resulting in a wide output spectrum while pumping with a single wavelength (often in the invisible range). The key parameters are the nonlinear coefficient and dispersion of the guide [Wadsworth 04 a].

Fibre nonlinearities are related to anharmonic motion of bound electrons under the influence of an applied field. Induced polarization in cylindrical fibres originates from 1st and 3rd order susceptibilities only, as 2nd order susceptibility vanishes for central symmetric glass. 3rd order susceptibility is responsible for 3rd order harmonic generation, four wave mixing (FWM) and nonlinear refraction. A good introduction to this field is given in [Agrawal 01]. Nonlinear refraction can be described as:

$$n = n_0 + n_2 I \tag{1.15}$$

where n_0 is the ordinary refractive index, n_2 is the nonlinear refractive index and I is the intensity of the light propagating through the medium. In the nonlinear fibre the phase shift Φ in the direction of propagation z is composed of 2 terms: linear and nonlinear. The nonlinear phase shift Φ_{nl} depending on the nonlinear coefficient γ and transmitted optical power P is denoted as follow:

$$\Phi_{nl} = \gamma P z \tag{1.16}$$

$$\gamma = \frac{2\pi n_2}{\lambda A_{eff}} \tag{1.17}$$

where A_{eff} is the fibre effective mode area. The smaller the effective mode area is the bigger the nonlinear coefficient and the phase shift are.

The explanation of SC generation is very complicated [Alfano 89]. Firstly, there are two different pulse regimes for continuum generation in PCF: ultrashort (femtosecond) pulses and picosecond/nanosecond pulses. In the first case, in the presence of the anomalous dispersion, pulses which do not change along fibre length or follow a periodic evolution pattern (called solitons) are formed [Agrawal 01]. Self-phase modulation, soliton effects and pulse walk-off are important considerations, and the propagation is described by the generalised nonlinear Schrödinger equation [Wadsworth 04 a]. In the second case SC generation can be understood by considering degenerate FWM [Wadsworth 04a, Serebryannikov 07]. By pumping a nonlinear medium at a frequency close to the zero dispersion wavelength (ZDW) of the medium

two sidebands (idler and signal) spaced at equal frequency intervals from the pump are generated (Fig.1.9). Phase matching and conservation of energy give the equations [Agrawal 01]:

$$2k_{pump} = k_{signal} + k_{idler} + 2\gamma P \tag{1.18}$$

$$2\omega_{pump} = \omega_{signal} + \omega_{idler} \tag{1.19}$$

where P is the peak pump power.

These phase matching conditions specify the wavelengths for peak gain in a given fibre, and will depend on the chromatic dispersion of the fibre. Fig. 1.9 represents a graphic solution of the phase matching illustrating the need for zero group velocity dispersion (GVD).

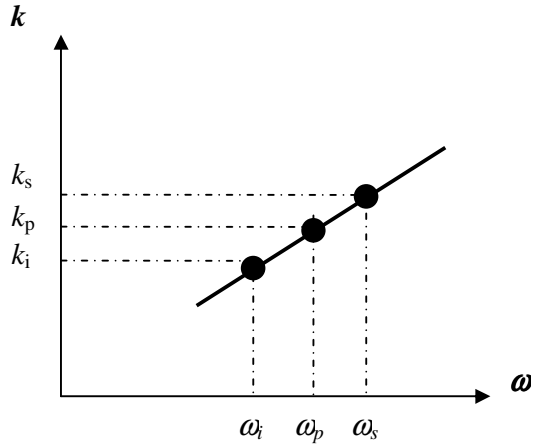

Fig. 1.9 Representation of the phase matching. Points must lie on a straight line with no second derivative, which is proportional to the GVD [Agrawal 01].

The relationship between dispersion and phase matching is critical for many nonlinear processes. PCFs can have nonlinear coefficients ranging from 3 orders of magnitude less than SMFs, or several orders of magnitude greater. A significant nonlinearity in a PCF can be reached through careful design of the fibre, or locally tapering it down to the smaller core size [Birks 00, Wadsworth 02, Leon-Saval 04a].

PCFs also opened up a range of new possibilities in dispersion control. It has been demonstrated that decreasing the fibre diameter shifts the zero dispersion wavelength (ZDW) down to smaller wavelengths [Wadsworth 02, Kudlinski 05] The holes along

the fibre not only affect the magnitude of the dispersion but also isolate the light from the surroundings even for small tapers [Birks 00]. Combining high nonlinear coefficient γ (small A_{eff}) with zero GVD is possible for very convienient pump wavelengths such as 1064 nm.

PCF SC can be used in place of other white-light sources in many characterisation and spectroscopy experiments, providing high brightness and broad spectral coverage simultaneously [Wadsworth 04 a]. Furthermore SC as emerging from PCF is more convenient for fibre coupling purposes than some incandescent sources, as the light is typically in a single mode. Broadband sources are also needed for the low-coherence-based imaging technique known as optical coherence tomography [Huang 91]. Here the use of PCFs results in unprecedented resolutions [Hartl 01]. Other applications of massive spectral broadening in PCFs were frequency standards [Udem 99] as a femtosecond laser comb in a PCF can be easily broadened to the optical octave required for determining the offset frequancy.

Chapter 2 Optical fibre transitions

Optical fibres are normally designed to be as uniform as possible along the direction of propagation. Any irregularities can cause coupling to higher order modes and loss in transmission. However if changes of structure in this direction are introduced smoothly, light can pass gradually from one fibre structure to another with low-loss. Such a smoothly-varying section is referred to as a fibre transition in this thesis. Depending on how this transition is made, it can generate some desirable effects as changing of mode size and shape, mode conversion or beam splitting, providing new possibilities in light control [Okamoto 86, Alder 00, Hunsperger 02, Choi 03, Belardi 05, Wadsworth 05, Nasilowski 05].

In this Chapter I describe two post-processing techniques used to make optical fibre transitions. The background of light propagation through fibre transitions is described. As an example of fibre transitions the null coupler idea is presented, a use of which is described in Chapters 5 and 6.

2.1 Fabrication of optical fibre transitions

There are two techniques developed and used in our photonics centre to produce fibre transitions. One of them is to make fibre tapers from stock fibres using a taper rig. The second technique uses fibre fabrication facilities in order to produce a preform which is then drawn into a fibre using the drawing tower, providing a fibre transition between two sections. The taper rig is a more compact and less expensive way of producing fibre transitions.

2.1.1 SMF tapers

The taper rig is composed of two motorised stages that stretch a fibre while it is heated by a burner mounted on a third stage (Fig. 2.1). The heated part therefore narrows to form a waist that is connected to untreated fibre ends by taper transitions

(Fig. 2.2). The whole resulting structure is called a tapered fibre, or (more loosely) a taper.

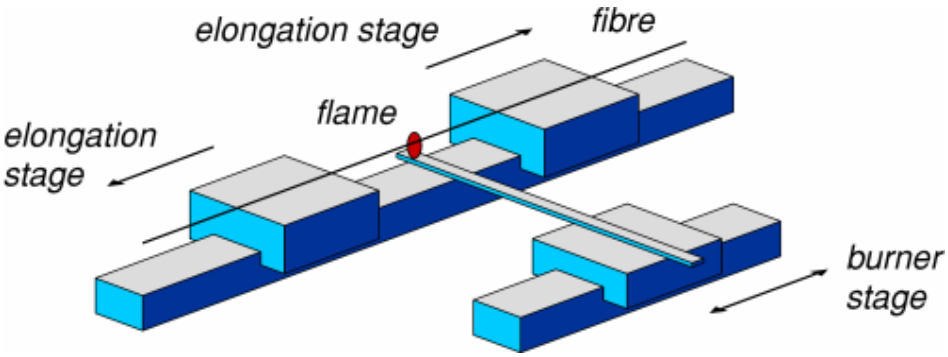

Fig. 2.1 Taper rig setup.

Fibre tapering is a convenient and effective way of dramatically modifying the nature of a fibre waveguide, while introducing hardly any loss of light. This powerful post-processing-technique can form taper transitions and waists of almost any shape and size with waist diameters down to 100 nm allowing precise control of taper parameters [Kenny 91, Birks 92].

Without the transition, input coupling into thin tapered waists would be impossible. In order to provide low loss these transitions should be sufficiently gradual. This *adiabaticity* condition is easily satisfied in practice [Birks 92] even for small diameter tapers. The light propagates with negligible loss (typically less than 0.1 dB) along the input transition into the waist where it can fill the entire fibre and then is recaptured by the growing fibre core at the output end (Fig 2.2).

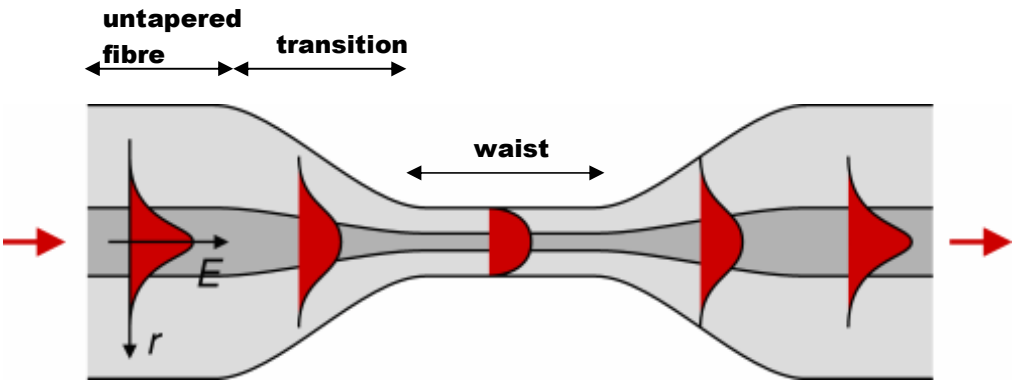

Fig. 2.2 Light propagation along a tapered fibre.

As well as tapering a fibre on its own, two parallel fibres can be fused and tapered together. This structure behaves like the directional coupler in Section 1.1.5 of Chapter 1, even though it is more complicated. Light entering one input fibre is split between the output fibres as described in Eq. 1.8 and 1.9. Depending on how similar two fibres are and how strongly they interact, all of the light can be coupled between them. However, if the fibres are dissimilar enough there is no power transfer which corresponds to the case where F^2=0. Such a device is called a null coupler, to be described in more detail in Section 2.2.2.

2.1.2 PCF tapers and ferrules

Tapering of PCFs is even more interesting as there is an additional degree of freedom, namely the size of the holes, which tend to shrink under surface tension when the fibre is heated. In order to keep the guided mode in the core of the fibre we need to preserve the holey structure in the cladding, even though there is always a little hole collapse. As tapering reduces the core size, it affects the dispersion of the fibre in ways that have been successfully applied in nonlinear applications such as supercontinuum generation [Birks 00, Coen 01, Wadsworth 02, Leon-Saval 04 a]. These nonlinear and dispersion properties depend on the size of the holes, as does the number of modes supported by the fibre. Other applications of tapered PCFs are in the area of optical sensors [Magi 05, Nguyen 05 b]. For example, when the holes collapse completely in the taper section, the guided light spreads out and interacts with the surrounding environment. Therefore changing the hole size in a controllable way in PCFs while

tapering is an important factor to optimize the optical properties of the fibre and thus leads to several new applications.

The tapering of PCF's can also help solve the problem of interfacing PCFs to other fibres with low loss. The interfacing of different fibres is an important problem because if the modes of the fibres are mis-matched there will be loss at the interface (see Section 1.1.6). The fibre taper rig described above can be used to make transitions that match between both fibres. However, the process of fibre drawing on a drawing tower can also be used to solve this problem [Leon-Saval 05 b]. A preform, called a ferrule, is made which incorporates one or more pieces of SMF which protrude from one end of the ferrule. One end of it is drawn down to a length of PCF, the core of which incorporates material from the entire SMF. These two fibres are connected via a gradual transition which results in a low optical loss. Fig. 2.3 shows an example of using such a ferrule transition for interfacing between a SMF and a PCF [Leon-Saval 04 b].

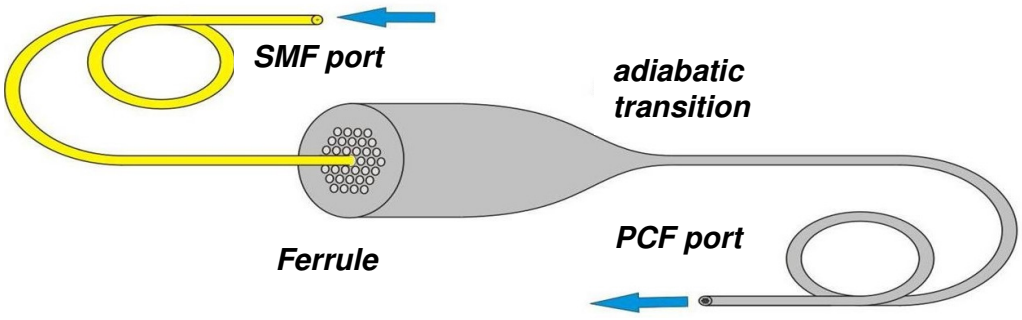

Fig. 2.3 Ferrule technique applied to SMF and PCF interfacing.

A ferrule transition with two dissimilar fibres in the central hole of the cane has been demonstrated as a mode convertor, to be described in Section 2.2.2.

Furthermore, low-loss ferrule transitions have been made with a greater number of SMFs in the ferrule: Chapter 7 describes the use of the ferrule technique to make multimode to single-mode transitions.

2.2 Transitions and mode guidance

2.2.1 Adiabatic transitions.

A fibre transition can profoundly change the field distribution of a mode. Severe structural changes of the core along a fibre introduce coupling to higher order modes or loss. However if the fibre transition is gradual enough there will be negligible coupling and low loss. Such a transition is described as adiabatic.

A taper transition can be divided along the propagation direction z into a sequence of thin slices (i_0, i_0+i), Fig. 2.4. Each slice at a position z supports its own "local modes" with propagation constants $\beta(z)$ which are defined as the modes of the uniform fibre of the same dimensions [Snyder 83]. Normally if light propagates through different slices there is some light coupling from one local mode to another one, which is called "local mode coupling". However, it can be shown that if the fibre transition is gradual enough, the coupling from this local mode is negligible and the local mode evolves adiabatically into the neighbour local mode of the next slice.

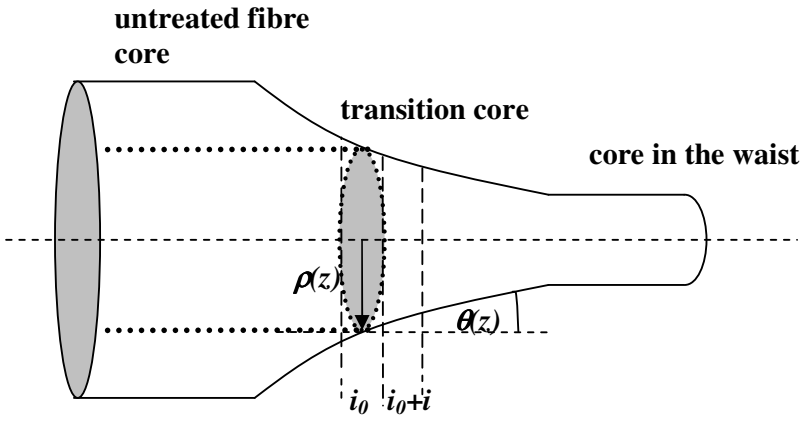

Fig. 2.4 Local mode concept. Each slice of the fibre transition has its local mode fields and propagation constants, which refer to a uniform fibre of the same physical parameters.

Theoretically the condition for low-loss is expressed through some adiabacity criterion [Love 91]. There is a length-scale criterion based on a comparison of the local taper length scale z_T with the beat length L_B between two possible closest modes m and n. If $z_T >> L_B$ then negligible coupling occurs and the fundamental mode propagates

adiabatically with negligible loss. This corresponds to a taper angle $\theta(z)$ much smaller than a local delineating angle $\theta_L(z)$:

$$\theta(z) < \theta_L(z) = \frac{\rho(z)(\beta_m - \beta_n)}{2\pi} \tag{2.1}$$

where $\rho(z)$ is the core radius, and β_m and β_n are the local mode propagation constants.

In practice a measurement of loss and/or purity of the mode at the fibre output can indicate whether a transition is adiabatic or not.

2.2.2 Null coupler

The null coupler is a device based on fibre transitions proposed by T. Birks [Birks 95] and developed by S. Leon-Saval [Leon-Saval 05]. It can be made by fusing together a parallel pair of dissimilar SMFs (eg. of different sizes) whilst tapering to form a fused coupler with a common waist. Depending on which fibre the light is launched into, a fundamental core mode evolves adiabatically into the fundamental mode or the second mode of the waist [Burns 75], as shown on Fig. 2.5.

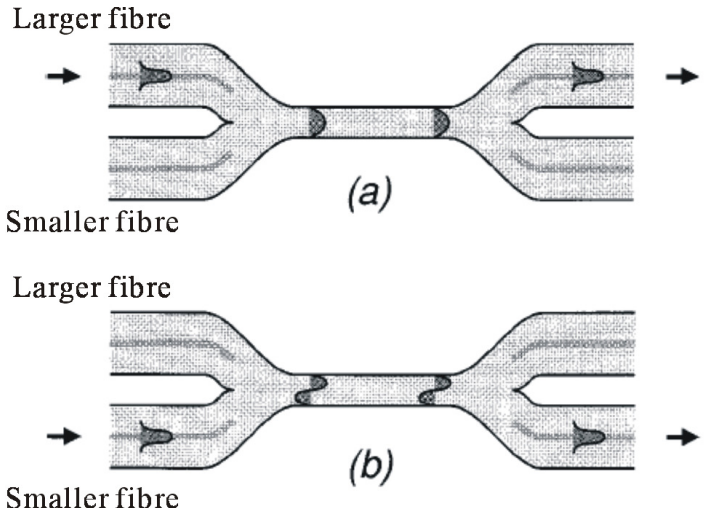

Fig. 2.5 Mode evolution.

The mode conversion is effective at all wavelengths (and any polarisation). So when we cleave the coupler at the waist and couple light just into the smaller fibre, we can get a mode convertor from the fundamental mode of the smaller fibre to the second

mode of the waveguide in the coupler waist [Birks 95]. Paradoxically, an ideal null coupler is a perfectly adiabatic device. This is because the fundamental mode of the smaller individual fibre is in fact the second mode of the pair of fibres (it has a smaller β than the mode of the larger diameter fibre). Null couplers can be made by pre-tapering one of a pair of identical fibres before forming the coupler, as described in Chapter 6. A discussion of adiabaticity in this structure is complicated by the pre-taper, which (strictly-speaking) is non-adiabatic with respect to the pair of fibres even if it is adiabatic with respect to the one fibre alone. However, the (ideal) null coupler beyond the pre-taper is still perfectly adiabatic.

This idea was implemented using the ferrule technique described in Section 2.1.2. Two SMFs with different propagation constants were introduced to one hole of a PCF preform which was then drawn down to the PCF, which in fact represents a null coupler embedded in a PCF. The device was shown to couple light from the LP_{01} mode to the LP_{11} mode with an extinction ratio better than 30 dB from 650 to 1750 nm wavelength [Leon-Saval 05]. Unfortunately, the core shape was elliptical, so the higher-order mode was LP_{11} rather than a hybrid HE or TE mode, and so could not be generalized, eg. to excite the circular LP_{02} mode needed for dispersion compensation. However, increasing the circularity of the core and/or decreasing the size of the core should make possible the excitation of higher order hybrid modes.

In Chapter 5 I describe an improved form of null-coupler-type mode convertor with a circular core, simply by post-processing a PCF. In contrast to ferrule drawing, no fibre fabrication is needed in our experiment. Instead, using our hole-blocking technique described in the next Chapter we demonstrated the fabrication of a TE_{01} mode convertor with low insertion loss.

Chapter 3 Hole inflation technique

Optical fibre tapering as described in the preceding Sections is a powerful post-processing technique. When applied to PCF it allows us to change not only the overall final diameter profile of the fibre along its length, but also the air-filling fraction. The hole size is a new degree of freedom that PCFs can offer. Control of hole size is of great interest in order to control dispersion properties, mode field diameter and the numerical aperture of a fibre [Knight 00, Mortensen 02, Kuhlmey 02, Reeves 02, Zsigri 04].

The shrinkage of holes while tapering is an expected and natural effect of surface tension and an excess of hydrostatic pressure is required to resist collapse, as explained in the next Section. Controlled hole shrinkage (at different rates) has been demonstrated in PCFs [Kakarantzas 02, Leon-Saval 04 a, Magi 04, Nguyen 05 a]. Even in small-pitch PCFs hole shrinkage has been minimised in order to preserve the hole structure by reducing the heating time and temperature [Kakarantzas 02, Leon-Saval 04 a, Nguyen 05 a]. Nevertheless in all cases the holes collapse at least partially.

However, a greater number of interesting devices could be provided if the fibre hole size could change the other way – getting enlarged. The effect of surface tension can be opposed by applying an internal pressure to resist collapse while heating. Provided there is an excess of hydrostatic pressure inside the holes they should expand.

Pressurisation of the holes of a PCF in order to change the mode field diameter (MFD) has been reported by [Birks 02]. Tapering with the ratio more than four times resulted in increased hole diameter to pitch ratio (d/Λ) starting from 0.46 to 0.66. Another way to prevent the holes from collapsing is by sealing the end of the fibre while drawing [Magi 04]. When a sealed volume of gas is heated, its pressure increases. In both cases the hole expansion was not significant and so the character of such a fibre was little changed. However, much more significant and better-controlled hole expansion is possible by applying a higher pressure directly.

In this Chapter I describe a new hole inflation technique that allows a controlled hole expansion in PCFs by heating the fibre while the holes are pressurised. By pressurisation of the holes it is possible to resist the hole collapse and indeed expand

the holes during tapering. In [Birks 02] ~ 30 % a hole size increase was demonstrated in this way, but I show that dramatic increases in air-filling fraction of more than 90% are possible. This enabled me to make low-loss transitions from an endlessly single-mode PCF (ESM PCF) with a large core and small holes to a highly nonlinear PCF with a small core and large holes. I show how such transitions help in the generation of supercontinuum light.

3.1 Surface tension and hole size

Whether a hole in fused silica shrinks or expands when the fibre is heated depends only on the pressure difference between the excess air pressure P in the hole and the effective pressure P_{st} due to the surface tension γ of the glass [Tabor 69]

$$P_{st} = 2\,\gamma / d \tag{3.1}$$

where d is the hole diameter. If $P > P_{st}$ then the hole will expand instead of collapsing.

Given the commonly-quoted value of $\gamma = 0.3$ J / m^2 for silica [Kingery 59], Eq. 3.1 is conveniently expressed in terms of pressure in bar and hole diameter in µm:

$$P_{st}\,(\text{bar}) = 6 / d\,(\mu\text{m}) \tag{3.2}$$

so an excess pressure of 6 bar is needed to keep a 1-µm hole in (unstable) equilibrium.

Although the viscosity of silica glass does change rapidly with temperature close to the softening point of 1700 °C, the surface tension varies little with temperature [Kingery 59].

3.2 Loss and adiabacity in the transitions

For transitions to have low optical loss, the guided mode must transform adiabatically through the transition, as described in the previous Chapter. In practice this means that any changes in mode size or shape in the transition must be over a length scale long compared to the diffraction of the guided mode [Love 87].

We consider transitions in both hole size and in core diameter, starting with ESM PCFs ($d/\Lambda \leq 0.4$ [Birks 97, Birks 99]) with core diameters of 5 or 12 µm, i.e. large compared to the wavelength. For such fibres the mode is well confined to the core at visible and near-infrared wavelengths. If the hole diameter d is increased by inflating the fibre without stretching it, the fundamental mode will still fill the core so the mode

field diameter (MFD) will not change much. For example the MFD is plotted against d/Λ for a PCF with a fixed solid core diameter of 5 μm in Fig. 3.1.

Field profiles are calculated using a full-vector plane-wave model [Pearce 05] for round holes and the MFD is calculated under the approximation that the mode field is scalar using

$$\mathrm{MFD}^2 = 4 \times \frac{\int_0^\infty r^2 \, I \, dA}{\int_0^\infty I \, dA} \tag{3.3}$$

where $I(r,\theta)$ is the mode intensity [Gambling 77]. The small change in MFD shown in Fig. 3.1 with hole diameter suggests that adiabaticity will be easy to fulfil for this type of hole expansion.

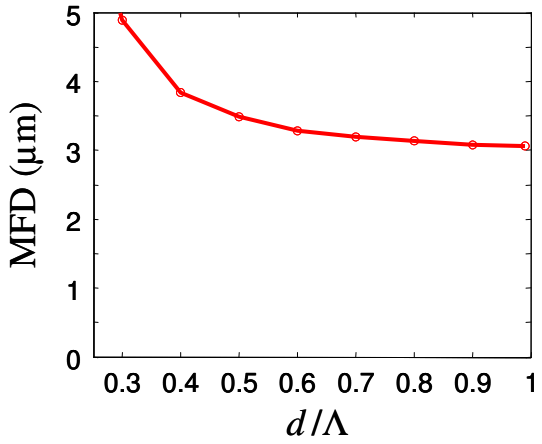

Fig. 3.1 Calculated MFD (by W. Wadsworth) at a wavelength of 1 μm for PCFs with a 5 μm diameter solid core and varying d/Λ.

Once the holes were inflated we then tapered the fibre by stretching it in a second process to form an interfaced highly-nonlinear PCF. This reduces the core diameter to 1-2 μm. Since this is just the standard tapering process that we have previously applied to PCF, we already know it should be adiabatic.

3.3 Experimental technique

As outlined in Section 3.2, two conditions must be met for hole expansion in PCF. Firstly the internal pressure must exceed that set by Eq. 3.2, and secondly the fibre must be heated long enough and hot enough to allow the expansion to take place.

Our procedure is summarised in Fig. 3.2. The holes at one end of a length of PCF were completely collapsed by heating the fibre in a fusion splicer. Then we used a gas cell with a fibre chuck and optical window (Fig. 3.3) to pressurise the other end of the fibre with dry nitrogen at up to 10 bar pressure whilst still allowing optical access for monitoring of the fibre transmission during processing. To heat a length of fibre in between in a controlled manner our standard flame-brush tapering rig was used [Birks 92]. The fibre was stretched slightly just to keep it taut while heated, typically to an extent that would reduce the transverse scale of the fibre by about 10% if the air filling fraction was unchanged. Transitions from unprocessed fibre to inflated fibre were made by heating a shorter length of fibre with each successive sweep of the burner.

The tapering parameters required for hole inflation are actually the opposite of those needed to taper with little hole collapse. To prevent hole collapse under surface tension without pressure we taper ‘fast and cold’, with a relatively cold flame to minimise the rate of hole collapse, and stretching as quickly as possible to minimise the processing time. In contrast, for hole inflation we must process ‘slow and hot’, using a relatively hot flame for rapid hole inflation and stretching slowly to increase the processing time. With constant flame conditions, tapering and burner speeds, we controlled the inflation of the holes by using different nitrogen pressures. After making a section of fibre with inflated air holes, the fibre could be tapered again but in a conventional ‘fast and cold’ process to reduce the fibre core diameter as required with little further change of air filling fraction.

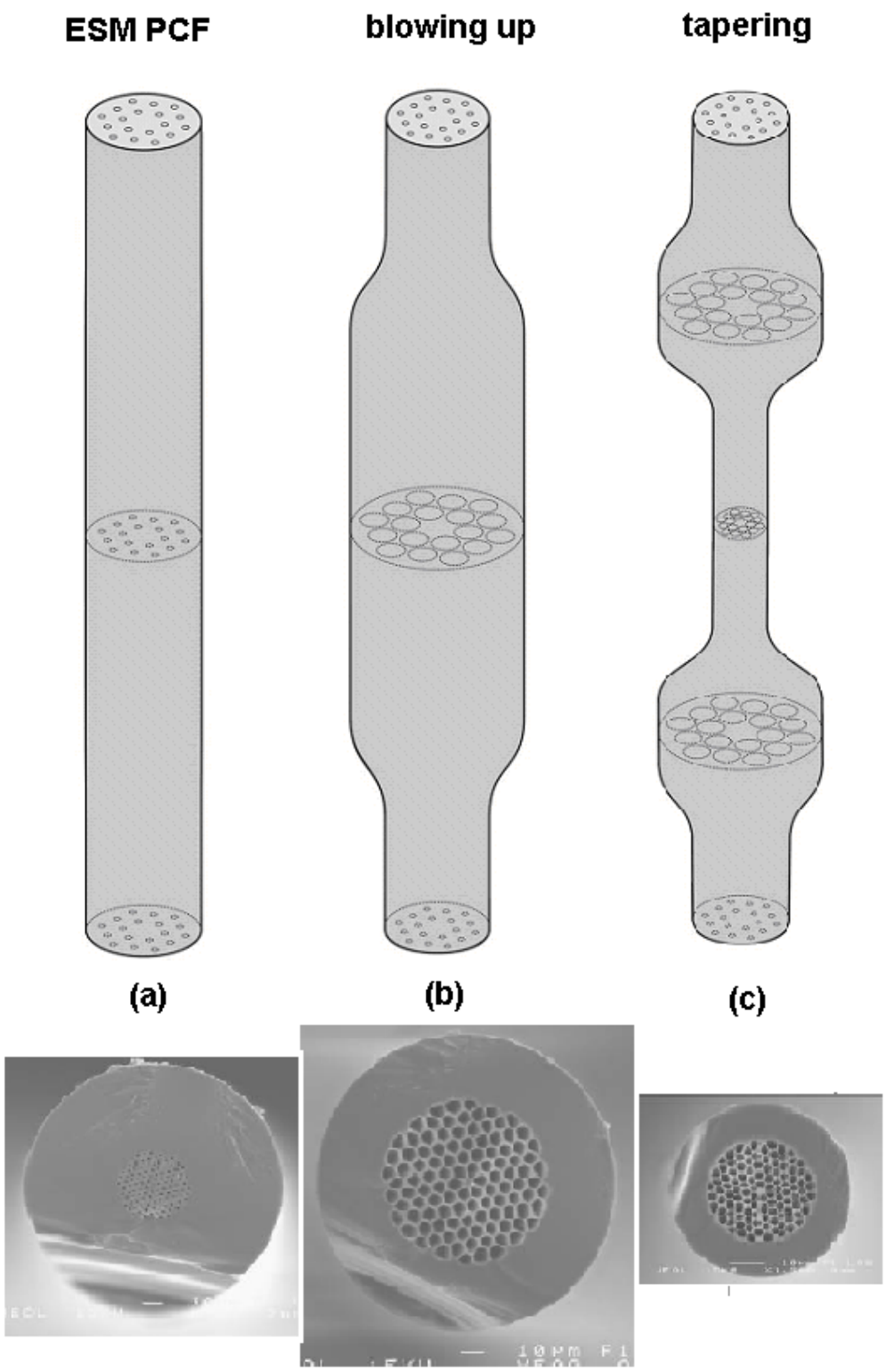

Fig. 3.2 Fibre inflation and tapering process to produce a 2-µm-core PCF with large air holes, connected at both ends to 5-µm-core PCF pigtails with small air holes. The example SEMs of the cleaved waist are to the same scale. The initial fibre was 125 µm diameter.

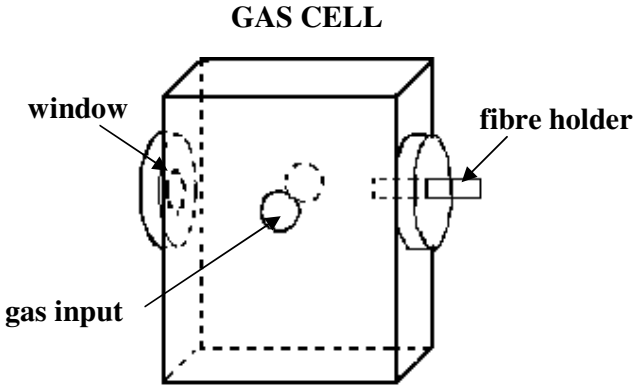

Fig. 3.3 Schematic figure of a gas cell.

The flame temperature is controlled through the ratio of butane to oxygen. However, in order to achieve a high enough temperature for significant hole inflation, the standard metallic burner was replaced by one made of silica providing a 2.8 mm flame (Fig. 3.4). This flame was hotter because metal burners absorb significant amounts of heat [Lienhard 01]. For a given butane to oxygen ratio, we found that the hole inflation was much easier to achieve with the glass burner.

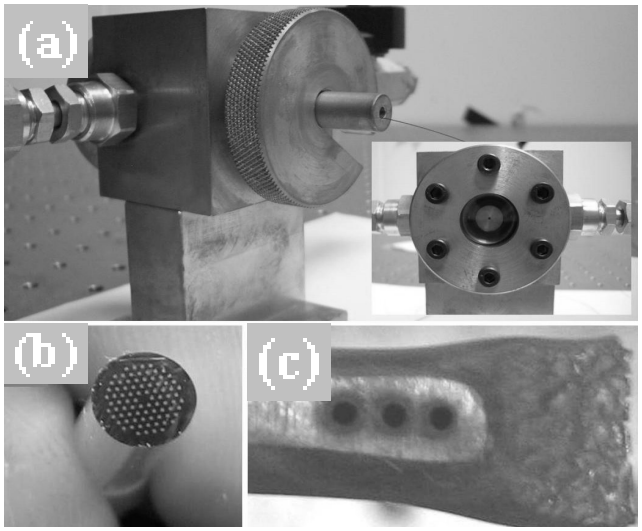

Fig. 3.4 Photos of (a) gas cell (b) glass burner (c) standard metallic burner. Photographs (b) and (c) are roughly at the same scale; in (c) the holes are 1 mm diameter.

3.4 Hole expansion control

To investigate the effect of different pressures, we inflated a 5-μm core ESM PCF with Λ = 3.2 μm, d/Λ = 0.43 and outer diameter OD = 125 μm, which was splice-compatible to conventional step-index fibre designed for 1060 nm light (e.g. *Corning HI 1060*). The hole diameter was 3.2 × 0.43 = 1.4 μm, so from Eq. 3.2 a pressure of 4.3 bar was required to counter surface tension. We formed 70 mm inflated sections with 30 mm transitions with a flame length of 2.8 mm and a processing time of ~280 s. The flame made 13 sweeps so one transition had 6 steps, the other 7 steps. The total time that for each portion of fibre in the waist spends in the flame was estimated to be 9 sec.

Figure 3.5 shows scanning electron micrographs (SEMs) of the fibre inflated at pressures from 6 to 10 bar under otherwise identical conditions. The more highly-inflated fibres have the "cobweb" structures of some highly nonlinear PCFs [Wadsworth 02], with a core suspended from thin webs and almost entirely surrounded by air, although the core diameter was of course much greater at this stage. Parameters measured from the SEMs are given in Table 3.1. For highly inflated fibres (8 and 10 bar) the hole size d in d/Λ is the distance across the flats of the rounded hexagonal holes. The initial core diameter (the solid region between the inside edges of the central ring of holes) was 5.0 μm. We define the core diameter as the distance between the inner edges of the inner ring of air holes:

$$d_{core} = 2\Lambda - d = \Lambda\left(2 - \frac{d}{\Lambda}\right) \tag{3.4}$$

During the processing the fibre was stretched slightly (as mentioned above), which in the absence of hole collapse or expansion would have proportionately changed the fibre's dimensions to those given under the heading "scaled fibre", the final core diameter being reduced by 8 % to 4.6 μm. The core diameters for all three inflated fibres were slightly smaller than this, indicating that there was some flow of glass from the core into the webs holding the core.

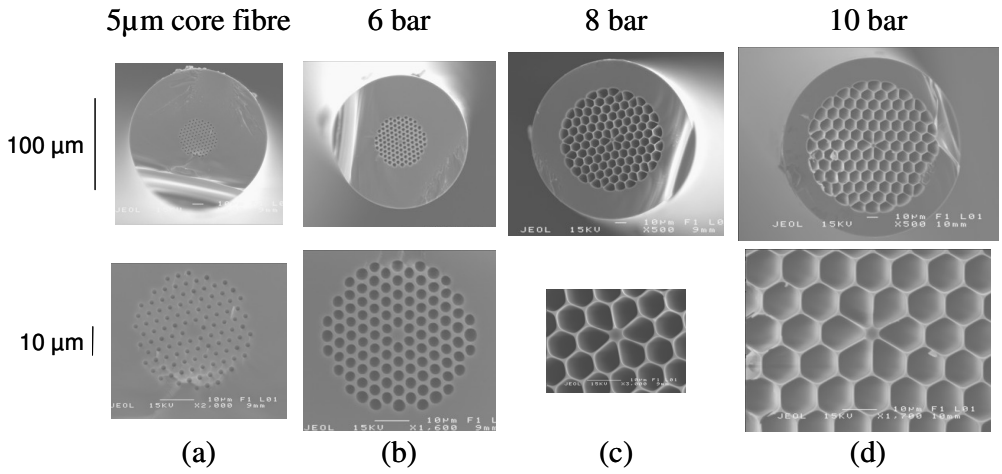

Fig. 3.5 SEMs of (a) the original 5-µm-core ESM PCF and (b)-(d) the same PCF inflated at pressures of 6, 8 and 10 bar respectively. All images in each row are at the same scale.

The increased air filling fraction in the inflated-hole fibres also increased their outside diameter. The scaled fibre should have an OD of 115 µm and contain 120 holes of 1.4 × 0.92 = 1.29 µm diameter. The total area of glass in the fibre cross-section can thus be calculated, and this will be the same for all the inflated fibres. A greater proportion of air in an inflated fibre will then necessarily increase the fibre OD in a predictable way. Monitoring fibre OD is standard in fibre drawing towers, and if implemented on an inflation rig would give a clear online indication of the hole size attained.

	Initial Fibre	Scaled Fibre	6 bar	8 bar	10 bar
OD (outer diameter)	125	115	121	144	163
d_{core}	5.0	4.6	4.0	4.0	3.7
d	1.4	1.29	2.9	8.0	10.5
Λ	3.2	2.9	3.8	8.3	10.8
d/Λ	0.43	0.43	0.74	0.96	0.98
Air filling fraction	0.16	0.16	0.50	0.91	0.95
Insertion loss (dB)	--	--	0.08	0.10	0.05

Table 3.1: Dimensions of the inflated PCFs shown in Fig. 3.5. The scaled fibre values are obtained by multiplying the initial fibre values by the same factor of 0.92, to represent the effect of the slight tapering if the holes did not deform.

Optical losses from 0.05 to 0.3 dB for 1550 nm light were measured during the inflation process. Losses at shorter wavelengths are expected to be even lower as the guided mode will be more strongly confined to the core and will therefore be less affected by changes in hole size.

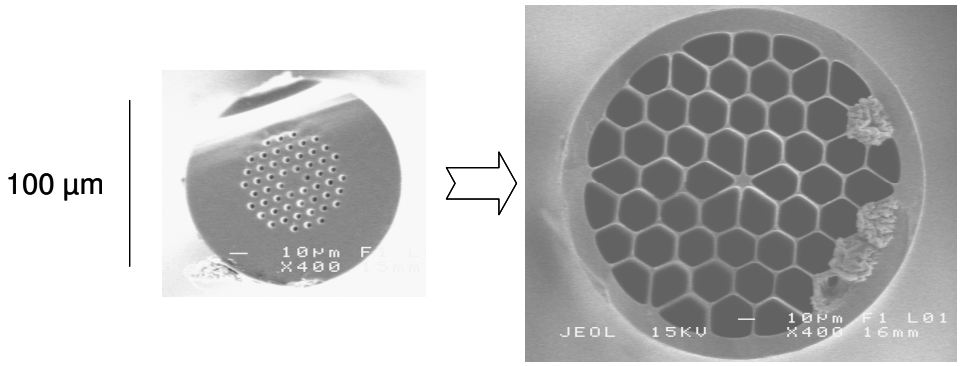

Fig. 3.6 SEMs of the 12-µm-core PCF before and after inflation, to the same scale. The inflated fibre has 210 µm OD.

A 12-µm-core ESM PCF was also processed in the same way. This fibre had Λ = 8 µm, d/Λ = 0.46 and OD = 125 µm. The mode field diameter matches standard SMF-28 at 1550 nm, allowing low-loss splices to conventional fibre systems. SEMs of this fibre before and after inflation are shown in Fig. 3.6. The maximum OD obtained in our experiments exceeded 400 µm, more than 3 times that of the un-inflated fibre.

3.5 Making highly nonlinear PCFs

Once a large-hole PCF had been made in this way, we then conventionally tapered the inflated section in a standard 'fast and cold' process to yield 100 mm long waists with core diameters of 1.1, 1.6 and 1.9 µm. The fibres were pressurised at 10 bar during this process so there is some further hole inflation, although the fibre is not processed hot enough or slowly enough to allow the holes to deform greatly. SEMs of these fibres are shown in Fig. 3.2 (a) and 3.7. Images of the initial and inflated fibres are essentially the same as Fig. 3.5 (a) and 3.5 (d). The scale reduction during tapering is shown by the bottom row of Fig. 3.7 which shows the tapered fibre at the same scale as the initial and

inflated fibres. Parameters of the inflated and tapered fibres are given in Table 3.2. Note that for tapered fibre (c) the fibre has been elongated by a factor of 3.7, so the area of glass in the fibre cross-section is also reduced by a factor of 3.7. However the final fibre diameter is almost the same as the initial diameter. The absolute hole diameters *d* in the tapered sections are all larger than in the initial fibre (holes in tapered fibre (a) would be as small as 0.37 μm without inflation or collapse).

The measured optical losses at 1550 nm for this second tapering stage ranged from 0.05 to 0.3 dB. The insertion loss of the entire structure (from initial ESM PCF to inflated PCF to small-core PCF, and back) was less than 0.4 dB for the 1.9 and 1.6 μm core samples, but was high for 1.1 μm core samples. For a 1.1 μm core diameter, the core is smaller than the measurement wavelength, so guidance may be expected to be weak. We note that the loss from mode mismatch if the untreated fibre was simply butted or spliced to 2 μm core high air filling fraction PCF would be at least 5 dB per junction.

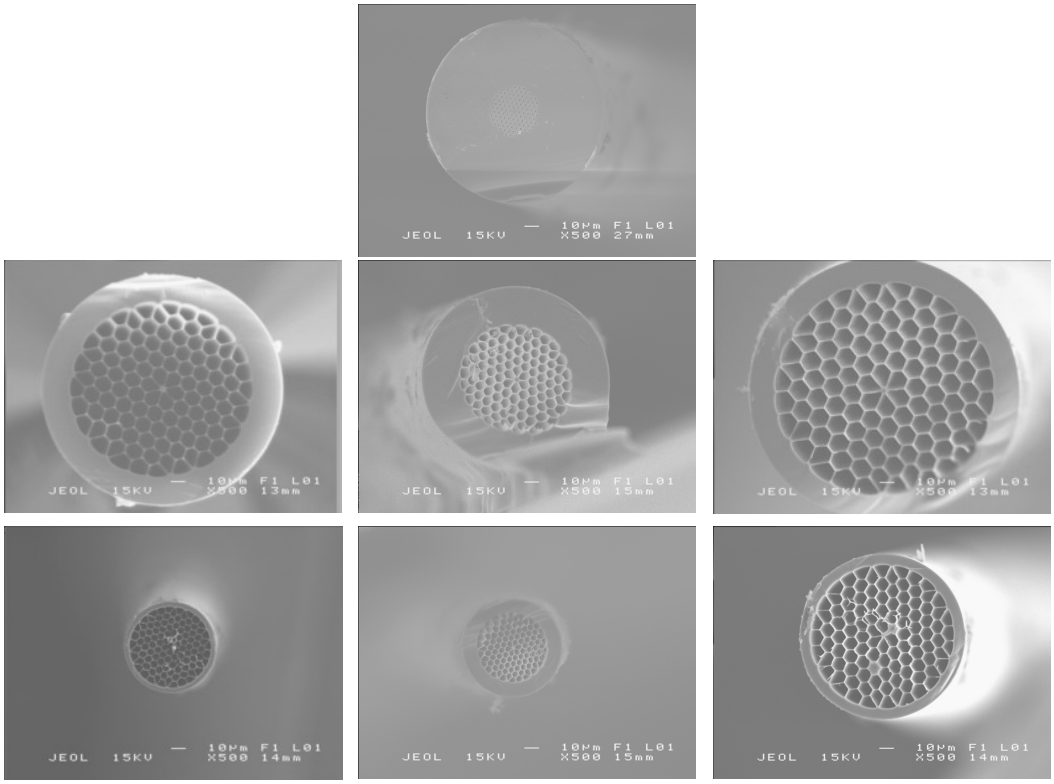

Fig. 3.7 SEM images of the inflated and tapered fibres. Top: initial PCF; Middle: inflated PCF; Bottom: tapered inflated PCF. All pictures to the same scale. Left to right; Final taper core diameters 1.1, 1.6 and 1.9 μm respectively.

		Total Elongation	OD (μm)	d_{core} (μm)	d (μm)	Λ (μm)	Loss (dB)	
(a)	Inflated fibre	1.18 (125-115 μm)	165	3.5	10.4	10.8	0.27	--
	taper	14.3 (125-33μm)	65	1.1	4.9	5.1	--	
(b)	Inflated fibre	1.18 (125-115 μm)	132	3.6	6.3	6.6	0.075	0.38
	taper	5.2 (125-55 μm)	69	1.6	3.7	3.9	0.30	
(c)	Inflated fibre	1.18 (125-115 μm)	192	3.6	12.6	12.7	0.28	0.34
	taper	3.7 (125-65 μm)	119	1.9	8.5	8.6	0.06	

Table 3.2. Parameters for the inflated and tapered fibres shown in Fig. 3.7

3.6 Nonlinear applications

3.6.1 Supercontinuum generation

The structures described in Section 3.5 have final waist sections similar to the PCFs and fibre tapers used for supercontinuum generation [Ranka 00, Birks 00, Chandalia 01, Wadsworth 02, Cordeiro 04, Leon-Saval 04 a], but with some advantages over both. The waist is a PCF (as in [Ranka 00, Coen 01, Chandalia 01, Wadsworth 02]), so the dispersion can be tuned by using different air hole sizes as well as by altering the core diameter. However, uniform PCFs [Ranka 00, Coen 01, Wadsworth 02] require that the input light is coupled into a very small core. This is alleviated in conventional fibre tapers [Birks 00, Cordeiro 04] because the input and output are conventional single-mode fibre pigtails. However, in conventional fibre tapers the guided mode is exposed on the outer surface and so is sensitive to environmental contamination, eg by dust. In contrast, in our device the input and output pigtails are single-mode fibres with a relatively large core diameter, but the waist is a PCF so the guided mode is enclosed and protected. A similar effect was achieved in a pioneering experiment by Chandalia *et al*. [Chandalia 01] where an otherwise conventional step-

index fibre had large holes in the cladding, which were used to confine the light when the fibre was tapered. Our device has the additional advantage that the PCF pigtails are close to being endlessly single mode, so they guide the whole continuum output in a robust single mode, whereas a conventional step-index core is unlikely to be single-mode and low loss over an octave or more in frequency. Our device is also fabricated from stock ESM PCF and does not require any special preform or fibre.

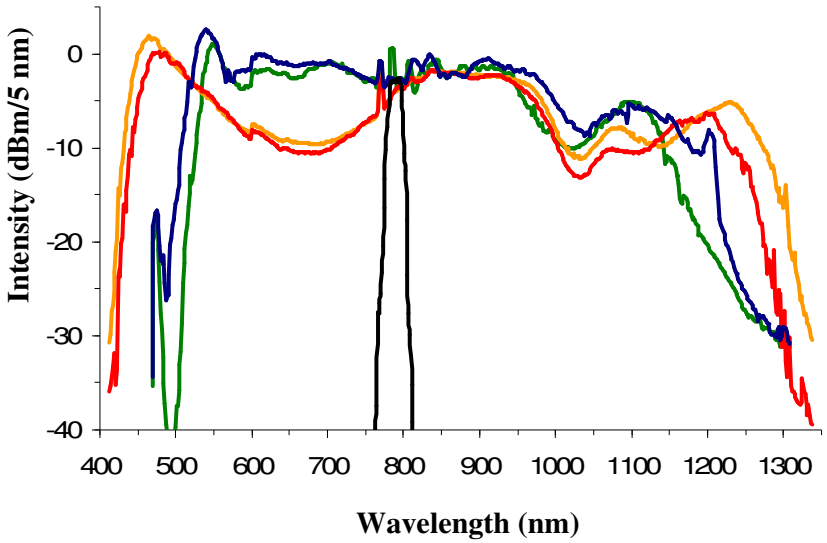

Fig. 3.8 Supercontinuum spectra for inflated fibres. Orange and red curves, tapered core diameter of 1.6 µm and coupled power of 123 and 92 mW respectively; blue and green curves, tapered core diameter of 1.9 µm and coupled power of 130 and 103 mW respectively.

Fig. 3.8 shows the continuum spectra produced by devices with 1.6 and 1.9 µm core diameters in the waist when pumped with a fs Ti:sapphire laser (790 nm, pulse duration ~200 fs, repetition rate 75 MHz) with ~100 mW average power coupled into the fibre. The input pigtail was cut to 6 cm length to avoid pulse broadening by the chromatic dispersion of the fibre before the tapered section. The output supercontinuum is naturally in the fundamental fibre mode, as the second mode (if excited) is only weakly guided and is easily stripped with a small bend. Although the inflated and tapered sections are strictly multimoded, we do not expect to excite any high-order modes as the nonlinear process occur in the fundamental mode of the multimode waist. The output continuum is then expected to reach the single mode output pigtail in the

fundamental mode and therefore will be output without loss. This is borne out in our nonlinear experiments, where the output power achieved is consistent with the small measured linear propagation loss in the structures, given in Table 3.2. The spectral extent of the continuum is as expected from previous experiments with similar active structures [Ranka 00, Birks 00, Wadsworth 02].

3.6.2 Visible supercontinuum generation

The previous Section has shown improved coupling for SC generation. However, as in most SC generation experiments, the range of wavelengths over which the supercontinuum is spread out rarely reaches half of the pump wavelength. This can be seen in Fig. 3.8. However if a shorter pump wavelength can be used, shorter-wavelength continuum can be generated.

Here we demonstrate bright single-mode *visible* continuum generation pumped by a simple compact 1062 nm Nd:LSB microchip laser (125 mW average power, 25 kHz repetition rate, 0.6 ns pulse duration, 5 μJ pulse energy). The hole inflation technique enables the whole process to be carried out in a monolithic all-fibre system. The process is in two steps. First we use four-wave mixing in a properly designed PCF to generate intense 734 nm pulses, which are then fed into a second PCF which generates supercontinuum from this output as the pump. The resulting total continuum spans the whole region from 400 nm to 1300 nm.

The experiment builds on the results of [Ranka 00] and [Wadsworth 04]. It has previously been demonstrated that PCF may be designed to convert 1064 nm pulses efficiently to wavelengths around 700 nm by four-wave mixing [Wadsworth 04]. It is also well established that small-core PCF is ideal for SC generation from pulsed sources at these wavelengths, e.g. from Ti:sapphire lasers [Ranka 00]. My colleague C. Xiong combined these two effects (Fig. 3.9) to generate a broad continuum spectrum spanning the visible and near-IR using a simple piece of inflated fibre produced by myself.

The two fibres required for the two-stage visible continuum generation are very different from each other. The first fibre (fibre A) is an endlessly single mode PCF with a core diameter of about 5 μm and small holes. This has a zero dispersion wavelength (ZDW) at 1103 nm and gives strong FWM gain at 734 nm, allowing >25% conversion

of the 1062 nm pump light over a 6 m length of fibre. The second fibre (fibre B) has a smaller core diameter of 2 μm and large air-holes. This fibre then has a ZDW at approximately 700 nm and thus displays strong modulation instability and continuum generation when pumped at 734 nm. The widely different core dimensions mean that it is not possible to splice the fibres together in a simple manner. To demonstrate the idea my colleague C. Xiong coupled light between the two fibres using free-space optics, and obtained the output SC spectrum shown in red in Fig. 3.11.

To improve the coupling we took a piece of type A fibre, and inflated and tapered part of it to form a section of type B, with a low-loss transition between the two sections. A schematic of the device and example electron micrographs are shown in Fig 3.9 and Fig. 3.10 respectively.

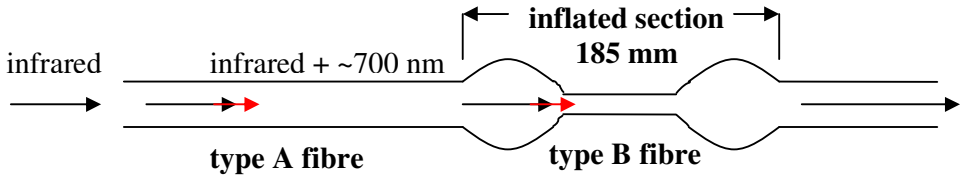

Fig. 3.9 Schematic for the two-stage visible generation process. Infrared 1062 nm laser light enters the input and is converted in the pigtail into ~700 nm light by four-wave mixing. The ~700 nm light acts as a pump for SC in the inflated fibre section.The output continuum is measured in the output fibre. Both input and output sections are endlessly single-mode fibre with a relatively large (5 μm diameter) core.

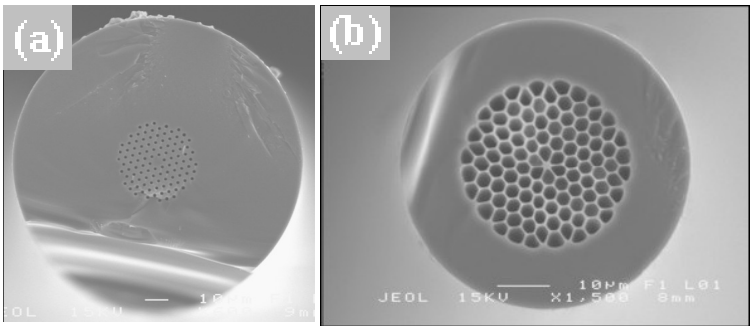

Fig. 3.10 SEM of (a) initial type A fibre before processing (OD 125 μm), (b) waist of inflated device. Images (a) and (b) are to the same scale.

First pressure is applied to the air holes in a length of fibre A with dry nitrogen at 6-10 bar. The fibre is then heated and stretched in a flame. The pressure makes the

holes expand, whilst the stretching reduces the transverse dimensions of the fibre. The result, shown in Fig. 3.10, is that the core diameter is reduced from 5 μm to 2 μm, whilst the air-filling fraction is increased. Thus the fibre in the waist region of the inflated device is equivalent to the bulk fibre B used above. All transitions were made gradual so that the insertion loss of the entire device was just 0.68 dB. The waist length is 120 mm.

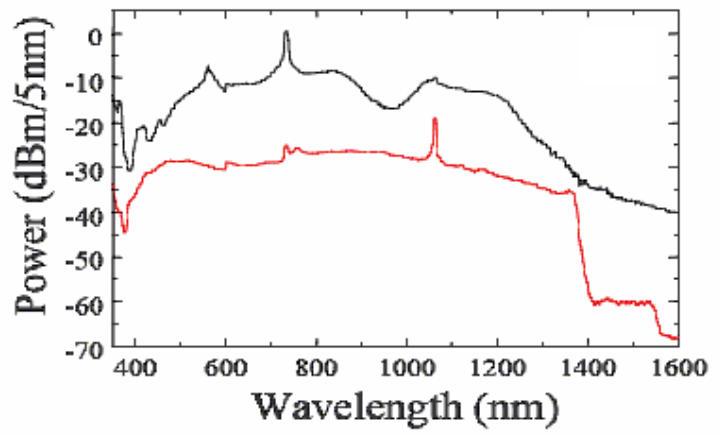

Fig. 3.11 Two fibres with free-space coupling (red) and the monolithic device (black). The apparent rising intensity towards 350 nm in all traces is an artefact of the spectrometer used.

.

The maximum output power for continuum generation in this device was 40 mW, considerably more than from the free-space coupled device. The spectrum is shown in Fig. 3.11. The spectrum is not quite flat as there is a strong peak at 561 nm due to accidental phase matching of the FWM process $2\,\omega_{734} - \omega_{1062} = \omega_{561}$. This will occur at some point in the transition as the ZDW sweeps from 1064 nm in fibre A to 700 nm in the waist. The effective length will be very short, but we still see a strong signal as there is pump field at the central frequency and the idler frequency to drive the process. Residual 734 nm light is also seen as the short device is unable to give full conversion.

We have demonstrated efficient visible continuum generation from a long-wavelength 1062 nm pump source by a two-stage process in a monolithic all-fibre device. The output fibre is single-mode at all wavelengths, which is ideal for delivery of such a broad continuum. Further enhancements are possible through transition design to enhance or reduce the peak at 561 nm, and fabricating more than one device in a single fibre to achieve a greater interaction length for the second stage.

3.7 Conclusions

In this Chapter a powerful post-processing technique has been described. We have demonstrated for the first time the thermal post-processing of a stock single-mode PCF to form a transition to a cobweb-type PCF structure with a smaller core but larger air-filling fraction. The inflation process can be well-controlled applying appropriate pressurisation. Generation of a supercontinuum has been demonstrated as one of the applications of inflated-hole structures. The insertion loss of complete structures was less than 0.3 dB. In these experiments all the holes were pressurised equally leading to the same inflation rate. In the next Chapter a differential hole inflation will be reported resulting in new core configurations and creation of additional cores along a length of the fibre.

Chapter 4 Differential pressurization

4.1 Introduction

The design of a PCF has many degrees of freedom, which are affected by tapering. For example core size and air-filling fraction can be varied on a cm-scale by tapering [Birks 92, Knight 97, Leon-Saval 04, Birks 04, Cordeiro 04]. In these experiments the shape of the core was little-changed, deviating at most only slightly from six-fold rotation symmetry and an essentially circular aspect ratio. However, core shape is an important parameter that affects the mode pattern and controls form birefringence. Furthermore, the number of cores is also of interest. Guided light can interact between parallel cores and couple between them. The shape and configuration of cores in a fibre can therefore be regarded as a new degree of freedom. Unusual core shapes and numbers can be formed during the fabrication of PCFs, but the local introduction of fibre transitions in core shapes or to additional cores along the fibre through tapering would provide new possibilities of light control.

Here I report the postprocessing of a PCF to change the shape of the core and to introduce secondary cores along its length. The approach is based on the inflation technique presented in the previous Chapter. We adapted this technique to change the core shape by two alternative methods of differential hole pressurisation: either exploiting surface tension to achieve different effective pressures in holes of different sizes; or applying different gas pressures to different holes by plugging some of them with glue at the end where pressure is applied.

A change of the core shape can be introduced using either method of differential hole pressurisation. Applying the first method to a PCF with 2 enlarged holes near the core results in unequal hole expansion where the bigger holes enlarged more and squashed the core, giving it and its mode patterns an elongated rectangular shape. With the second method we choose to pressurise all the cladding holes apart from one or more holes placed in line next to the core. When the fibre was heated the unpressurised holes collapse, adding extra solid unit cells to the core and giving it an elongated shape. We demonstrated that all-fibre anamorphic core-shape transitions made using both

methods can provide low-loss coupling of light between fibres and diode lasers. In other experiments ellipticity introduced into a core induced birefringence in the inflated section of a single-mode PCF.

With the second method the change of the core shape is made by blocking holes in the direct neighbourhood to the core adding new silica area to it. However if no physical connection is established between the original core and the blocked hole, it forms an additional separate core. Multi-core fibres have many interesting properties [MacPherson 01, MacPherson 03, Leon-Saval 05 b], but special fabrication techniques must be employed. Now using the adapted hole inflation technique we can easily introduce secondary cores along a piece of the PCF. We introduced a second core with a gradual transition. Input light excited only one supermode and therefore no light interaction between the cores. Such a device could potentially be used as a bend sensor.

4.2 Differential hole pressurization

In the preceding Chapter equal pressurisation of all PCF holes was demonstrated in a fibre where all of the holes were the same size. As a result inflation was identical for each hole. However, different rates of hole expansion occur when the hole sizes are different because the effective pressure due to surface tension differs (Eq. (3.2)). Therefore bigger holes expand quicker relative to smaller ones. Dramatic changes in core shape are therefore possible without blocking any holes if the initial fibre has a suitable distribution of hole sizes. The hydrostatic pressure common to all holes changes the "bias point" (eg whether two holes shrink at different rates or one expands while the other shrinks), giving an independent way to control the size of any one hole.

In order to demonstrate differential hole size pressurization without making a fibre specially, an existing polarisation-maintaining (PM) PCF with two holes bigger than the others (Fig. 4.1 a) was used. This fibre was pressurised to 7 bar and inflated. The bigger holes enlarged more as expected and squashed the core, giving it and its mode patterns an elongated rectangular shape, Fig. 4.1 b) c). The transition loss was 0.03 dB at 1550 nm.

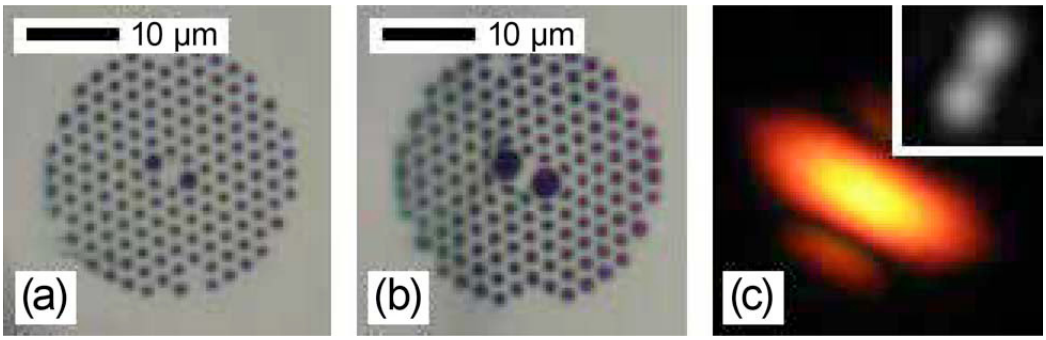

Fig. 4.1 Micrographs of PM PCF (a) before and (b) after inflation. (c) Output images of far-field for visible light and (inset) near-field at 1000 nm, not to scale.

Such transitions to rectangular cores can provide low-loss coupling of light between fibres and diode lasers or integrated optic waveguides with non-circular modes. Such an experiment has been carried out using this device with the elongated core section and will be described in Section 4.3. In due course, suitable fibre designs could be conceived and implemented for various shape transitions.

4.3 Blocking holes

4.3.1 Introduction

If all the holes are of the same size and the same pressure is applied to the fibre, differential hole pressurisation is still possible if one or more holes are plugged at one end of the PCF, not letting the pressure get in. Selected holes are blocked at the end where pressure is applied (all the holes at the other end being sealed as before). The plug of glue keeps such a hole near atmospheric pressure while its (open) neighbours become pressurised, Fig. 4.2. When the fibre is heated, each plugged hole collapses as its neighbours expand, leaving a new solid "unit cell" in the fibre's cross-section.

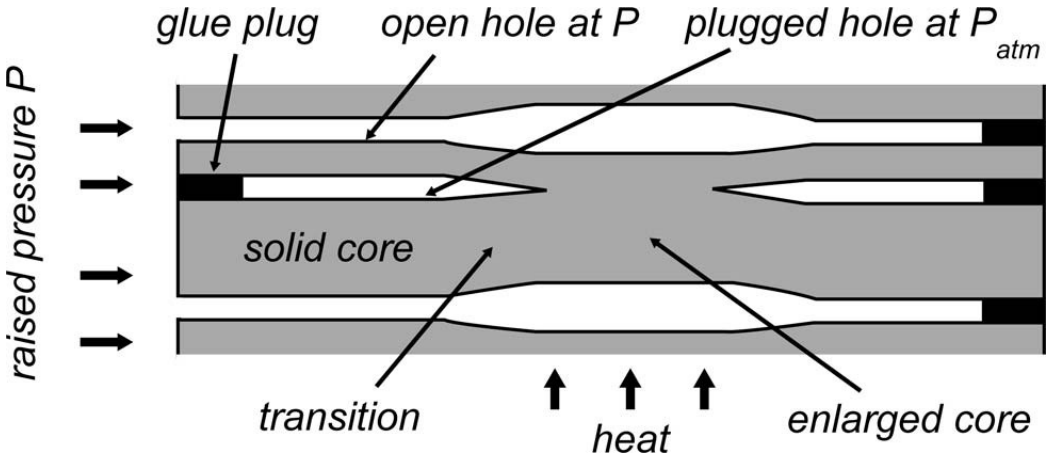

Fig. 4.2 Differential pressurisation in a PCF by blocking selected holes.

In all cases, the plugging of selected holes in an endface need only be done once for a whole length of fibre to give thousands of transitions in 1 km of PCF.

4.3.2 Hole blocking method.

The holes at the endface of a PCF are blocked using UV-sensitive glue. A tiny fibre tip is used to dispense the glue. The glue distribution setup consists of 2 xyz stages (Fig. 4.3). One of them positions the target fibre, and other one serves as a tip holder. To make hole blocking reproducible this method should be controllable in every possible aspect. A camera with a large-zoom microscope images the fibre endface and the position of the tip on a screen. Fig. 4.4 shows a target fibre, another fibre storing a supply of glue and a fibre tip. The method relies on picking up a small amount of glue by the tip and positioning it under the target fibre hole to be blocked. By approaching such a fibre to the tip, the glue can be placed on the hole to be blocked.

As shown on the Fig. 4.4 fibre holes as small as 4 μm can be blocked with a tip of comparable diameter using our setup. However in order to block fibre holes of smaller diameter we first use the inflation technique of Chapter 3 just to make a fibre section with holes large enough to see and block (Fig. 4.5).

When the glue is in place, it is cured using UV light, then pressure is applied as described in Chapter 3.

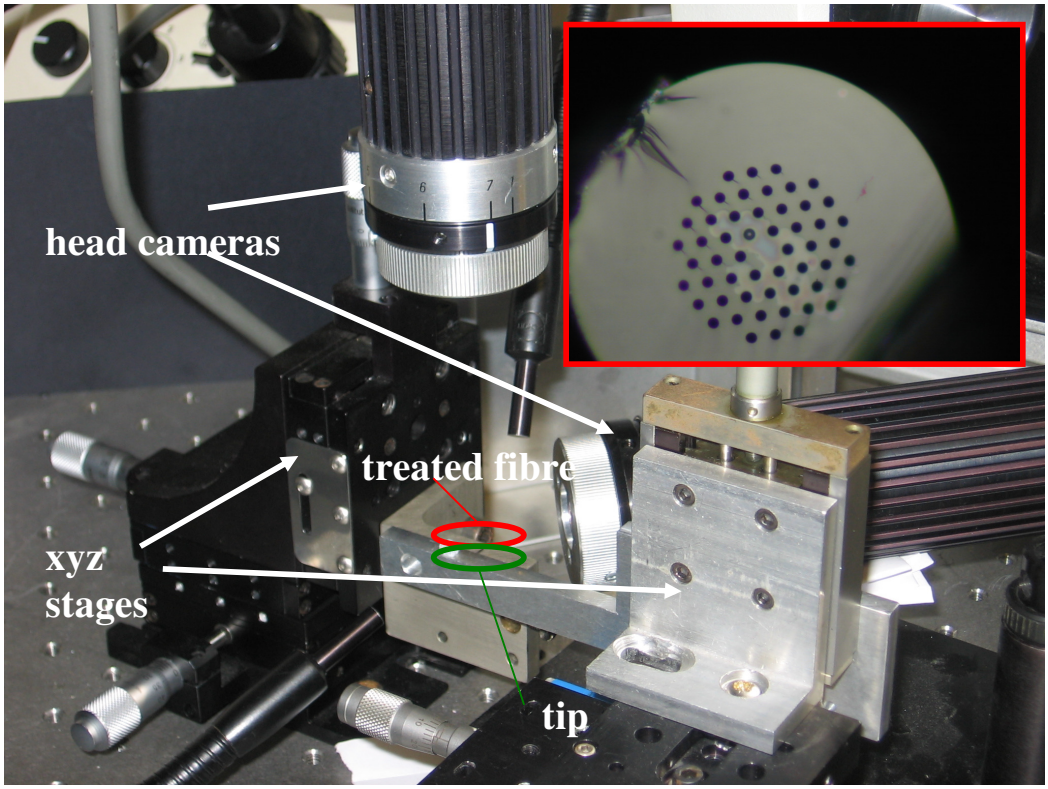

Fig. 4.3 Glue dispensing setup. The picture in the corner shows the cross-section of the fibre with one hole filled with the glue next to the core, at “11 o’clock”.

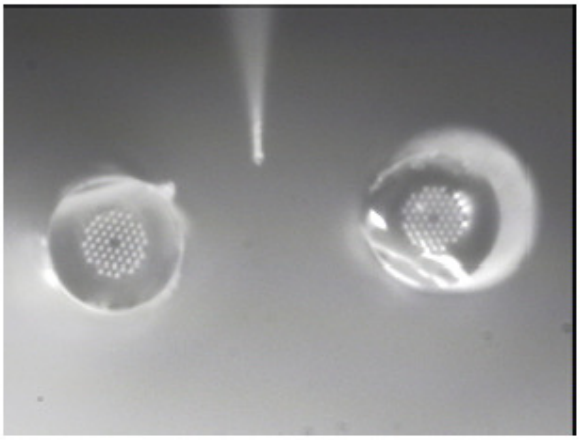

Fig. 4.4 Target fibre (left), the fibre storing glue (right) and movable tip (centre) under the microscope.

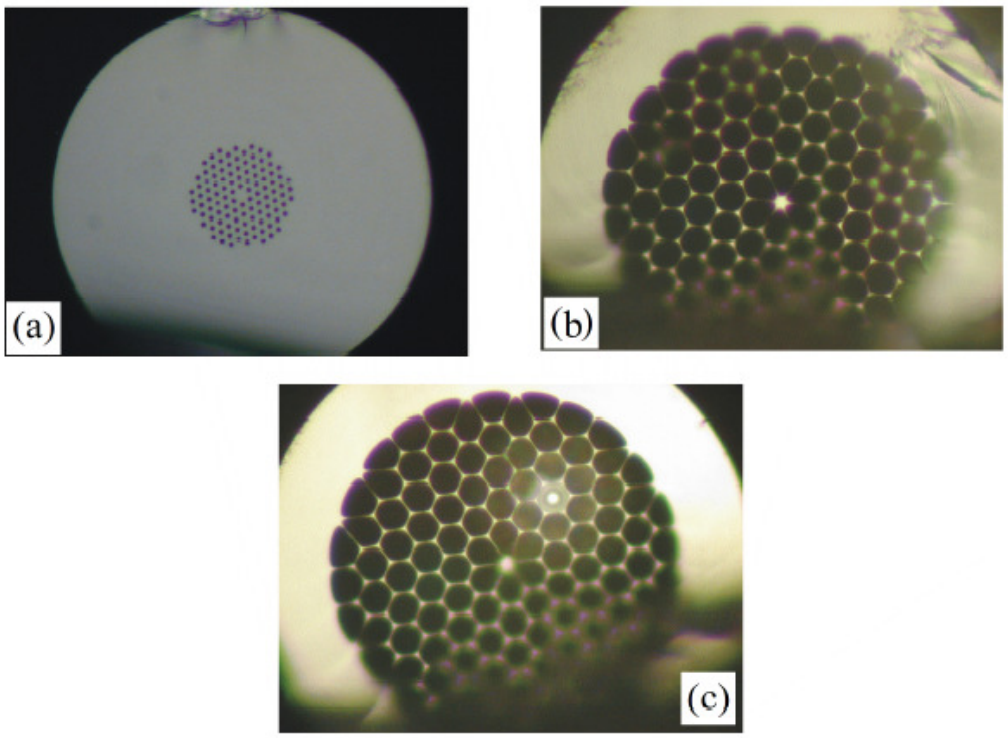

Fig. 4.5 Preinflation procedure in small-hole PCFs. (a) original fibre (b) inflated fibre cross-section (c) inflated fibre cross-section with one hole blocked.

It is important to allow enough time for the holes along the whole length of fibre in the experiment to reach equilibrium pressures. The flow of gas depends on the length and the diameter of the hole. Therefore pressurization can be time-consuming, especially for longer pieces of fibre. The same applies to the process the other way – depressurisation. For example some time (up to two hours) is needed before moving a pre-inflated fibre to the glueing stage. Otherwise, the glue can be pushed out and spill over in a neighbour hole.

4.3.3 Making fibre transitions

The method for plugging the holes has just been explained, but it is also important to explain how transitions to a different core size or shape or to a newly-introduced core are formed.

In order to form a gradual low-loss transition the hot-zone length is varied. As the burner progresses back and forward in an oscillatory way along a stretching fibre its

distance is shortened every time it changes direction, Fig. 4.6. The length of the waist is determined by the final distance travelled by the burner.

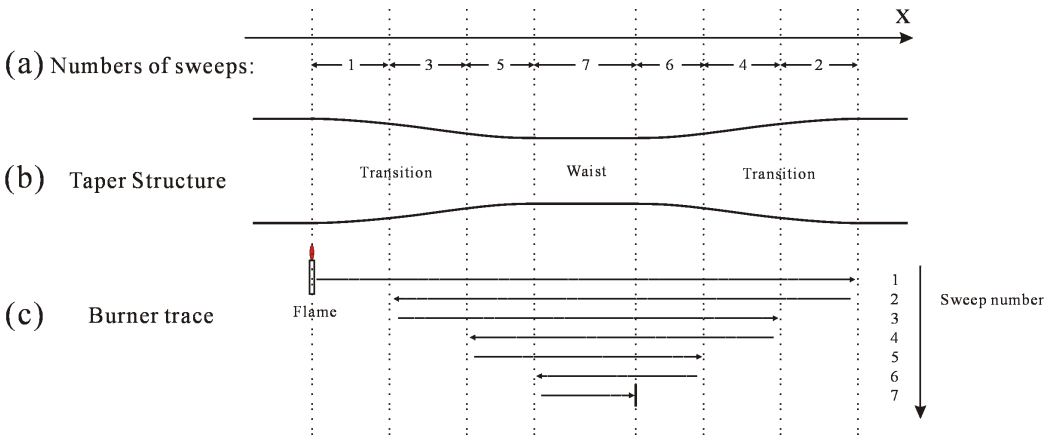

Fig. 4.6 Schematic diagram [Lai 06 b] of the movement of burner to form core shape transitions: (a) number of sweeps experienced by each section of fibre, (b) the fibre structure along the taper and (c) the motion of burner in practice.

This results in a gradually changed longitudinal fibre cross-section. If a single-core fibre is heat-treated in a such way, a gradual core transition is formed between the waist and the original fibre. If the hole inflation technique is applied and one hole is not pressurised one can expect a gradual hole collapse along the heated length. The hole collapses slightly every time is heated and finally collapses completely (in the waist) adding a new silica material cell.

Abrupt transitions are possible by increasing the hot zone length so that every time the burner changes direction it reaches to the previously-heated point of the fibre. As the fibre is being stretched the burner must go further and further every time.

4.4 Core shape change through hole blocking.

For our experiments we used an ESM PCF with a non-birefringent ~12 μm diameter core, as shown on inset picture (Fig. 4.3). It is commercially available and it is splice compatible with SMF-28 telecoms fibre. We used the hole blocking technique to create low-loss transitions to elliptical, rectangular and other-shaped cores.

4.4.1 Blocking one hole – elliptical core

Here we blocked one hole to give the core a pronounced elliptical shape and hence form-birefringence, which could be enhanced by tapering the core down in size.

Dry nitrogen at a pressure of 5.3 bar was supplied to the appropriate end of the fibre to pressurise all the holes except the one blocked with glue, which remained at atmospheric pressure. A section of the pressurised fibre was stripped of its coating and tapered down using an oxy-butane flame on our fibre tapering rig. The taper ratio was 4:1, meaning that the fibre's diameter would have reduced by this ratio if there had been no changes in relative hole sizes; ie the area of glass in the fibre's cross-section was reduced by 16:1. The transition loss of the fibre with one hole collapsed was measured by the cut-back technique to be <0.4 dB at 1550 nm wavelength.

The tapered waist was then cleaved, leaving a 3 cm transition between ~1 m of the original (input) fibre at one end and 9 cm of inflated-and-tapered (output) fibre at the other end.

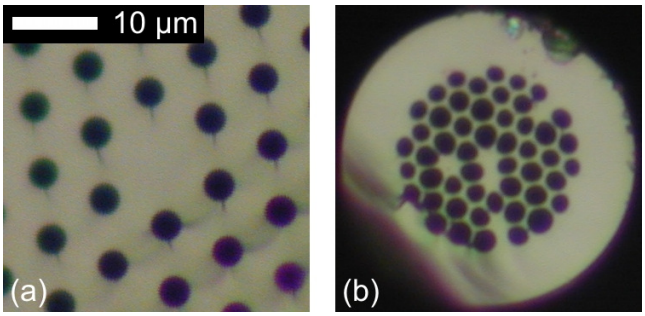

Fig. 4.7. The PCF (a) before and (b) after inflation and tapering with one hole blocked next to the core.

Fig. 4.7 is an optical micrograph of the cleaved waist, together with the original fibre to the same scale. The pressurised holes inflated as described in the preceding section, but the unpressurised hole collapsed completely instead. The "circular" core at the centre of the original fibre has reduced in size by the tapering and become "elliptical" by the addition of solid material from the collapse of the adjacent hole. The dimensions of the core are now roughly 4.6 × 2.1 µm, an aspect ratio exceeding 2:1. It can be seen that three other holes also collapsed, unintentionally, forming new cores in the fibre. However, they were well-enough isolated to have no observable effect on propagation in the central core. The holes were probably blocked by water

condensation on the fibre endface (a particularly humid day in a lab without air conditioning).

To characterise the birefringence of the output fibre, polarisation beating with wavelength was recorded by launching polarised light from a broadband source into the input fibre, and passing the output light to an optical spectrum analyser via a polariser at 45º to the optical axes of the fibre. Fig. 4.8 is the output spectrum.

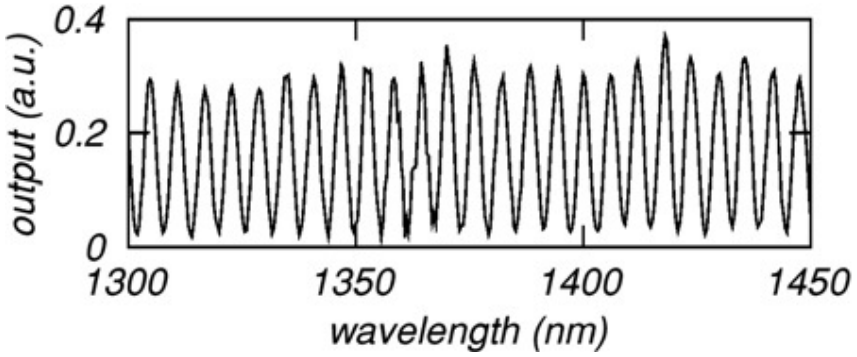

Fig. 4.8 Measured polarisation beating.

The spectral beat period $\Delta\lambda$ is related to the beatlength L_B and the fibre length L by [Ortigosa-Blanch 00]

$$L_B = \frac{\Delta\lambda}{\lambda} L \left[\frac{\lambda}{L_B} \frac{dL_B}{d\lambda} \right] \tag{4.1}$$

The factor in brackets is of order unity, so since the output fibre is 9 cm long and $\Delta\lambda$ = 5.95 nm from Fig. 4.8, the equation gives an estimate for the beatlength of ~390 μm. This compares well with the value of 280 μm calculated for a 4.6 × 2.1 μm rectangular silica core in air [Snyder 86]. (This value is highly sensitive to the dimensions, which can be only imperfectly known from our optical micrograph.) Repeating the measurement with the input fibre alone confirmed that it did not contribute significantly to the birefringence.

The simple periodic form of Fig. 4.8 indicates that the output is in a single mode regime. If more than one mode had been excited to a significant extent, their different birefringences would have resulted in a more complicated beating spectrum.

Fig. 4.9 (a) is a near-field image of the output for 1430 nm light at the input. Only the central core was lit up, no light being evident in parasitic cores. The near-field

pattern, and the simple symmetrical centrally-peaked far-field pattern we observed for red light (not shown), indicate that the light was in the fundamental mode even though the core was almost certainly multimode.

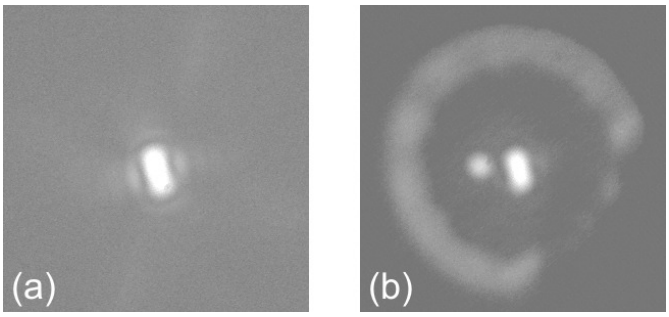

Fig. 4.9 Near-field images at the output (a) with the input fibre present and (b) with the input fibre removed so that cladding features are illuminated.

4.4.2 Blocking more than one hole – rectangular core

It is not straightforward to block a given hole in the fibre endface, and even harder to block four. However, using this technique, four holes in the same line were blocked with glue to produce a core with an even greater aspect ratio. Fig. 4.10 (a) shows the endface of the fibre with glue in defined holes.

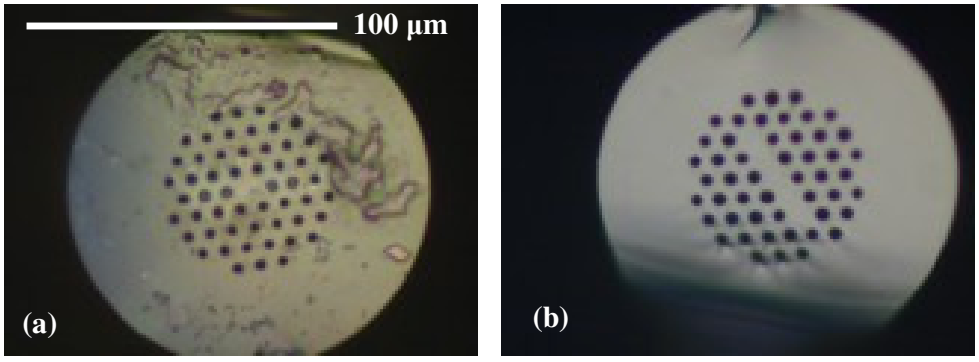

Fig. 4.10 The PCF (a) before and (b) after inflation. The four glued holes are in a nearly-horizontal line in (a).

The fibre was pressurised at 3 bar and tapered down. Four unpressurised holes situated at the same line as the core collapsed during processing due to the surface

tension. It is important to control how much the holes are inflated. On one hand, if the holes are too small then light can leak into the solid outer cladding past the holes at the ends of the core. On the other hand, if the holes are too big then those along the sides of the core impose a corrugated edge to the core that disrupts the mode pattern, Fig 4.11.

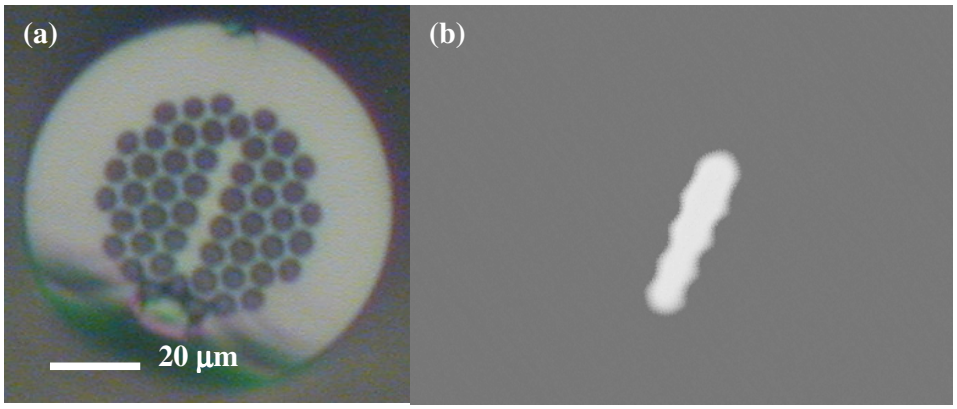

Fig 4.11 Optical micrographs of (a) processed fibre with a corrugated edge (b) mode shape of this fibre (near-field).

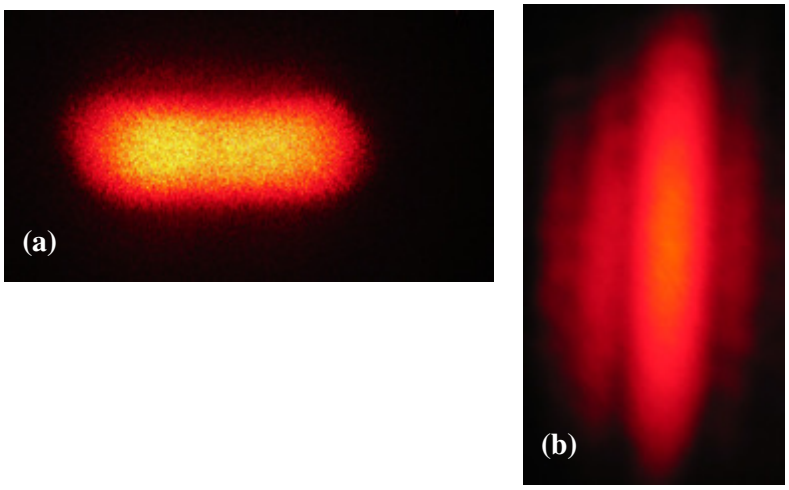

Fig. 4.12 Optical micrographs of (a) near and (b) far field spectrum of the output waist for He-Ne laser.

The dimensions of the tapered inflated waist core were now roughly 5 × 1 µm. The transitions of the fibre with 4 holes collapsed were 60 mm long and the insertion loss was only 0.2 dB at 1550 nm wavelength, corresponding to 0.1 dB per transition.

Red light from a He-Ne laser was coupled to around 70 cm of untreated fibre followed by 50 mm long transition to the inflated waist fibre of Fig. 4.11. Fig. 4.12 presents near and far-field images of the fibre output. The near field pattern is strongly elongated with intensity concentrated in the central core section. In the far-field distribution the central intensity is accompanied by some diffraction fringes.

Two further experiments demonstrated by our colleague Ke Lai showed the versatility of hole blocking. Five holes were plugged so that they and the core formed a ring with an open hole in the middle. Inflation gave low-loss transitions (0.25 dB each at 1550 nm) to an annular core (Fig 4.13 (a)) and hence a ring shaped mode (Fig. 4.13 (b)). A simple beam expander (0.2 dB loss at 1550 nm) was formed by inflation after the six holes around the core had been plugged (Fig. 4.13 (c)).

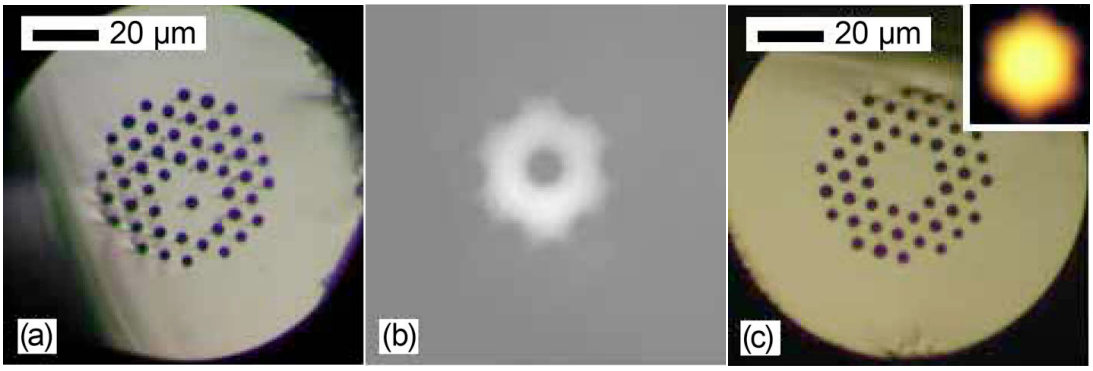

Fig. 4.13 (a) Micrograph of fibre A after inflation to give an annular core. (b) Output near-field image at 1000 nm. (c) fibre A after inflation to give an expanded core, with (inset) to give a near-field image for visible light, not to scale

4.5 Coupling from diode lasers

In the previous sections ESM fibre transitions to rectangular cores were demonstrated using two alternative differential pressurization techniques. Such transitions can provide low-loss coupling of light between fibres and diode lasers or integrated optic waveguides with noncircular modes. To demonstrate improved coupling from a diode laser, we inflated and tapered the ESM fiber to give a 3:1 rectangular core (by plugging two holes) and an outer diameter of 60 µm. The aspect ratio roughly matched the ratio of divergence angles specified for a diode laser (Fig. 4.14).

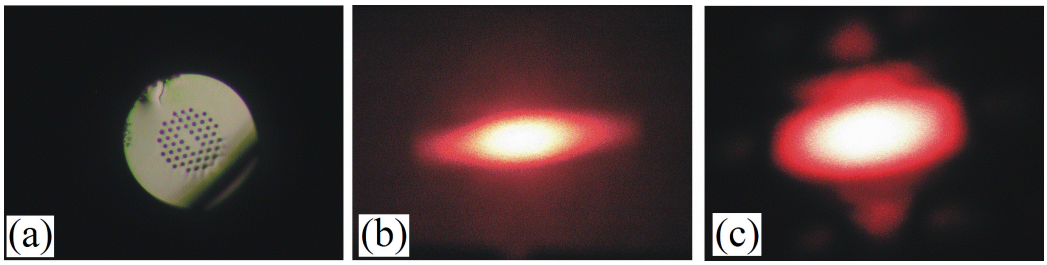

Fig. 4.14 (a) Optical micrograph of fibre with a core aspect ratio 3:1. Far-field images of the output at 658 nm from the laser diode (b) and the rectangular fibre core(c).

The laser's visible output (658 nm) simplified alignement but raised the transition loss to 0.9 dB; the light must spread out further in the transition relative to its wavelength, making adiabaticity harder to achieve.

Light was coupled from the laser to the rectangular core using a spherical coupling lens, then to the circular core via the transition. We could couple 12.5 mW of the 22.4 mW laser output (measured before the lens) through to the circular core, hence a coupling efficiency of 56%. This compared with 42 % for a conventional fibre (single-mode at 658 nm) after similarly optimizing the alignment. Our transition improved coupling despite the relatively high loss of the transition; without that loss, the efficiency would have been ~ 70%, which we would expect to approach for longer wavelengths. By further tapering (and with enough inflation to suppress leakage loss) butting the fibre against the diode laser emitter should be sufficient without the need for a lens at all.

The other device with the rectangular core (Fig. 4.1) was used in the experiment with laser diode coupling. The elongated shape of the mode at the output of the device is shown in Fig. 4.1 (c). Although its shape corresponds to the diode laser mode (Fig. 4.14 (b)), it did not yield better coupling efficiency than 36%. The use of a specially designed PM fibre would be a solution to consider for better coupling results especially where state of polarisation matters.

4.6 Introducing a secondary core into the fibre

Multiple-core fibres open up new opportunities for exploiting the interaction of light between the cores. They are often proposed for sensing applications [Vallee 94, Blanchard 00, MacPherson 01, MacPherson 03], and wavelength-dependent coupling

to the neighbouring secondary waveguide has applications in spectral filtering [Safaai-Jazi 91, Saitoh 05]. Extra defects/cores can be introduced into a PCF during the fibre fabrication process. Very often only a short piece of a specially designed fibre is needed to get a desired interaction of light between the cores. For these reasons the hole inflation technique is very helpful.

Below I present an experiment based on 2-core PCFs. The second core was introduced using the adapted hole inflation technique. The appearance of the second core can be abrupt or gradual, which affects the behaviour of the device. I demonstrate results for gradual transitions.

4.6.1 Secondary core

PCFs can be used as bend sensors to monitor the deformation of a structure. In an early paper [Blanchard 00] a three-core PCF was designed so that there was no significant coupling between the single-mode cores. Bending of the fibre introduces a relative optical phase difference between light propagating in the cores which can be measured interferometrically.

Here I demonstrate a similar approach but with a two-core fibre section made by the hole inflation technique. The cores are connected to ESM PCF outputs through adiabatic fibre transitions. Single-mode outputs have the advantage (compared to the fibre assembly examined in the report mentioned above) of allowing a simpler interrogation system. Only the transmitted power needs to be detected in place of the complex analysis of a spatial interference pattern.

4.6.2 Principle of operation of the device.

Introducing a second core beside the initial core in a gradual and adiabatic way (with a long fibre transition) will cause the fundamental core mode of the single-core fibre to evolve into the fundamental (even) supermode of the 2-core fibre section, as explained in Section 2.2.1 of Chapter 2. The reverse mode evolution is expected in the output transition (Fig. 4.15). Light present in both cores should be in phase. Fig. 4.15

shows the schematic configuration of proposed PCF device for bend sensing applications.

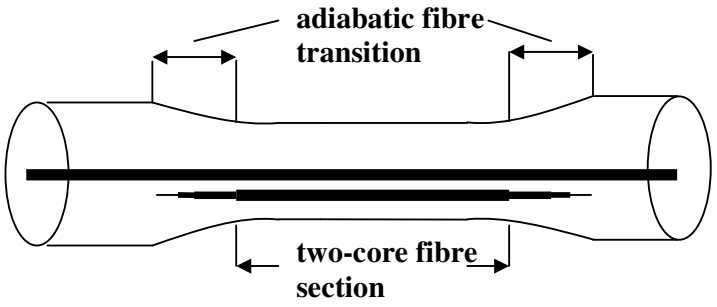

Fig. 4.15 Schematic configuration of the two-core fibre device.

When the two-core fibre section is deformed, a differential strain is introduced between the cores in the plane of deformation. That, in turn, introduces a relative optical phase which couples light into the odd mode, which is not transmitted to the single-mode output core. The optical phase difference $\Delta\phi$ between light propagating in the cores depends on the angle of bend (Ψ) [Blanchard 00]:

$$\Delta\phi = 1.14\frac{2\pi\delta}{\lambda}\psi \tag{4.2}$$

where δ is the distance between the cores and λ is the wavelength. The reduced transmission allows us to monitor the bend.

4.6.3 Transitions made from stock ESM PCF

Standard ESM PCF (Fig. 4.16 (a)) was used in which a second core was introduced by hole blocking technique. First, the fibre with one hole blocked at the endface was pressurised at 5 bar and then tapered with a gradual transition (see Fig. 4.6) resulting in 2-core waist with the configuration shown in Fig. 4.16 (b). The insertion loss was 0.4 dB for the whole device.

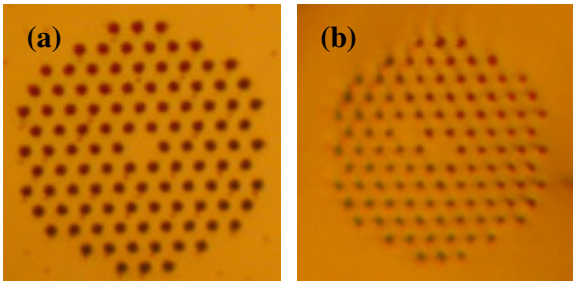

Fig. 4.16 Optical micrographs (to the same scale) of the holey part of the (a) initial 5 um-core ESM PCF, (b) 115-um tapered ESM PCF with introduced core.

The transmission spectrum was measured and no spectral beating was observed (Fig. 4.17) which suggests that the transition is adiabatic. Then the fibre waist was cleaved in order to look at the mode pattern. Fig. 4.18 presents the near and far-field mode patterns of the device for different wavelengths. They show that the power distribution in the cores is not equal, even though it improves for longer wavelengths. Reducing the size and the distance between two cores through tapering (which would increase C in Eq.1.7 and also increase F^2) improved the result, but still did not provide equal illumination of the cores.

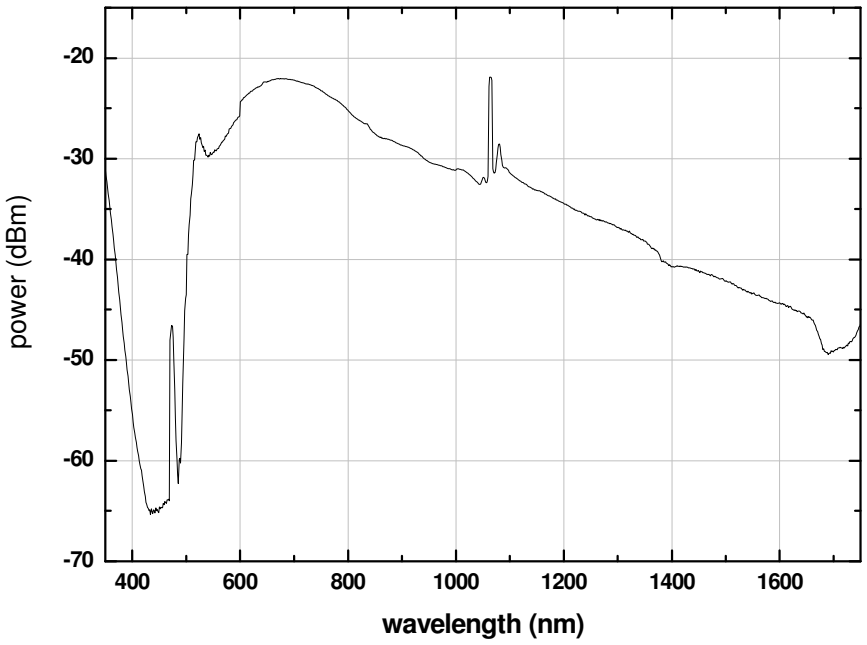

Fig. 4.17 Spectral transmission at the output of the two-core fibre section (two transitions present).

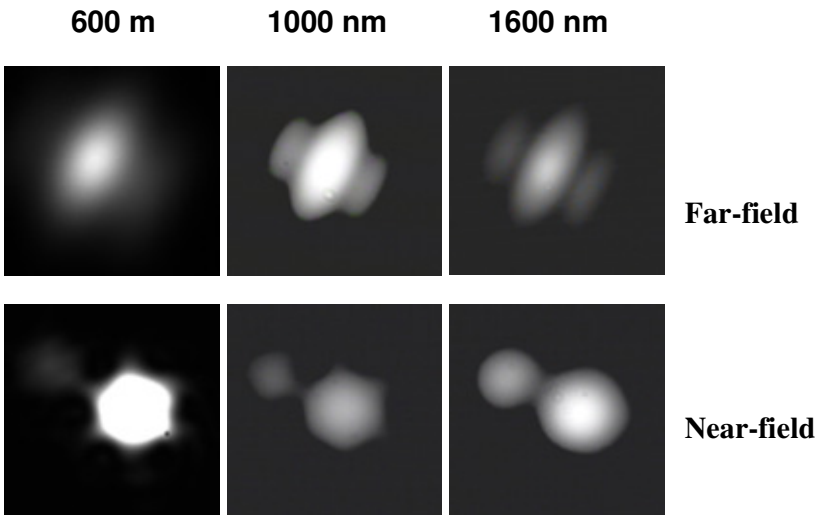

Fig. 4.18 Near and far-field mode patterns at the two-core waist for 600 nm, 1000 nm and 1600 nm wavelength transmission.

This result can be explained by considering how the fibre was made. The preform of the stock fibre contained a rod in the centre which after drawing to fibre becomes the original core. The amount of silica in the rod differs from the amount of silica in each capillary that gives the holes in the fibre. Therefore, when we collapse one hole, the core that is created will be smaller than the original core. This makes the directional coupler asymmetric (Section 1.1.5).

If this asymmetry is the cause of unequal illumination, we need a new fibre which could provide two equal cores.

4.6.4 Transitions made from special ESM PCF.

To achieve symmetric cores, a special ESM PCF was designed and fabricated. This fibre's original core was introduced in the fibre drawing process in the same way that the secondary core was introduced by hole collapse later on the taper rig. The fibre was drawn from a preform composed only from capillaries (with no rod) during its fabrication process. When the cane (Fig. 4.19 a) was drawn to the fibre, the central hole was collapsed to yield a single core (Fig. 4.19 b). Thus when a cladding hole is collapsed to form a secondary core, it will be the same size as the original core.

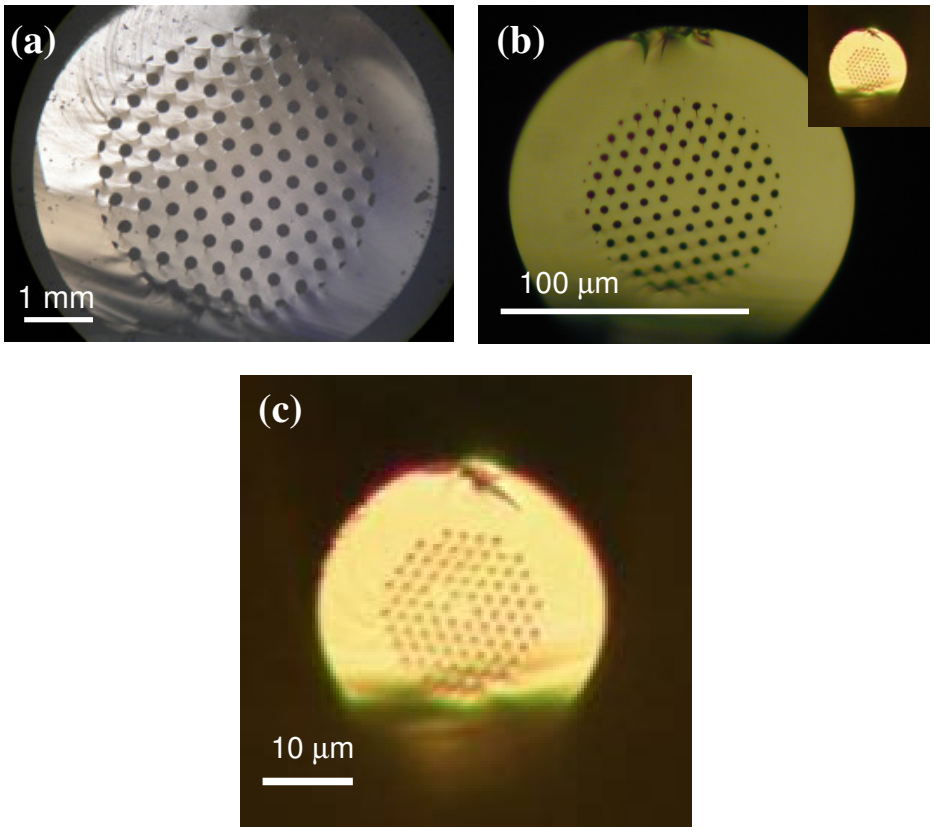

Fig 4.19. (a) Cross-section of a 4.75 mm diameter preform with no core rod, (b) drawn ESM PCF endface of 125 µm diameter, (inset) 31 µm diameter two-core fibre section to the same scale, and (c) enlarged inset in (b).

Following the procedure used to make a two-core section as before (first introducing the core then tapering) did not yield the expected result as some spectral beating was observed. Our explanation is that the transition length into and out of the two-core fibre section is not long enough to be adiabatic.

Tapering before adding the second core allows more gradual transitions. We replaced the glass burner with the standard metallic burner. Because this has a much colder flame than the glass burner, it is more suitable for producing long transitions in hole size providing the starting diameter is small enough. Secondly, the smaller the core, the easier it is to make transition adiabatic. Therefore we first tapered the fibre from 125 µm to 80-µm diameter then introduced the core along the tapered section, then tapered this down again with a taper ratio of around two.

The insertion loss of the resulting device was large at around 3 dB for 1550 nm. However this time no spectral beating at the output was observed for wavelengths

longer than 1200 nm (Fig. 4.20). (We believe that the significant coupling for shorter wavelengths is due to the multimode regime of the imperfect ESM fibre). Cleaving the waist shows that the light is present in both cores and more importantly the power distribution for a wide range of wavelengths (650-1550 nm) appears to be equal (Fig. 4.21). Therefore our device behaves in the expected way for longer wavelengths as the intensity in both cores is almost equal with no light interaction (Fig. 4.20), and we excite here only the fundamental supermode in the waist. The desired even supermode generator has therefore been demonstrated.

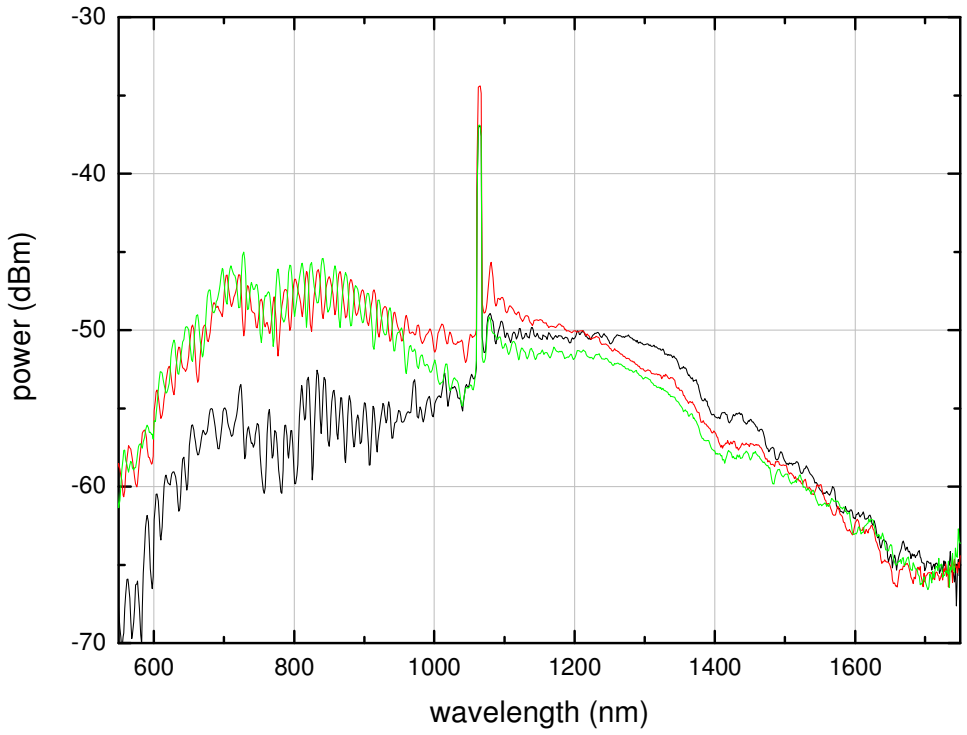

Fig. 4.20 Spectral transmission received at the output of the two-core fibre section with two transitions (black line), and in the waist from the original core (red line) or introduced core (green line).

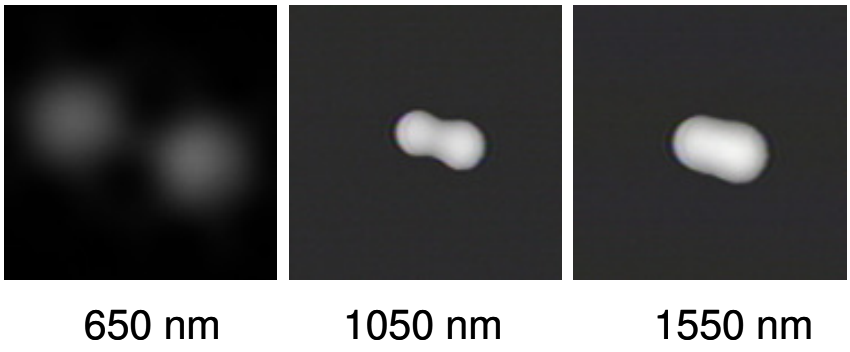

Fig. 4.21 Near-field mode patterns recorded at the output of the two-core fibre section.

It is also possible to introduce a second core while keeping the transition length close to zero. An abrupt transition ensures the coupling of the fundamental mode to both even and odd fundamental modes of the 2-core waveguide, as explained in the Section 1.1.5. The interaction of light between two equal cores would lead to sinusoidal spectral beating. Different lengths of such a two-core section would allow modulation of the spectrum in order to get a bandpass filter as proposed by [Okamoto 86], but without any splices between two-core fibres.

4.7 Conclusions

In this Chapter two alternative differential pressurisation methods have been described. These methods were used to change the core shape in widely-available stock ESM PCFs on a cm-scale.

An elongated core shape (and mode shape) was achieved through the pressure-like effect of surface tension. Other changes in core shape were provided via the hole blocking technique. For example a low-loss taper transition in a PCF was demonstrated by collapsing one hole, where the core shape change from "circular" (6-fold rotational symmetry) and non-birefringent to "elliptical" (2-fold rotation symmetry) with an aspect ratio exceeding 2:1. A very short birefringence beat length of about half a millimetre was measured. As well as showing how strong variations in birefringence can be achieved, our result is also a demonstration of a general new technique with a much wider applicability. More radical changes of core shape were described where 4 holes were blocked resulting in a rectangular core with aspect ratio 5:1. This is the first

time that such a transition in core shape has been reported in PCFs. Improved laser diode coupling exceeding 50 % using such fibre transitions for mode matching has been demonstrated.

Then, using our powerful hole blocking technique a separate core was introduced beside the original core. Two-core fibre section with adiabatic transitions was demonstrated using a specially-designed ESM PCF. In the device only the even supermode was excited.

Many cores of different configurations and shapes can be implemented in a PCF using the hole blocking technique. In the next Chapter this technique will be used to produce new devices and demonstrate striking effects related to mode conversion.

Chapter 5 Mode convertor in PCF

In Chapter 4 we demonstrated the potential of the hole blocking technique. Changing of the core shape and introduction of a secondary core into a fibre structure were reported. However the diversity of cores configurations offered by hole blocking technique can be explored further to provide other interesting new devices. Introducing a secondary core into the structure in an appropriate way can affect the guided mode of the entire structure. Like the null coupler [Birks 95], described in Sections 1.1.5 and 2.2.2, such a structure can act as a mode convertor. The symmetry of the device determines the output mode [Snyder 83].

In this Chapter I report a low-loss PCF mode convertor from the fundamental LP_{01} mode to the TE_{01} & HE_{21} modes in the second-order LP_{11} set of modes.

5.1 Motivation

Mode convertors couple light from one fibre mode to another. They have applications in dispersion compensation [Poole 92, Ramachandran 05], nonlinear optics [Hu 06] and atom guiding [Zhan 03] for example. Here we demonstrate coupling from the fundamental LP_{01} mode to the circularly symmetric TE_{01} mode, which has applications for atom guidance.

The mode convertor in some dispersion compensators and other fibre devices is usually a long-period grating with a period matching the beat length between the modes. This means that the strength of the grating must be closely controlled to give complete coupling between the modes. If the grating is even slightly too strong or too weak the modes will be over- or undercoupled, increasing the residual power in the input mode and reducing the extinction ratio. The grating is also a resonant device, giving complete conversion only over a band of wavelengths. This can make the extinction ratio and the operating wavelength sensitive to its environment.

Mode conversion relying on adiabatic propagation rather than resonant coupling has many adventages over the approach presented above. Its extinction ratio is

determined only by the adiabaticity of the transition. Such a mode convertor should be effective at all wavelengths, and very stable environmentally.

An LP_{02} mode convertor of this type was made by my colleague Ke Lai [Lai 06 a] using the hole blocking technique I developed. Here I describe a TE_{01} mode convertor I made using the same technique. This device lacked the symmetry that prevented coupling to the TE_{01} mode in the previous device.

5.2 Construction and explanation

Here we describe a device that can generate modes in the LP_{11} set from an input in the fundamental mode. Understanding its operation relies on the order of modes in multimode fibres (discussed in Chapter 1 and summarised here in Fig. 5.1) and the fact that, symmetry permitting, light stays in a mode of a given order along a waveguide transition that is gradual enough to be adiabatic.

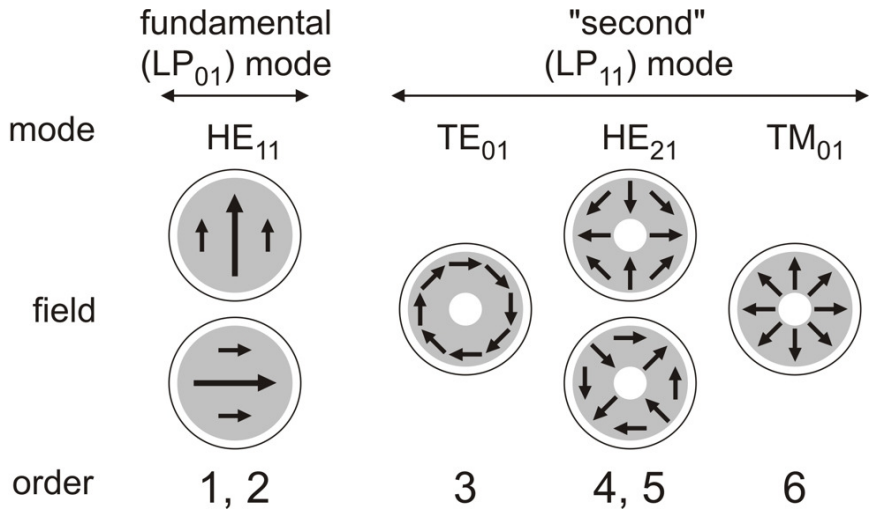

Fig. 5.1 Schematic diagram showing the electric field directions of the six lowest-order polarisation modes of a circular multimode fibre core. (The patterns are similar for a hexagonal core, but the LP_{11} patterns are sensitive to elliptical deformations.) The propagation constant decreases and the mode order increases from left to right. The HE modes are degenerate pairs.

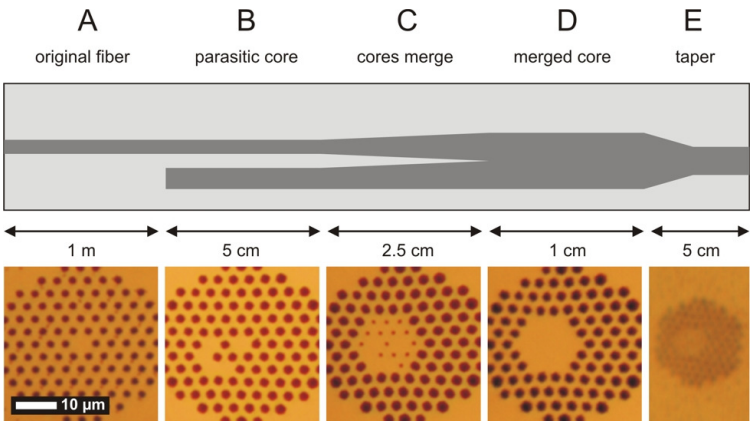

Fig. 5.2 (upper) Schematic longitudinal cross-section of the PCF mode convertor, showing core areas in dark grey. (lower) Optical micrographs of the holey region in the cleaved fibre in each of sections A-E, to the same scale.

The mode convertor resembles the LP_{02} device [Lai 06 a], in which a large parasitic core was formed symmetrically around the original central core of a single-mode PCF. However, in the present case the parasitic core is formed asymmetrically, to one side of the original core, so that the output is in the next mode of any symmetry (ie, LP_{11}) rather than the next symmetric mode (ie, LP_{02}) [Birks 95].

The device was made in three stages and cross-sections along the final structure are shown in Fig 5.2. In the first stage, four holes were plugged with glue at one end of the fibre (section A) before that end of the fibre was pressurised and a section half-way along the fibre was heated on the taper rig. The plugged (and therefore unpressurised) holes collapsed where heated to locally form the arc-shaped parasitic core of section B. In the second stage, 14 holes were plugged and the fibre pressurised and heated again to yield the single merged hexagonally-symmetric core of section D. The heating time was varied so that the holes collapsed gradually (and hence adiabatically) along the transitional section C between B and D, the image in the figure being roughly at the midpoint of the transition. In the third stage, part of section D was heated and stretched to halve its width and form section E. Finally the structure was cleaved in section E to yield two separate devices.

The waist can support several modes, including those of Fig. 5.1, but only four of them can be excited via the cores of section B. This is because the cores support four polarisation modes in total (two polarisations of LP_{01} in each core). These evolve

adiabatically into the four lowest-order polarisation modes of the waist. However, the 4th and 5th modes in the waist are the two degenerate HE_{21} modes (Fig. 5.1).

Light enters in the fundamental mode of the original core in section A. The light stays there in section B because the transition between A and B is abrupt. However the parasitic core, being larger, now supports the fundamental mode of the two-core system analogously to the structure of LP_{02} mode convertor. The light in section B must therefore be in the second mode of the system. If the transition via section C is gradual enough to be adiabatic, the light must remain in the second mode and so ends up in the LP_{11} mode of the merged core in section D. The reduction in size to section E makes it easier to access the individual TE_{01} and HE_{21} components of the LP_{11} set, the distribution of power between these components depending on the input polarisation [Birks 95].

5.3 Results

The lengths of sections A, B, C and D in the final device were roughly 1 m, 50 mm, 25 mm and 10 mm respectively, and the transition to section E was 24 mm long. (Uniform sections like A could of course be arbitrarily short.) A very low loss of just 0.3 dB at 1550 nm wavelength was measured from the input in section A to the output in section E by the cut-back technique, with index-matching gel applied to strip away any light in cladding modes. As shown in Fig. 5.3 (a) the far-field intensity pattern at the output of the device always had a null on the axis for various wavelengths (from 1000 to 1500 nm) and input polarisations, and as the input and output fibres were moved, indicating the absence of light in the fundamental LP_{01} mode. We measured an extinction ratio of 20 dB from the intensity profile (Fig. 5.3 (b)) of the farfield pattern, this value being limited by the dynamic range of the measurement.

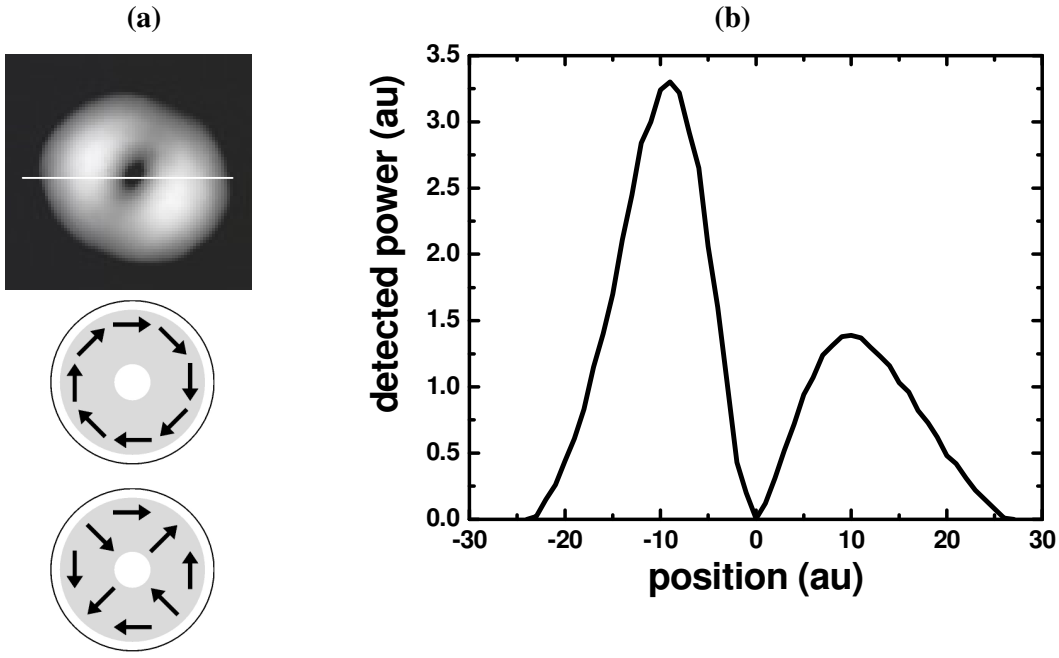

Fig. 5.3 (a) Measured output far-field pattern and schematic TE_{01} & HE_{21} modes showing electric vector orientation. (b) Intensity distribution along the line shown across the far-field pattern in (a).

Fig. 5.4 (a) is an image of the far-field after adjusting the input polarisation to obtain the ring-shaped pattern expected for a pure TE_{01} or HE_{21} mode. Which of these two modes is present can be determined by placing a polariser at the output. As can be seen by inspecting the electric field vector directions in Fig. 5.3 (a), this passes a two-lobed "LP_{11} - like" intensity pattern in both cases. If the polariser is rotated, the lobes of the transmitted pattern also rotate. However, for a TE_{01} mode the lobes rotate in the same direction as the polariser, whereas for an HE_{21} mode the lobes rotate in the opposite direction [Birks 95]. As shown in Fig. 5.4 (b), in this case the transmitted patterns rotated in the same direction as the polariser, indicating the TE_{01} mode. For the orthogonal input polarisation the rotation was in the opposite direction (not shown) as expected for the HE_{21} mode. The device can therefore be used for the efficient excitation of the TE_{01} or HE_{21} members of the LP_{11} mode set, and hence an azimuthally-polarised free-space beam.

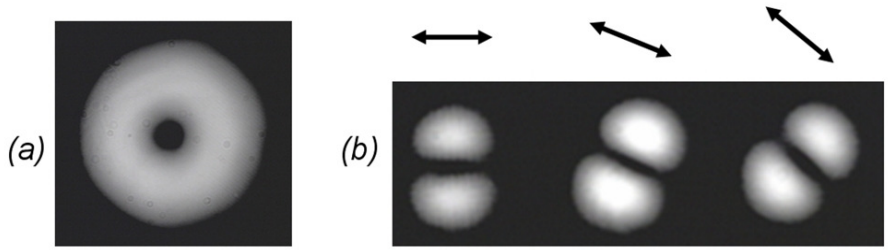

Fig. 5.4 (a) Measured output far-field pattern of the PCF mode convertor at 1500 nm. (b) (to a different scale) Far-field patterns after passing the light through a polariser oriented to transmit electric field along the arrows shown above.

5.4 Conclusions

A TE_{01} fibre mode convertor has been demonstrated. The method is based on controlled hole collapse in a PCF, and can be generalised to other modes by collapsing different patterns of holes with different symmetries or adjusting the size of the parasitic core to turn the mode of the original core into a third or even higher-order mode of the two-core system. By optical reciprocity, such devices should also work in reverse. They may be proposed for dispersion compensation but can be also used to explore the nonlinear propagation of pure higher-order modes in PCFs [Birks 01].

Chapter 6 Mode convertor in SMF

In the previous Chapter a PCF-based second-order mode convertor was described. The hole blocking technique was used to introduce a second core into the structure, enabling the mode conversion.

In this Chapter I describe a second-order mode convertor in which, in contrast, no special fibers are used. This all-fibre device converts light from the fundamental mode to the second-order set of modes in SMF, without using PCFs. It is a twisted fused coupler made from few-moded SMF fibres.

6.1 Principle of operation

Our device is based on the null-coupler polariser described in Section 2.2.2 of Chapter 2, which is an adiabatic fused coupler with a circular waist cross-section made from dissimilar standard fibres. Like the device of the previous Chapter the waist of the coupler supports several modes but only the 4 lowest-order polarisation modes can be excited via the input fibres. Light entering the coupler in the fundamental mode of one input fibre passes through the multimode waist and evolves into the fundamental mode at the output of the same fibre. However, the 4^{th} and 5^{th} modes in the waist are the two degenerate HE_{21} modes (Fig. 5.1). A 45° twist of the coupler couples light directly from one to the other, for which there are no more core modes available in the output fibres. One polarisation state of the smaller input fibre is therefore lost. The principle is summarised in Fig. 5.1 of Chapter 5.

In contrast, here the mode convertor is a similar twisted null coupler but operated at a short-enough wavelength that the fibres are multimode, so there are more guided core modes available in the output fibre. Light coupled by a 45° twist into the "spare" HE_{21} mode in the waist now has somewhere to go: it evolves into the lowest-order LP_{11} mode of the two fibres, namely the TE_{01} mode of the larger fibre, if the coupler really is adiabatic. Suitably-polarised light entering the smaller input fibre should therefore emerge in this mode. The twist response should clearly be periodic with a period of

90°, a further 45° twist returning the light to the original HE_{21} mode in the waist and hence to the smaller fibre at the output.

6.2 Fabrication and results

We made our null coupler from Corning SMF-28, a standard telecoms fibre that is single-mode at a wavelength of 1550 nm. However, we carried out our experiments at 633 nm, where the fibre is few-moded. 40 mm of one of two lengths of this fibre was pre-tapered to reduce its outer diameter from 125 μm to 90 μm, before a coupler with a waist of length 30 mm and diameter 1.78 μm was formed from the pair of now-dissimilar fibres. Fig. 6.1 shows an SEM image of the circularly-formed waist of a coupler made identically to the one whose characteristics are described below.

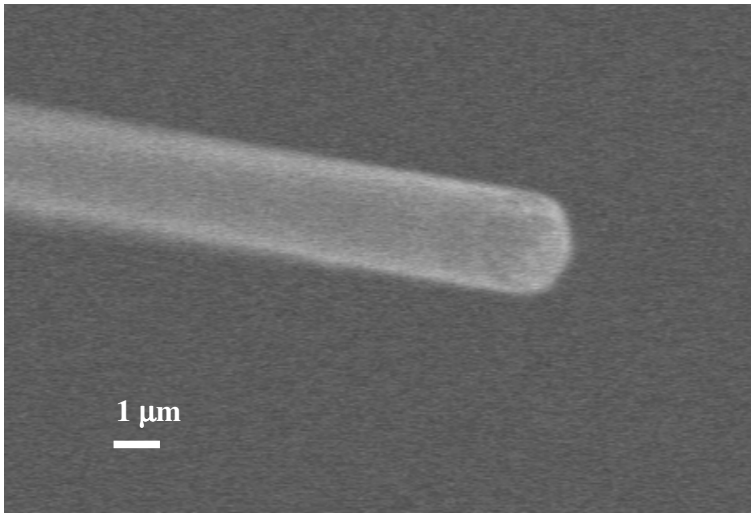

Fig. 6.1 SEM of the cleaved circularly-formed coupler waist.

The excess loss of the coupler as made was 1.9 dB and the splitting ratio between the pre-tapered and un-pretapered fibres was 3 %, ie it was a reasonable (if lossy) null coupler. To ensure that light entered the device in only the fundamental mode, we tapered 40 mm of the input fibre to a diameter of 30 μm and surrounded it in index-matching gel. This made the fibre locally single-mode at 633 nm and acted as a filter for higher-order modes.

633 nm light was passed through a polariser and half-wave plate and launched into the pre-tapered fibre via the mode filter. We could identify the right input polarisation for mode conversion by adjusting the polarisation until twisting the coupler had minimum effect on transmission (polarisation #1) and then rotating the wave plate to select the orthogonal polarisation #2. Twisting of the coupler had a dramatic effect for this polarisation.

Output powers measured in the two output fibres are plotted against twist angle in Fig. 6.2, together with far-field images of the light emerging from the two output fibres for two extreme cases. For a twist angle of 45°, over 80 % of the output light was transferred to the un-pretapered fibre and emerged in a ring-shaped intensity pattern with a central minimum.

This pattern behaved as expected for a TE_{01} mode when a polariser was placed at the output and rotated, Fig. 6.3. A further 45° rotation returned the light to the pre-tapered output fibre. This behaviour is just as expected from the discussion above.

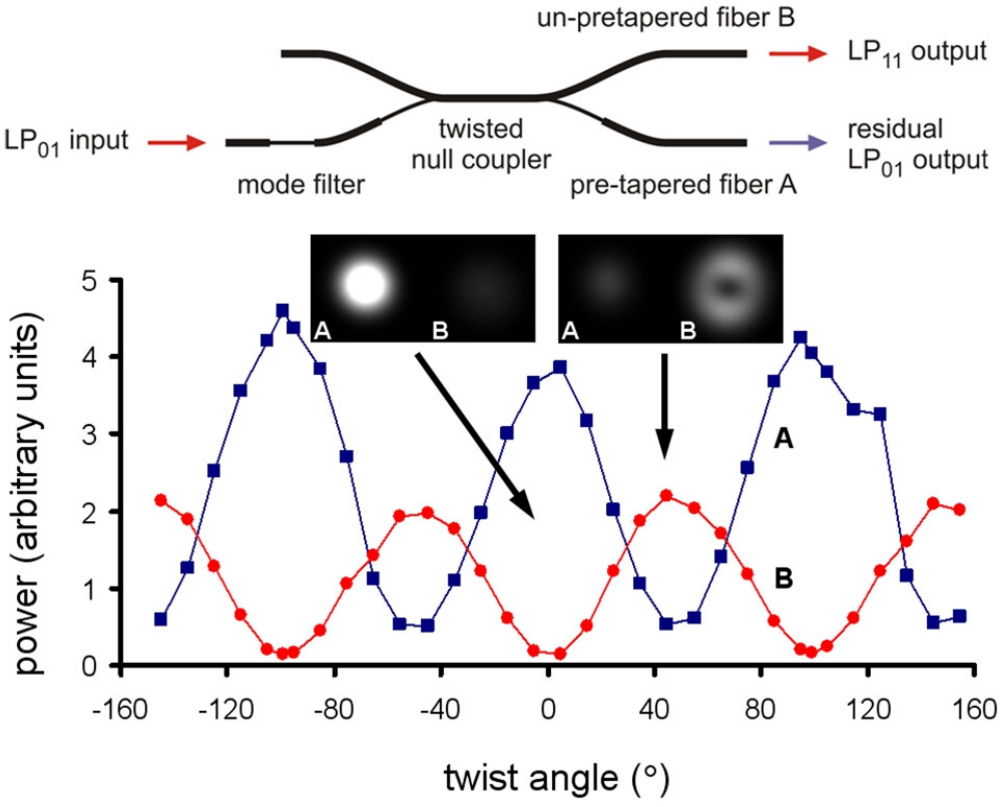

Fig. 6.2 (upper) Schematic diagram of a null coupler mode convertor. (lower) Powers in the pre-tapered (A) and un-pretapered (B) output fibres of such a device at 633 nm versus twist angle, for input light in the pre-tapered fibre with its polarisation adjusted to maximise the twist dependence. The insets show far field images from the two fibres for the twist angles indicated.

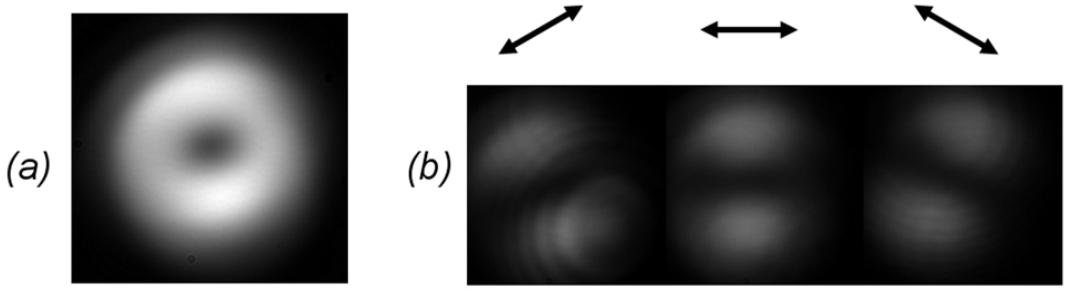

Fig. 6.3 (a) Measured output far-field pattern of a null coupler mode convertor at 633 nm. (b) (to a different scale) Far-field patterns after passing the light through a polariser oriented to transmit electric field along the arrows shown above.

The loss characteristics of the device were unexpected. The 1.9 dB loss of the coupler as fabricated is far from typical of our tapering rig, and similar null couplers were made with losses as low as 0.3 dB at the same wavelength when untwisted. However as can be seen in Fig. 6.2 an additional ~1.5 dB of light was (reversibly) lost when the coupler was twisted by 45°, and other similar devices suffered similar losses on twisting. In all cases the additional loss was correlated to TE_{01} light emerging from the un-pretapered fibre and, as in Fig. 6.2, the light was recovered when the couplers were further twisted to return the light to the pre-tapered fibre. Furthermore there was no additional loss with the other polarisation (#1) for which twisting does not couple light to the un-pretapered fibre. We therefore conjecture that the additional loss is a result of the coupler's output transition not being gradual enough to be adiabatic for higher-mode propagation. This can be remedied by making the transition longer, in which case the twisted coupler represents an effective way of generating a TE_{01} mode (and hence an azimuthally-polarised beam) from a gaussian-like fundamental mode using only conventional fibres and well-known processes.

6.3 Conclusions

A TE_{01} mode convertor has been demonstrated. The method is based on a fused coupler made from conventional fibre and so does not require any PCF. It should be possible to concatenate two or more of them to "pump up" the mode order of the light further, and perhaps generate very high-order modes [Birks 01].

Chapter 7 Multimode to multiple single-mode transitions

This Chapter describes work aimed to produce low-loss multimode to multiple single-mode fibre transitions. This short project was funded by the Anglo-Australian Observatory (AAO). The AAO needs to couple each "pixel" of a telescope image to a fibre. The most suitable fibre is a multimode fibre (MMF) characterized by a high numerical aperture (*NA*). The night sky background is rich in bright infrared spectral lines due to atmospheric OH emission which can overwhelm a faint astronomical image. In order to get rid of them and improve the contrast, fibre Bragg gratings can be used as selective light filters [Bland-Hawthorn 04]. However, Bragg gratings in multimode fibre will reflect a different wavelength for each mode, making the outcome unsuitable. One solution would be a fibre device consisting of a number of conventional single-mode fibres (SMF) connected to a MMF via fibre transitions Fig. 7.1 (a). Insertion of fibre gratings between single-mode ports of two such devices would give the required response, Fig. 7.1 (b).

This concept was implemented using the ferrule technique described in Section 2.1.2, to join 19 SMFs to a multimode PCF output port [Leon-Saval 05 c]. A PCF ferrule's central holes are filled with SMFs. Then one end of the ferrule is drawn to a PCF MMF fibre connected to the 19 SMFs via a transition, Fig 7.1 (c). A good filter spectrum with a narrow spectral width was demonstrated but the device suffered from high loss. The loss can be due to two mechanisms, either a mode number mismatch or non-adiabacity of the transition [Birks 05]. Further work on a device with 37 SMFs demonstrated successful control of NA and core size leading to mode-number matching [Leon-Saval 06, no published work]. However the transitions were still lossy at best ~ 6 dB.

It was not practical to improve adiabaticity by lengthening the transitions in this experiment, because transition length was fixed by the size of our furnace. However, decreasing the number of SMFs will also improve the loss as the adiabacity criterion becomes less rigorous [Birks 05]. Although this makes the device less effective for the AAO's application, the hope was that the smaller port count would enable us to

demonstrate that these devices can be made low loss. Here the aim is to make 1×7 transitions by the same process, Fig. 7.1.

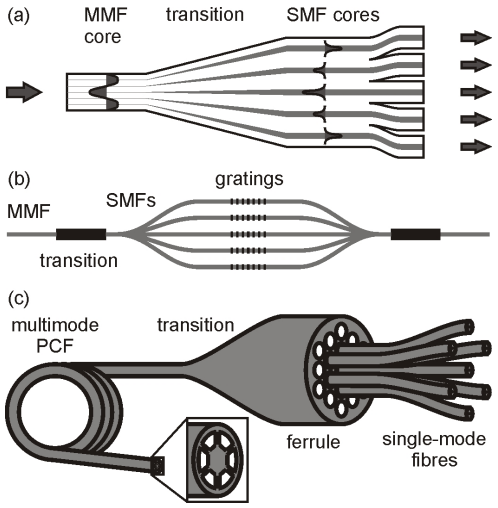

Fig. 7.1 (a) Schematic taper transition between an MMF and several SMFs [Leon-Saval 05 c]. Each MMF mode evolves into a supermode of weakly-coupled SMF cores and is distributed between separate output SMFs, and vice versa. (b) MMF grating device made by inserting SMF gratings between two transitions. (c) Schematic implementation using a PCF ferrule filled with multiple SMF and then drawn to a multimode PCF in a fibre drawing tower.

7.1 Objectives

The final objective of the work was to provide the AAO with two MMF-SMF transitions with:

- 7 ports of Corning SMF-28 single-mode fibre
- 1 port of multimode PCF with a core diameter of 20 μm and an *NA* of 0.12 or more, supporting 7 modes
- operating wavelength of $\lambda = 1550$ nm
- loss less than 1 dB
- packaged to be robust enough for handling and shipping

The MMF characteristics were chosen for compatibility with the AAO's experiments, but also so that the number of (spatial) modes would match the number of SMFs. The number of modes in an MMF can be expressed as [Crisp 01]:

$$N = \frac{\pi^2 d^2 NA^2}{4\lambda^2} \tag{7.1}$$

where d is the core diameter, NA is the numerical aperture and λ is the wavelength. This expression is the same as Eq. 1.4 but divided by 2 to count spatial modes rather than polarisation modes.

The number of SMFs was chosen to conform to hexagonal packing in the PCF ferrule.

Our principal research task was to control the NA of the MMF via the geometry of the holes. The effective index of a PCF is mainly determined by the size of the silica structures in the cladding [Birks 97, Wadsworth 04 b].

7.2 Fabrication

The fabrication of ferrule canes by drawing silica capillaries, stacking them in a hexagonal array (Fig. 7.2) and then drawing them to the cane is described in Section 1.2.2 of Chapter 1. Each of the 7 large holes in this cane was filled with an SMF, then one end was drawn to a multimode PCF port (Fig. 7.1 c) as described in Section 2.1.2 of Chapter 2.

From effective-index calculations carried out by Sergio Leon-Saval I designed a ferrule for producing a multimode PCF from stock silica capillaries with pitch Λ= 7.5 μm, a relative hole size d/Λ of 0.45 and core diameter of 20 μm. The bore diameters were chosen for the best chance of giving the target MMF. The inner 7 holes must end up big enough to accept SMFs, whereas the smaller outer holes will form the holes in the final MMF.

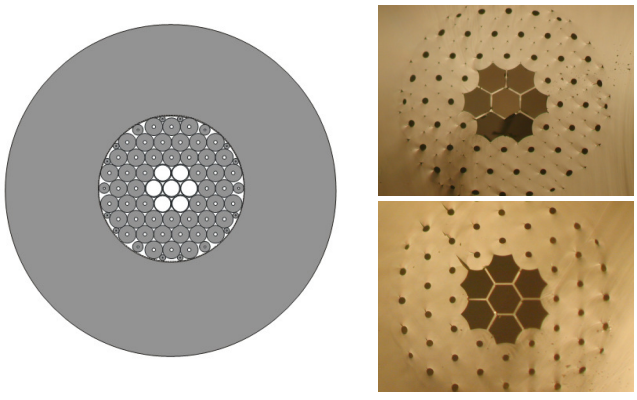

Fig. 7.2 (left) Design of the stack, made from tubes of 1.32 mm OD and 1.22 or 0.26 mm ID. (right) Photos of two ferrules drawn from the stack. Due to variations in the drawing process, the upper ferrule has small interstitial holes in the cladding whereas the lower one does not.

7.3 Results

Several metres of ferrule of diameter 3.2 - 3.6 mm were drawn from a single stack, Fig. 7.2. A total of 12 transitions A-L were made, Fig. 7.3. Optical micrographs of their MMF ports are shown in Fig. 7.4, and a summary of their structural and optical characteristics is given in Table 7.1.

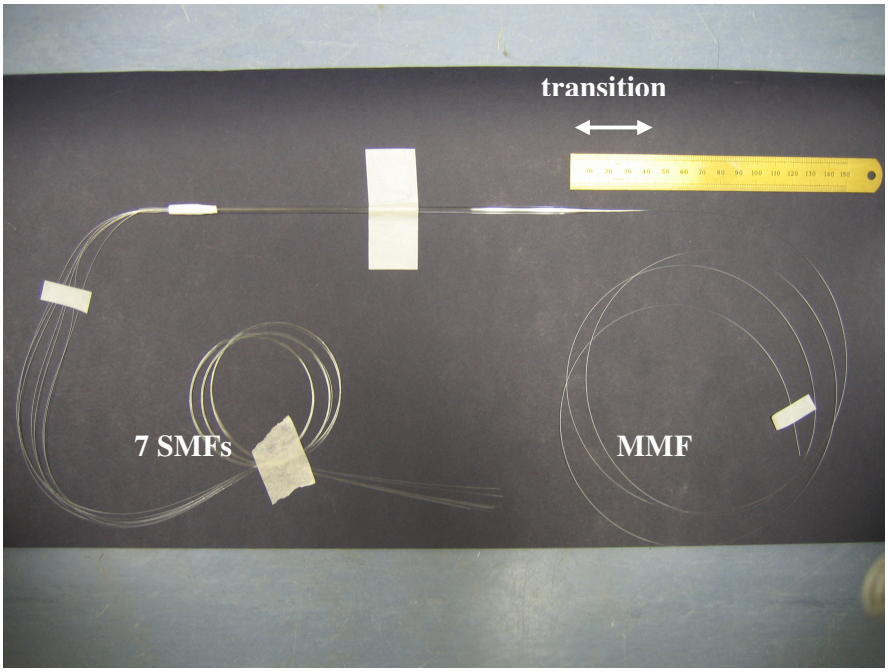

Fig. 7.3 A photo of a typical complete MMF-SMF taper device.

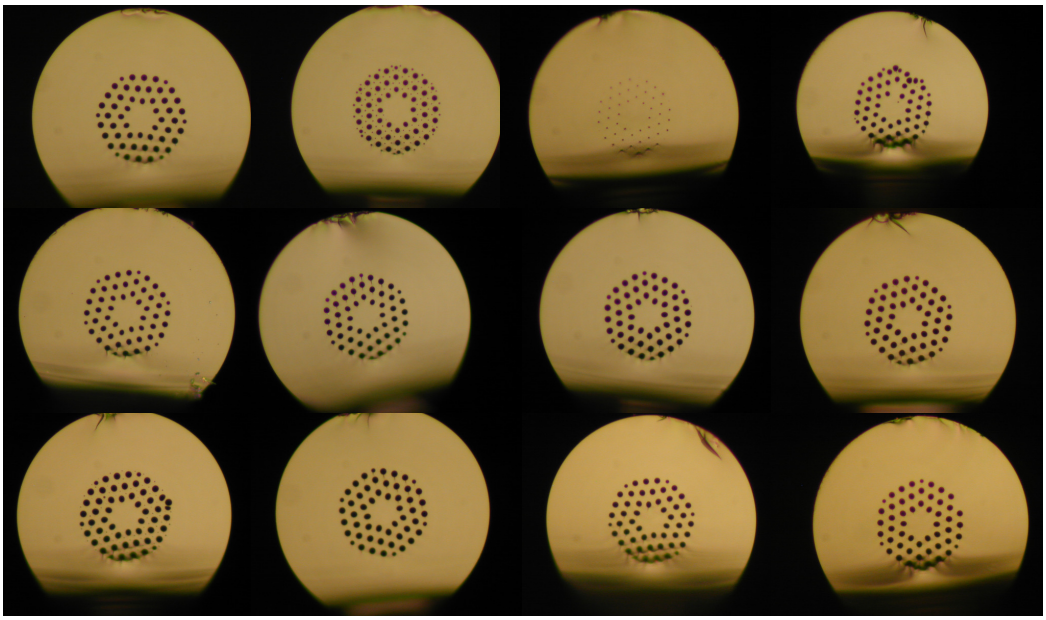

Fig.7.4 Photos of the MMFs in transitions A to L (reading from left to right, then top to bottom) to the same scale. The outer diameter (*OD*) of A is 132 µm.

taper	A	B	C	D	E	F	G	H	I	J	K	L
OD (µm)	132	128	127	116	131	128	129	130	130	130	126	131
Core diam (µm)	21	21	22	19	21	20.5	20.5	20.5	21.5	21	20	21.5
Λ (µm)	7.8	7.6	6.6	6.6	3.4	7.5	7.9	7.9	8.0	7.8	7.8	7.9
d/Λ	0.44	0.39	0.14	0.44	0.43	0.45	0.47	0.48	0.46	0.50	0.46	0.47
NA	0.17	0.14	0.13		0.16	0.15	0.18	0.18	0.21	0.19	0.14	0.16
loss of each SMF path (dB)	2.5	8.6		36.6	5.4	2.0	0.3	0.55	0.19	0.28	0.4	0.2
	2.7	8.7		38.0	5.6	2.0	0.3	1.8	0.21	0.48	0.5	0.3
	3.7	11.0		38.2	6.8	2.0	0.33	1.8	0.29	1.9	1.1	1.0
	3.8	11.1		45.0	7.0	2.2	0.7	4.5	0.3	2.4	1.8	1.45
	4.2	12.2		>45	7.7	4.3	1.1	4.7	0.35	6.5	2.6	3.3
	4.2	12.4		>45	9.9	5.4	3.2	6.2	0.43	9.5	4.6	3.7
	4.2	13.1		>45	11.7	6.2	4.2	7.3	0.5	bn	8.0	bn
mean loss (dB)	**3.56**	**10.7**		**>30**	**7.3**	**3.1**	**1.2**	**3.2**	**0.32**	**3.1**	**2.1**	**2.1**
MMF loss (dB/m)	1.8	3.3		32	6.0	1.2	0.1	0.05	0.1	0.4	0.2	0.2

Table 7.1 Measured characteristics of the 12 MMF-SMF taper samples, bn = broken.

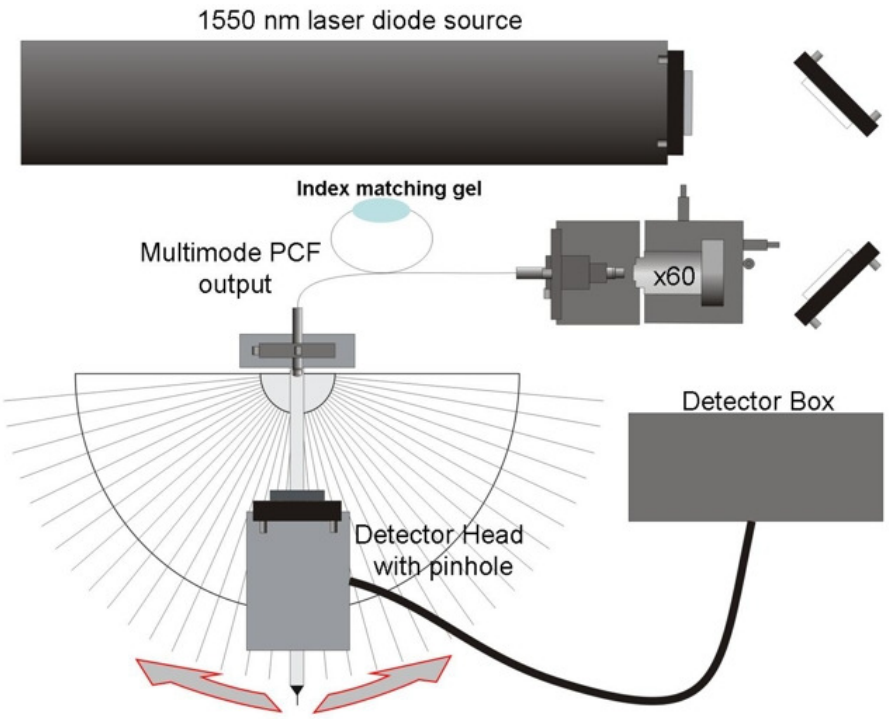

Fig. 7.5 Measurement of NA from the angular distribution of light emerging from a detached length of MMF.

The dimensions were simply taken from optical micrographs, the core diameter being measured across corners. The *NA* was found by measuring the angular dependence of the intensity emerging from a piece of the MMF using a movable photodiode (Fig 7.5). Losses were measured by launching light from a 1550 nm diode laser into each SMF in turn and measuring the output from the MMF. This was compared to the input power using the cutback technique. Index-matching gel was applied to the outside of the (uncoated) MMF to strip away cladding modes and prevent any light they support from contaminating the measurement. The average losses in the table are averaged as linear transmission coefficients and then expressed in dB. Samples J and L each suffered the breakage of one SMF port, incorporated as a zero transmission for that path when calculating average loss. Sample C did not transmit any light at all, presumably because the holes in the cladding were too small to confine light to the core.

The attenuation of a section of each MMF was also measured in the same way.

The processes used to make all 12 samples were identical, except that from sample G onwards greater care was taken over cleanliness while filling the ferrules with SMFs.

The avoidance of finger contamination will reduce scattering losses in the final tapers, and indeed losses were reduced which allowed us to make our first low-loss devices. This can be most clearly seen in the measured values for the MMF attenuation. Before avoiding contamination, the "best" value was 1.2 dB/km. After avoiding contamination, the "worst" value was 0.4 dB/km.

Sample I is clearly low loss, with an average loss of about 0.3 dB. Its *NA* of 0.21 is a little high, such that the MMF would support roughly 21 modes instead of the 7 that would correspond to mode-number-matching. The next best sample is G, with an average loss of 1.2 dB. If these two tapers were joined together via their SMF ports with no additional splice losses, and assuming only the lowest 7 modes are excited in the input MMF, the net loss would be 1.52 dB. (This assumes that the n^{th} lowest-loss ports of each taper are spliced together, which is the optimum configuration. The worst case would be 1.57 dB, if the ports are spliced together in reverse order.) The 7-way split would allow a 7-fold improvement in optical throughput in the proposed assembled OH-suppression device if it had no loss, so if such a device was assembled from samples G and I there would be a 4.9× improvement in throughput (assuming perfectly optimised input coupling into the MMF and the single SMF with which the comparison is being made).

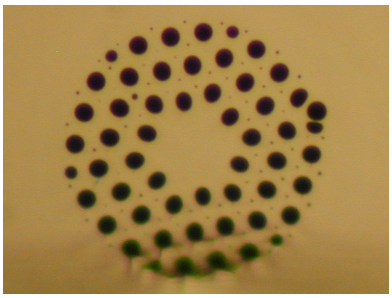

Fig. 7.6 A close-up of the best sample I.

Small residual holes can be seen in the cladding in the micrograph for sample I and some others, Fig. 7.6. These are interstitial holes between the capillaries in the original stack that did not completely close up during drawing. They are unlikely to cause any loss (as demonstrated by sample I) but could raise the *NA*, as they will reduce the effective refractive index of the cladding.

7.4 Conclusions

One low-loss 1×7 MMF-SMF transition was made, thus providing an existence theorem for the manufacturability of "low-loss" multimode to multiple single-mode transitions, although the *NA* was greater than the target. As shown in Fig 7.1, two such transitions are needed to make a filter for each pixel in the telescope image. The total number required will therefore be twice the number of pixels. However, for spectroscopic studies a small number of pixels may be adequate. The two best samples if used together could provide a 4.9× improvement in throughput in an OH-suppression device.

Chapter 8 Summary

8.1 Summary

This thesis focuses on the fabrication of new fibre transitions in PCFs (and SMFs) and the propagation of light in these structures. I made fibre transitions using post-processing techniques, amongst them a new hole inflation technique in PCFs has been developed and used. As powerful tools they allowed us to fabricate some interesting optical devices which have been demonstrated.

Hole inflation technique

This new post-processing technique which I developed, in connection with tapering, offers very easy control of the hole size along a cm-scale piece of PCF. Introducing a required pressure into all holes at one end of the fibre (the other end being sealed) and heating results in expansion of the holes. Additionally, this technique can be easily adapted to create new cores, or even change the shape of the original core. The latter can be achieved by two alternative methods. The first method is based on differential pressure due to surface tension for different hole sizes, so dramatic changes in core shapes are possible without blocking any holes if the initial fibre has a suitable configuration of hole sizes. Otherwise, blocking one or more holes prevents build up of pressure in those holes, which as a result will collapse when heated by the flame whereas others (which are still pressurized) will expand.

- This technique enabled us to get low-loss adiabatic transitions (insertion loss less than 0.3 dB for 1550 nm) between an original fibre and a fibre section with enlarged holes. The maximum outer diameter of the expanded fibre section reached 400 μm, more than 3 times that of the untreated fibre.

- Highly nonlinear PCFs have been demonstrated using this technique. They were made on a cm-scale from stock 5-μm diameter core ESM PCF (no special

preform or fibre needed) where the inflated section, connected to the single-mode pigtails through transitions of less than 0.4 dB loss, became nonlinear through tapering by factor of 3.7. SC generation using a Ti-Sapphire laser was reported.

- Using the hole inflation technique a monolithic all-fibre system was fabricated with a linear loss of 0.68 dB, for supercontinuum generation down to 400 nm when pumped with a simple compact 1062 Nd:LSB microchip laser.

- For the first time dramatic changes in core shape have been reported in PCFs. In a birefringent fibre, the differential pressure due to two larger holes on both sides of the core squashed the core, giving its mode patterns an elongated rectangular shape. The transition loss was 0.03 dB at 1550 nm. In other experiments, one, two or four holes next to the core were blocked leading to a significant change of the core shape approaching even a 5 :1 aspect ratio with a transition loss of 0.1 dB.

- A 3-cm-long low-loss (less than 0.4 dB) PCF taper transition from “circular” to “elliptical” core shape was demonstrated. The aspect ratio exceeded 2:1 and a very short birefringence beatlength of about half a millimetre was measured.

- Improved coupling from diode lasers to a rectangular core made by the inflation technique was reported. The coupling efficiency was up to 56% for 658 nm (compared to 42% for a conventional fibre).

- We succeeded in locally forming a two-core fibre section by hole blocking.

- We demonstrated a low-loss (0.3 dB at 1550 nm wavelength) PCF mode convertor from the fundamental LP_{01} mode to the TE_{01} & HE_{21} modes based on a null-coupler produced using the hole inflation technique. An extinction ratio of 20 dB was measured, this value being limited by the dynamic range of the measurement.

Tapering of SMFs

Fibre tapering is a convenient and effective way of dramatically modifying the nature of a fibre waveguide, while introducing hardly any loss of light. This powerful post-processing-technique can form taper transitions and waists of almost any shape and size with waist diameters down to 100 nm allowing precise control of taper parameters.

- A mode convertor from the fundamental mode to the second-order set of modes in SMF using tapering was demonstrated. We made a twisted fused coupler from two dissimilar fibres with the outer diameters of 125 μm and 90 μm, and a coupler waist of length 30 mm and 1.78 μm diameter. The excess loss of the coupler, as made, was 1.9 dB. By twisting of the waist, over 80 % of the output light was transferred to the un-pretapered fibre and emerged in a ring-shaped TE_{01} mode. It should be possible to concatenate two or more of them to "pump up" the mode order of the light further, and perhaps generate very high-order modes.

Ferrule technique

This technique unlike the previous ones implies the use of the fibre drawing tower. It has been proven to be a very versatile method. Fibre transitions are made by drawing a part of a preform (incorporating a number of fibres protruding from one end) into a PCF. They can provide with low-loss multimode to single-mode transitions as has been proposed to make a device for OH-line suppression.

- One low-loss (insertion loss less than 1 dB) 1×7 MMF-SMF transition was demonstrated, providing an existence theorem for their manufacturability although the *NA* was greater than the target. The two best samples if used together could provide a 4.9× improvement in throughput in an OH-suppression device.

References

[Agrawal 01] Govind P. Agrawal, "Nonlinear Fiber Optics", Academic Press (San Diego), 3rd ed, 2001.

[Alder 00] T. Alder, A. Stöhr, R. Heinzelmann, and D. Jäger, "High-Efficiency Fiber-to-Chip Coupling Using Low-Loss Tapered Single-Mode Fiber", IEEE Photonic Technology Letters 12, pp 1016-1018, 2000.

[Alfano 89] R. Alfano (Ed.), The Supercontinuum Laser Source, Springer (Berlin),1989.

[Alkeskjold 04] T. T. Alkeskjold, J. Lægsgaard, A. Bjarklev, D. S. H. Anawati, J. Broeng, J. Li, S.-T. Wu, "All-optical modulation in dye-doped nematic liquid crystal photonic bandgap fibers," Opt. Express 12, pp. 5857-71, 2004.

[Argyros 05 a] A. Argyros, T. A. Birks, S. G. Leon-Saval, C. M. B. Cordeiro, F. Luan, P. St.J. Russell, "Photonic bandgap with an index step of one percent," Opt. Express 13, pp. 309-14, 2005.

[Argyros 05 b] A. Argyros, T. A. Birks, S. G. Leon-Saval, C. M. B. Cordeiro, P. St.J. Russell "Guidance properties of low-contrast photonic bandgap fibres", Opt. Express 13, pp. 2503-11, 2005.

[Belardi 05] W. Belardi, G. Bouwmans, L. Provino and M. Douay "Form-induced birefringence in elliptical hollow photonic crystal fiber with large mode area" IEEE J. Quantum Electron. 41, pp. 1558-1564, 2005.

[Birks 00] T.A. Birks, W.J. Wadsworth and P.St.J. Russell, "Supercontinuum generation in tapered fibers," Opt. Lett. 25, pp.1415-1417, 2000.

[Birks 01] T. A. Birks, W. J. Wadsworth and P. St.J. Russell, "Supercontinuum generation in fused fiber couplers", Proc. CLEO, pp. 412-413, 2001.

[Birks 02] T.A. Birks, G. Kakarantzas, P.St.J. Russell and D.F.Murphy, "Photonic crystal fibre devices", Proc SPIE, 4943, pp 142, 2002.

[Birks 05] T. A. Birks, S. G. Leon-Saval, J. Bland-Hawthorn, M. Englund "Adiabaticity in multicore fibre transitions" Proc. Workshop on Optical Waveguide Theory and Numerical Modelling, Sydney Australia, 2005.

[Birks 06] T. A. Birks, S. Leon-Saval, A. Witkowska, K. Lai, and W. Wadsworth, "Novel methods pair holey fibers with conventional fibers," Laser Focus World, vol. 42, pp. 70-73, 2006.

[Birks 92] T. A. Birks and Y. W. Li, "The shape of fiber tapers," IEEE J. Lightwave Technol. 10, pp. 432-438, 1992.

[Birks 94] T. A. Birks, S. G. Farwell, P. St.J. Russell, C. N. Pannell, "Four-port fiber frequency shifter with a null taper coupler", Opt. Lett. 19, pp. 1964, 1994.

[Birks 95] T. A. Birks, D. O. Culverhouse, S. G. Farwell and P. St. J. Russell, "All fibre polariser using a null coupler," Opt. Lett. 20, pp.1371-1373, 1995.

[Birks 97] T.A. Birks, J.C. Knight, and P.St.J. Russell, "Endlessly single-mode photonic crystal fibre," Opt. Lett. 22, pp. 961-963, 1997.

[Birks 99] T. A. Birks, D. Mogilevtsev, J. C. Knight, P. St.J. Russell, J. Broeng, P. J. Roberts, J. A. West, D. C. Allen, J. C. Fajardo "The analogy between photonic crystal fibres and step index fibres" Proc. Opt. Fiber Commun. Conf. (OFC '99, San Diego, California) paper FG4, 1999.

[Blanchard 00] P M Blanchard, J G Burnett, G R G Erry, A H Greenaway, P Harrison, B Mangan, J C Knight, P St J Russell, M J Gander, R McBride and J D C Jones, "Two-dimensional bend sensing with a single, multi-core optical fibre", Smart Mater. Struct. 9, pp. 132-140, 2000

[Bland-Hawthorn 04] J. Bland-Hawthorn, M. Englund, G. Edvell, "New approach to atmospheric OH suppression using an aperiodic fibre Bragg grating", Opt. Express 12, pp. 5902-5909, 2004.

[Born 64] M. Born, E. Wolf, "Principles of optics", 3rd ed., Pergamon, Oxford, 1964.

[Buck 04] J. A. Buck, "Fundamentals of Optical Fibers", John Wiley and Sons (New York), 2004.

[Burns 75] W. K. Burns and A. F. Milton, IEEE J. Quantum Electron., QE-li, 32, 1975.

[Chandalia 01] J.K. Chandalia, B.J. Eggleton, R.S. Windeler, S.G. Kosinski, X. Liu, C. Xu, "Adiabatic coupling in tapered air-silica microstructured optical fiber," IEEE Photonics Technol. Lett. 13 (1), pp. 52-54, 2001.

[Choi 03] S. Choi and K. Oh, "A new LP02 mode dispersion compensation scheme based on mode converter using hollow optical fiber", Opt. Commun. 222, pp. 213-219, 2003.

[Coen 01] S. Coen, A.H.L. Chau, R. Leonhardt, J.D. Harvey, J.C. Knight, W.J. Wadsworth and P.St.J. Russell, "White-light supercontinuum generation with 60 ps pump pulses in a photonic crystal fiber", Opt. Lett. 26, pp.1356-1358, 2001.

[Cordeiro 04] C. M. B. Cordeiro, W. J. Wadsworth, T. A. Birks and P. St.J. Russell, "Octave supercontinuum generated in tapered conventional fibres by a nanosecond 1064 nm laser", presented at Conf. Lasers Electro-Opt., paper CThC2, 2004.

[Cregan 99] R. F. Cregan, B. J. Managan, J. C. Knight, T. A. Birks, P. St. J. Russell, P. J. Roberts, D. C. Allen, "Single-mode photonic band gap guidance of light in air" Science 285, pp. 1537-1539, 1999.

[Crisp 01] J. Crisp, "Introduction to fiber optics", 2nd edition, Newnes, 2001.

[Derickson 97] D. Derickson, Fiber Optic Test and Measurement, Prentice Hall, 1997.

[Diament 90] P. Diament, "Wave transmission and fiber optics", Macmillan publishing company, 1990.

[Gambling 77] W. A. Gambling, H. Matsumura, "Simple characterisation factor for practical single-mode fibres", Electron. Lett. 13, pp. 691-693,1977.

[Ghatak 98] A. Ghatak, K. Thyagarajan, "Introduction to fiber optics" Cambridge University Press, 1998.

[Hartl 01] I. Hartl, X. D. Li, C. Chudoba, R.K.Ghanta, T.H.Ko, and J.G.Fujimoto, "Ultrahigh-resolution optical coher-ence tomography using continuum generation in a air-silica microstructure optical fiber", Opt. Lett. 26, pp.608, 2001.

[Hu 06] M.-L. Hu, C.-Y. Wang, Y.-J. Song, Y.-F. Li, L. Chai, E. E. Serebryannikov, A. M. Zheltikov "A hollow beam from a holey fiber" Opt. Express 14, p.4128-4134, 2006.

[Huang 99] D. Huang, E.A.Swanson, C. P. Lin, J.S.Schuman, W.G.Stinson, W.Chang, M.R.Hee, T.Flotte, K.Gregory, C. A. Puliafito, and J.G.Fujimoto, "Optical coherence tomopgraphy", Science 254, pp.1178, 1991.

[Hunsperger 02] R.G. Hunsperger, "Integrated Optics, theory and technology", 5th edition, Springer, 2002.

[Jeunhomme 83] L.B. Jeunhomme, "Single-mode fibre optics", Marcel Dekker, 1983
[Joannopoulos 95] J. D. Joannopoulos, R. D. Meade, J. N. Winn, "Photonic crystals", (Princeton University Press), 1995.

[Kakarantzas 02] G. Kakarantzas, T.A. Birks, P.St.J. Russell, "Structural long-period gratings in photonic crystal fibers", Opt. Lett. 27 (12), pp. 1013-1015, 2002.

[Kawasaki 81] B. S. Kawasaki. K. O. Hill and R. G. Lamont, "Biconical-taper single-mode fiber coupler", Opt. Lett. 6, pp. 327-328, 1981.

[Keiser 00] G. Keiser, "Optical Fibre Communication", Third Edition, McGraw-Hill, NewYork, 2000.

[Kingery 59] W.D. Kingery, "Surface tension of some liquid oxides and their temperature coefficients", J. Am. Ceramic Soc. 42 (1), pp. 6-10, 1959.

[Knight 00] J. C. Knight J. Arriaga, T. A. Birks, A. Ortigosa-Blanch, W. J. Wadsworth, and P. St. J. Russell., "Anomalous dispersion in photonic crystal fibers", IEEE Phot. Tech. Lett. 12, pp. 807-809, 2000.

[Knight 96] J.C. Knight, T.A. Birks, P.St.J. Russell, and D.M. Atkin, "All-silica single-mode fiber with photonic crystal cladding", Optics Letters 21, pp. 1547-1549, 1996.

[Knight 98 a] J. C. Knight, J. Broeng, T. A. Birks, P. St. J. Russell, "Photonic Band Gap Guidance in Optical Fibers", Science 282, pp. 1476, 1998.

[Knight 98 b] J. C. Knight *et al.*, "Large mode area photonic crystal fibre", Electron. Lett. 34, pp. 1347, 1998.

[Kudlinski 05] A. Kudlinski, A. K. George and J. C. Knight J. C. Travers, A. B. Rulkov, S. V. Popov and J. R. Taylor, "Zero-dispersion wavelength decreasing photonic crystal fibers for ultraviolet-extended supercontinuum generation", Optics Express 14, pp.5715-5722, 2006.

[Kuhlmey 02 a] B.T. Kuhlmey, T.P. White, G. Renversez, D. Maystre, L. C. Botten, C. Martijn de Sterke, R.C. McPhedran, "Multipole method for microstructured optical fibers. II. Implementation and results", J. Opt. Soc. Am. B 19, pp. 2331, 2002.

[Kuhlmey 02 b] B. T. Kuhlmey, R. C. McPhedran, and C. M. de Sterke, "Modal "cut-off" in microstructured optical fibres", Opt. Lett. 27, pp. 1684-1686, 2002.

[Lai 06 a] K. Lai, S. G. Leon-Saval, A. Witkowska, W. J. Wadsworth and T. A. Birks, "Wavelength-insensitive LP01 to LP02 fibre mode convertor using photonic crystal fibre inflation", ECOC 2006, postdeadline,Th423, 2006.

[Lai 06 b] K. Lai, "Core shape transitions in photonic crystal fibres", Master Degree thesis, University of Bath, 2006.

[Leon-Saval 04 a] S.G. Leon-Saval, T.A. Birks, W.J. Wadsworth, P.St.J. Russell and M.W. Mason, "Supercontinuum generation in submicron fibre waveguides", Opt. Exp. 12, pp. 2864-2869, 2004.

[Leon-Saval 04 b] S.G. Leon-Saval, G. Kakarantzas, A.K. George, T.A. Birks and P.St.J. Russell, "Splice-less interfacing of conventional fibers to photonic crystal fibers", paper CThCC7 at Conference on Lasers and Electro-Optics (CLEO'04, San Francisco, California USA), 2004.

[Leon-Saval 05 a] S. G. Leon-Saval, T.A. Birks, A.K. George, W.J. Wadsworth and P. St.J. Russell, "Wavelength-independent high-extinction fibre mode convertor", paper CThZ2 at Conference on Lasers and Electro-Optics (CLEO'05), 2005.

[Leon-Saval 05 b] S.G. Leon-Saval, T.A. Birks, N.Y. Joly, A.K. George, W. J. Wadsworth, G. Kakarantzas, and P. S. J. Russell, "Splice-free interfacing of photonic crystal fibers", Opt. Lett. 30, pp.1629-1631, 2005.

[Leon-Saval 05 c] S.G. Leon-Saval, T.A. Birks, J. land-Hawthorn, M. Englund, "Single-mode performance in multimode devices", Optical Fiber Communication Conference, 2005. Technical Digest. OFC/NFOEC, PDP25, 2005.

[Lienhard 01] J.H. Lienhard, "A heat transfer textbook", Phlogistonpress, 3rd edition, 2001.

[Love 87] J.D. Love, "Spot size, adiabaticity and diffraction in tapered fibres", Electron. Lett. 23, pp. 993-994, 1987.

[Love 91] J.D.Love, W.M.Henry, W.J.Steward, R.J.Black, S.Lacroix, F.Gonthier, "Tapered single-mode fibres and devices. Part 1:Adiabacity Criteria", IEE Procedings-J 138, 1991.

[Luan 04] F. Luan, A. K. George, T. D. Hedley, G. J. Pearce, D. M. Bird, J. C. Knight, P. St.J. Russell, "All-solid photonic band gap fiber", Opt. Lett. 29, pp. 2369-71, 2004.

[MacPherson 01] W.N. MacPherson, *et al* ., "Remotely addressed optical fibre curvature sensor using multicore photonic crystal fibre", Optics Commun. 193, pp. 97-104, 2001.

[MacPherson 03] W. N. MacPherson, J. D. C. Jones, B. J. Mangan, J. C. Knight and P. St. J. Russell, Opt. Comm., "Two-core photonic crystal fibre for Doppler difference velocimetry", Vol. 223, pp. 375-380, 2003.

[Magi 04] E. C. Mägi, P. Steinvurzel, and B.J. Eggleton, "Tapered photonic crystal fibers", Optics Express 12, pp. 776, 2004.

[Marcuse 72] D. Marcuse, "Light transmission optics", Van Nostrand-Reinhold, New York, 1972.

[Marcuse 81] D. Marcuse, "Principles of optical fiber measurements", Academic Press, 1981.

[Mortensen 02] N.A. Mortensen, J.R. Folken, P.M. W. Skovgaard, and J. Broeng, "Numerical Aperture of Single-Mode Photonic Crystal Fibers", IEEE Photonics Technology Letters 14, pp. 1094, 2002.

[Nagel 82] S.R. Nagel, J.B.MacChesney, and K.L. Walker, "An overview of the modified chemical vapor deposition (mcvd) process and performance", IEEE J. of Quant. Electron., pp. 459, 1982.

[Nasilowski 05] T. Nasilowski *et al*. "Temperature and pressure sensitivities of the highly birefringent photonic crystal fiber with core asymmetry" Appl. Phys. B 81, pp. 325-331, 2005.

[Nguyen 05 a] H.C. Nguyen, B.T. Kuhlmey, M.J. Steel, C.L. Smith, E.C. Magi, R.C. McPhedran, B.J. Eggleton, "Leakage of the fundamental mode in photonic crystal fiber tapers", Opt. Lett. 30, pp.1123-1125, 2005.

[Nguyen 05 b] H. C. Nguyen[1], B. T. Kuhlmey[1], E. C. Mägi[1], M. J. Steel[1, 2], P. Domachuk[1], C. L. Smith[1] and B. J. Eggleton, "Tapered photonic crystal fibres: properties, characterisation and applications", Applied Physics B: Lasers and Optics 81, No 2/3, 2005.

[Okamoto 86] K. Okamoto and J. Noda, "Fibre-optic spectral filters consisting of concatenated dual-core fibres", Electron. Lett. 22, pp. 211-212, 1986.

[Ortigosa-Blanch 00] A. Ortigosa-Blanch, J. C. Knight, W. J. Wadsworth, B. J. Mangan, T. A. Birks and P. St. J. Russell, "Highly birefringent photonic crystal fibers", Opt. Lett. 25, pp. 1325-1327, 2000.

[Paschotta] R. Paschotta, "Encyclopedia of laser physics and technology", http://www.rp-photonics.com/encyclopedia.html

[Pearce 05] G. J. Pearce, T. D. Hedley and D. M. Bird, "Adaptive curvilinear coordinates in a plane-wave solution of Maxwell's equations in photonic crystals", Phys. Rev. B 71, pp. 195108, 2005.

[Poole 92] C. D. Poole, J. M. Wiesenfeld, A. R. McCormick, K. T. Nelson, "Broadband dispersion compensation by using the higher-order spatial mode in a two-mode fiber", Opt. Lett. 17, pp. 985-987, 1992.

[Ramachandran 05] S. Ramachandran, "Dispersion-Tailored Few-Mode Fibers: A Versatile Platform for In-Fiber Photonic Devices", J. Lightwave Technol. 23, pp. 3426, 2005.

[Ranka 00] J. K. Ranka, R. S. Windeler and A. J. Stentz, "Visible continuum generation in air-silica microstructure optical fibers with anomalous dispersion at 800 nm", Opt. Lett. 25, pp. 25-27, 2000.

[Reeves 02] W.H. Reeves, J.C. Knight, and P.St.J. Russell, P.J. Roberts, "Demonstration of ultra-flattened dispersion in photonic crystal fibers", Opt. Express 10, pp. 609, 2002.

[Russell 03] P.St.J. Russell, "Photonic crystal fibers," Science 299, pp. 358-362, 2003.

[Safaai-Jazi 91] A. Safaai-Jazi, J.C. McKeeman, "All-fiber spectral filters with nonperiodic bandpasscharacteristics and high extinction ratios in the wavelength range 0.8μm<λ<1.6 μm", Journal of Lightwave Technology 9, pp. 959, 1991.

[Saitoh 05] K. Saitoh, N. J. Florous, M. Koshiba, and M. Skorobogatiy, "Design of narrow band-pass filters based on the resonant-tunneling phenomenon in multi-core photonic crystal fibers", Opt. Express 13, pp. 10327-10335, 2005.

[Serebryannikov 07] E.E. Serebryannikov, A.M. Zheltikov, "Supercontinuum generation through cascaded four-wave mixing in photonic-crystal fibers: When picoseconds do it better", Optics Communications 274, pp. 433–440, 2007.

[Snyder 83] A. W. Snyder, J. D. Love, "Optical waveguide theory", Chapman and Hall, London, 1983.

[Snyder 86] A. W. Snyder and Xue-Heng Zheng, "Optical fibers of arbitrary cross sections", J. Opt. Soc. Am. A 3, pp. 600, 1986.

[Steinvurzel 04] P. Steinvurzel, B. T. Kuhmley, T. P. White, M. J. Steel, C. M. de Sterke, B. J. Eggleton, "Long-wavelength anti-resonant guidance in high index inclusion microstructured fibers", Opt. Express 12, pp. 5424-33, 2004.

[Tablor 69] D. Tabor "Gases, Liquids and Solids", Penguin Books, Harmondsworth UK, 1969.

[Udem 99] Th. Udem, J. Reichert, R. Holzwarth & T.W.Hänsch, "Absolute Optical Frequency Measurement of the Cesium D_1 Line with a Mode-Locked Laser", Phys. Rev. Lett. 82, pp.3568, 1999.

[Vallee 94] R. Vallée, D. Drolet, "Practical coupling device based on a two-core optical fiber", Applied Optics 33 Issue, pp.5602-5610, 1994.

[Wadsworth 02] W.J. Wadsworth, A. Ortigosa-Blanch, J.C. Knight, T.A. Birks, T.P.M. Man and P.St.J. Russell, "Supercontinuum generation in photonic crystal fibers and optical fiber tapers: a novel light source", J. Opt. Soc. Am. B 19, pp. 2148-2155, 2002.

[Wadsworth 04 a] W.J. Wadsworth, N. Joly, J.C. Knight, T.A. Birks, F. Biancalana, P.St.J. Russell, "Supercontinuum and four-wave mixing with Q-switched pulses in endlessly single-mode photonic crystal fibres", Optics Express 12 , pp. 299, 2004.

[Wadsworth 04 b] W. J. Wadsworth, R. M. Percival, G. Bouwmans, J. C. Knight, T. A. Birks, T. D. Hedley, P. St.J. Russell, "Very high numerical aperture fibers", IEEE Photon. Technol. Lett. 16, pp. 843-845, 2004.

[Wadsworth 05] W. J. Wadsworth, A. Witkowska, S. G. Leon-Saval and T. A. Birks, "Hole inflation and tapering of stock photonic crystal fibres", Opt. Express 13, pp.6541-6549, 2005.

[Zhan 03] Q. Zhan, "Radiation forces on a dielectric sphere produced by highly focused cylindrical vector beams" J. Opt. A 5, pp. 229-232, 2003.

[Zsigri 04] B. Zsirgi, J. Lægsgaard and A. Bjarklev, "A novel photonic crystal fibre design for dispersion compensation", J. Opt. A: Pure Appl. Opt. 6, pp. 717–720, 2004.